COMENIUS UNIVERSITY IN BRATISLAVA

FACULTY OF MATHEMATICS, PHYSICS AND INFORMATICS

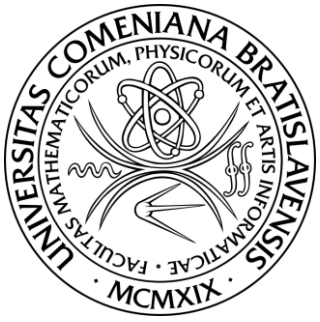

A QUANTITATIVE ANALYSIS AND CHARACTERIZATION OF MOUSE CA1 NEURON CLASSES:

A KNOWLEDGE BASE FOR COMPUTATIONAL MODELS

Diploma Thesis

2020 Nicole Vella

COMENIUS UNIVERSITY IN BRATISLAVA

FACULTY OF MATHEMATICS, PHYSICS AND INFORMATICS

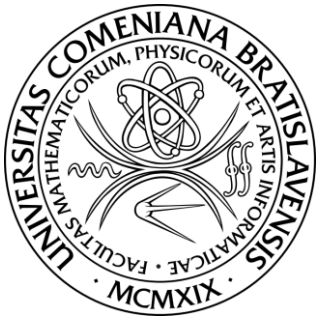

A QUANTITATIVE ANALYSIS AND CHARACTERIZATION OF MOUSE CA1 NEURON CLASSES:

A KNOWLEDGE BASE FOR COMPUTATIONAL MODELS

Diploma Thesis

Study program: Cognitive Science

Field of study: 2503, Cognitive Science

Supervising department: Department of Applied Informatics

Supervisor: prof. RNDr. Ľubica Beňušková, PhD.

2020 Nicole Vella

Univerzita Komenského v Bratislave
Fakulta matematiky, fyziky a informatiky

14398571

ZADANIE ZÁVEREČNEJ PRÁCE

Meno a priezvisko študenta: Nicole Vella
Študijný program: kognitívna veda (Jednoodborové štúdium, magisterský II. st., denná forma)
Študijný odbor: informatika
Typ záverečnej práce: diplomová
Jazyk záverečnej práce: anglický
Sekundárny jazyk: slovenský

Názov: A quantitative analysis and characterization of mouse CA1 neuron classes: A knowledge base for computational models
Kvantitatívna analýza a characterizácia neurónov tried CA1 u myší: Znalostná báza pre výpočtové modely

Anotácia: Výpočtová neuroveda umožňuje vývoj techník, pomocou ktorých sa dá celá mozgová štruktúra simulovať a testovať bez potreby in vivo alebo in vitro prístupov. Avšak, tento prístup si vyžaduje dáta; a dáta o mozgu, väčšinou kvôli zložitosti mozgu sú neúplné a neštrukturované. Hoci mnoho výskumu bolo urobené na myšiach, momentálne neexistuje žiadna databáza, ktorá obsahuje počty buniek a ich distribúciu potenciálne použiteľné pre myšací model a toto znamená výzvu pre presnosť výpočtových modelov a simulácie.

Cieľ: Kvantifikovať a charakterizovať rozličné typy glutamátových tak aj GABA neurónových buniek v oblasti CA1 mozgu myší. Zhromaždiť, organizovať a prezentovať tieto dáta, aby slúžili ako znalostná databáza pre ďalšie štúdie.

Literatúra: Bezaire, M. J., & Soltesz, I. (2013). Quantitative assessment of CA1 local circuits: knowledge base for interneuron#pyramidal cell connectivity. Hippocampus, 23(9), 751-785.
Jinno, S., & Kosaka, T. (2006). Cellular architecture of the mouse hippocampus: a quantitative aspect of chemically defined GABAergic neurons with stereology. Neuroscience Research, 56(3), 229-245.

Vedúci: prof. RNDr. Ľubica Beňušková, PhD.
Katedra: FMFI.KAI - Katedra aplikovanej informatiky
Vedúci katedry: prof. Ing. Igor Farkaš, Dr.

Dátum zadania: 25.02.2019

Dátum schválenia: 25.02.2019

prof. Ing. Igor Farkaš, Dr.
garant študijného programu

.....
študent

.....
vedúci práce

Comenius University in Bratislava
Faculty of Mathematics, Physics and Informatics

THESIS ASSIGNMENT

Name and Surname:	Nicole Vella
Study programme:	Cognitive Science (Single degree study, master II. deg., full time form)
Field of Study:	Computer Science
Type of Thesis:	Diploma Thesis
Language of Thesis:	English
Secondary language:	Slovak

Title: A quantitative analysis and characterization of mouse CA1 neuron classes: A knowledge base for computational models

Annotation: Computational neuroscience is allowing for the development of techniques where whole brain structures can be simulated and tested on without the need of an in vivo or in vitro approach. This, however, requires data; and brain-related data, mostly due to the complexity of the brain, are especially sparse and unstructured. While plenty of research is carried out on mice, there is currently no database containing cell numbers and distributions for the mouse model and this poses a challenge on the accuracy of computational models and simulations.

Aim: To quantify and characterize the different neuron classes, both glutamatergic and GABAergic neurons in the CA1 region of the mouse brain. Collect, streamline and present the data so as to serve as a knowledge base for future studies.

Literature: Bezaire, M. J., & Soltesz, I. (2013). Quantitative assessment of CA1 local circuits: knowledge base for interneuron#pyramidal cell connectivity. Hippocampus, 23(9), 751-785.
Jinno, S., & Kosaka, T. (2006). Cellular architecture of the mouse hippocampus: a quantitative aspect of chemically defined GABAergic neurons with stereology. Neuroscience Research, 56(3), 229-245.

Supervisor:	prof. RNDr. Ľubica Beňušková, PhD.
Department:	FMFI.KAI - Department of Applied Informatics
Head of department:	prof. Ing. Igor Farkaš, Dr.
Assigned:	25.02.2019
Approved:	25.02.2019

prof. Ing. Igor Farkaš, Dr.
Guarantor of Study Programme

Student

Supervisor

Declaration

I hereby declare that the work presented in this thesis is original and the result of my own investigations. Formulations and ideas taken from other sources are cited as such.

……..

Acknowledgements

Foremost, I would like to express my thanks to my supervisor prof. RNDr. Ľubica Beňušková, PhD. for her support and guidance during this project and RNDr. Kristína Malinovská, PhD. for keeping me heading forward during tough times.

I could not have done this without the invaluable input from Szabolcs Káli, PhD., Gabor Nyiri, PhD., and Julian Budd, PhD., from the Hungarian Academy of Sciences, Budapest, who have shared vital advice throughout my journey of completing my thesis.

I also want to thank all my close family and friends who have been there for me, providing me with the necessary strength and support and most importantly for lifting my spirits. Lastly, my gratitude goes to my boyfriend Michal, who has had to put up with my daily struggles, emotional turmoil and quick meals. We now know that canned tomato sauce can save lives.

Abstrakt

V dobe, keď nám výpočtová sila a technologické postupy umožňujú simulovať celé mozgové oblasti mozgu, vzniká silná potreba pre dáta, ktoré sú nevyhntutné pre takéto modely. Avšak, súčasné experimentálne dáta, ktoré sú k dispozícii sú roztrúsené a nejednotné, kvôli rozličným zdrojom, z ktorých pochádzajú a kvôli rozličným metódam a technikám, ktoré slúžia na ich získanie. Hipokampálna oblast CA1 u myší patrí medzi najviac anatomicky študovanú oblasť mozgu vďaka relatívnej jednoduchosti a dostupnosti transgenetických myší. Táto štruktúra je oknom do neurálnych základov kognície, pamäti a emočného kontextu našej epizodickej pamäti. Avšak, úplne kompletný anatomický model hipokampu myší, ktorý by zahŕňal všetky bunkové detaily, sa zatiaľ nepodarilo simulovať aj kvôli roztrúseným dátam. V tejto štúdii sme klasifikovali a kvantifikovali cez extenzívny prehľad dostupnej literatúry a jej metaanalýzu, glutamátergné a GABAergné neuróny pre oblasť CA1 hipokampu myší. Pomocou extenzívnych výpočtov sme zorganizovali dáta a prezentujeme ich v dorzo-ventrálnej osi. Takáto kvantitatívna báza znalostí je nevyhnutnou požiadavkou nielen pre simulácie, ktoré sú založené na dátach, ale aj ktoré sú určené na široko škálové simulácie ale tiež inšpirujú a inšpirujú a sústreďujú sa na budúce experimentálne projekty, ktoré sú zamerané na súčasné medzery v dátach, a tým pádom ich cieľom je pokryť holistický profil hipokampálneho regiónu CA1myší.

Keywords: CA1, hipokapmus myší, interneurón, pyramidálna bunka, quantitatívny odhad, báza znalostí, veľké dáta

Abstract

In an age where computational power and technological advances have allowed us the possibility to simulate whole brain regions, the data necessary for such models is in high demand. Currently available experimental data, however, is both sparse and non-uniform, due to the various sources it is extracted from and the different methods and technologies used for its procurement. The mouse hippocampus CA1 region is one of the most anatomically studied brain structures due to its relative simplicity and availability of transgenic mice. The structure itself is a window into the neural bases of cognition; representing the processing, storage and emotional flavouring of our episodic memories. A complete anatomical model, down to the cellular level of the mouse hippocampus, however, has not yet been simulated, with data scarcity being one of the main culprits for the delay. In this study, therefore, through an extensive literature review and data mining, the constituent glutamatergic and GABAergic neurons of the CA1 region of the mouse hippocampus were classified and quantified. By means of extensive calculations, the data has been streamlined and presented with laminar dorso-ventral accuracy. Such a quantitative knowledge-base is not only a requirement for data-driven, large-scale computational simulations but also acts to inspire and focus future experimental projects onto current gaps in the data thus aiming towards a more holistic histological profile of the mouse CA1 hippocampal region.

Keywords: CA1, mouse hippocampus, interneuron, pyramidal cell, quantitative assessment, knowledge-base, big data.

Table of Contents

List of figures.

1. Introduction

At an age where data is becoming the new currency and the machinery of the brain is slowly unravelling before our eyes, it is computational models, built on available experimental data, which are likely to usher us into the great discoveries of our mental workings and possibly even shedding light on the hard problem of consciousness. However, it is a long and tedious road ahead, paved with widely spaced and ragged stepping stones and what we aim for in this research is to smoothen those stones and bring them a little bit closer together.

This study mainly focuses on the gathering of data for a potential mouse hippocampus simulation. Through vast literature reviews, data streamlining and extensive calculations, the neural cell types of the CA1 region of the mouse hippocampus have been classified and quantified.

Since the hippocampus is the main structure accountable for episodic memory, this report starts with the definition of memory, its importance to our existence as humans and a summary of how experiential information is processed within our brain from the moment of perception to its possible long-term storage (Chapter 2). The neural bases of each stage are highlighted, finally ending at the hippocampus, the main area of memory consolidation and retrieval (Chapter 3). Special focus is given to the anatomical constitution of the structure and a detailed reasoning and justification for focusing primarily on the mouse brain is given (Chapter 4).

Since classification of cell types within the CA1 has been and still is an evolving subject, our best collective evaluation of the classification of both glutamatergic (excitatory principal neurons) and GABAergic (inhibitory interneurons) neurons was put together from various literature sources, with each cell type described, whenever possible, in terms of its origin, morphology, immunochemistry and electrophysiology (Chapter 5). The quantifications of each cell type were then calculated based on mined data and immunocytochemistry. Quantifications are specific to the dorsal and ventral parts of each of the CA1 strata.

The possible implications of our findings were then discussed with special focus on behavioural, clinical and potential future technological advancements which can be based on or facilitated by data such as that provided in this study (Chapter 6).

2. Memory and its neural correlates

Memory, both natural and artificial, is the storage of information within a system. Information is simply contextualised and interpreted data which in turn can be reduced to values attributed to certain parameters (*Definition of INFORMATION*, n.d.). The system, in the case of us humans, is the nervous system, in particular the brain, and the information is represented experience. This experience can be conscious or unconscious, subjective or arguably objective, sensory-derived or thought-generated. Within the human brain, all forms of known memory are represented by synaptic firings, strengths, frequencies and configurations within neural circuits of their respective memory systems (Eichenbaum, 2008).

Memory is what ties together our past, present and future. It is what makes us able to recognise, build, react and create in an increasingly efficient manner based on past experience. Arguably, being the most intelligent and most hyper social living organisms on the planet, humans are possibly the creatures most reliant on memory for a functional

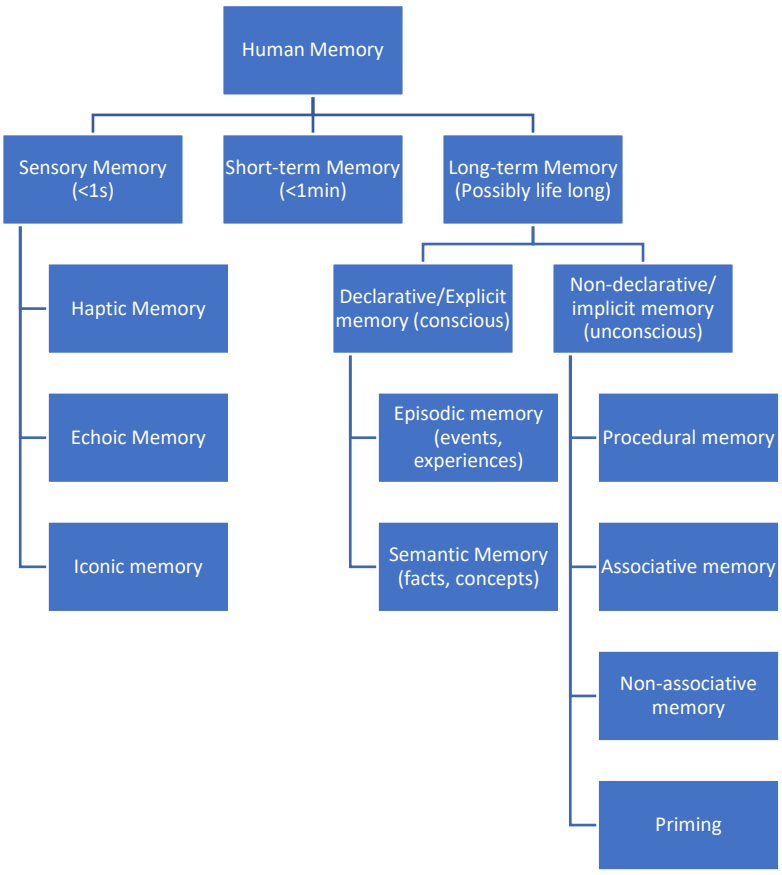

Fig. 2. 1 Memory classification chart
As adapted from Camina and Güell (2017)

everyday life. Memory allows us to learn skills, movements and language, automates behaviour, improves our judgement in detecting danger and helps us adapt to environmental and social dynamic situations. Without memory we would be, to say the least, aimless and shameless.

2.1. Sensory Memory

As memory is a very complex phenomenon, it is generally broadly classified into different classes depending on its persistence and modality (**Fig. 2. 1**). The shortest-lived memory is what is known as sensory memory which includes visual, auditory, tactile, olfactory and gustatory feelings of events (Cowan, 2008). The first three dimensions, being the most heavily researched, were dubbed iconic, echoic and haptic memory respectively. Taking iconic memory as a representative, Coltheart (1983) and Sperling, (1960), characterised iconic memory as having a large capacity of 9 to 12 characters and a short duration of less than one second. Having initially been described as pre-categorical, Loftus and colleagues, (1992) re-evaluated the sensory memory process by demonstrating that familiar symbols such as letters and numbers were already significantly more likely to be remembered at this early stage suggesting probable categorization and filtration of data.

Di Lollo's model (Di Lollo, 1980) depicts iconic memory as consisting of two components. The first component, the persistence of vision, is the pre-categorical representation that is determined by the physical parameters and their sensation by retinal photoreceptors, together with the neurons responsible for transmitting the signal to the primary visual cortex (V1) of the occipital lobe. This persistence lasts between 100 and 300ms. The second component is the persistence of information which lasts about 800ms and involves the maintenance of the post-categorical memory as it transitions from V1 to inferior temporal cortex through V2 and V5. This is the pathway taken by visual data entering visual short-term memory (STM) within the visuospatial sketchpad (Camina & Güell, 2017).

2.2. Short term memory and Working Memory.

S TM is the ability to store experiential data for a limited period of time during which said data is either "deemed worth" proceeding to long term memory (LTM) or simply forgotten forever. Working memory (WM) is arguably a subcategory of STM which can be described

as the transient state of a memory during which it is prone to manipulation or utilisation within and as part of executive functions. Gathercole, (2008) describes WM as a mental jotting pad on which we note down information for brief periods of time depending on demand and cognitive activities. Gathercole further depicts WM as a limited capacity and fragile system which can be easily disrupted and whose contents, once lost, are permanently erased.

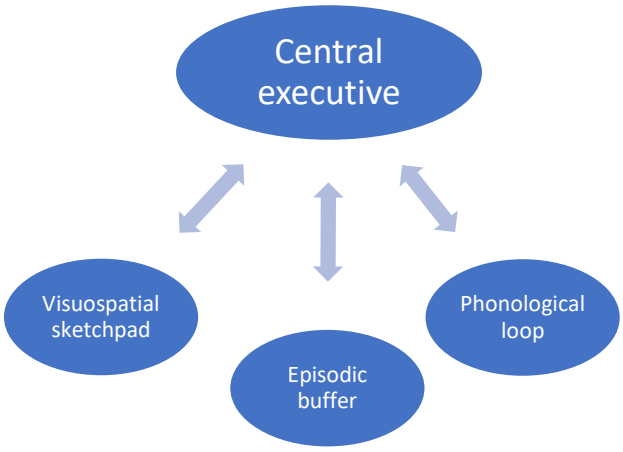

Fig. 2. 2 The Baddeley (2000) working memory model

The Baddeley (2000) (**Fig. 2. 2**) WM model suggested a dynamic and looping system, majorly requiring attention and modulated by executive functions. The model is made up of four components. Two components are slave systems which could function simultaneously without major mutual interference; the visuospatial sketchpad for visual memories, and the phonological loop for auditory memories. These are integrated and given context by the third component, the episodic buffer and regulated by a fourth component, the central executive (Gathercole, 2008). This is, however, a very limited view since, as also backed up by brain imaging techniques (Eriksson *et al*., 2015) WM constellations are much more complex than just two loops and unsurprisingly represent more than just visual and auditory memory processes. Visualised in **Fig 2. 3.** below, this component-processes view, states that no process and, therefore, no brain structure is specific to WM. The WM system is the result of several component processes which include prospection, attention, perceptual and LTM representations and can embody any representation (verbal, visual, spatial, etc.) including learned or temporary sequences and procedures such as following a set of instructions.

Therefore, by extension, they engage the many different brain regions comprising such representations. Luck and Vogel (1997) claimed that most WM capacity estimates of healthy young adults fall within 3 and 4 simple items though this can be extended by "chunking" several simple items together (Eriksson *et al.*, 2015). It has also been found to be at least true for visual memories, that the site of memory encoding (elaborated on below) is also the site of WM maintenance – in this case, the visual cortex. This, however, makes the memory vulnerable for disruption by task-irrelevant stimulus processing (Miller *et al.*, 1993). As for the executive processes, which mainly boil down to maintenance and

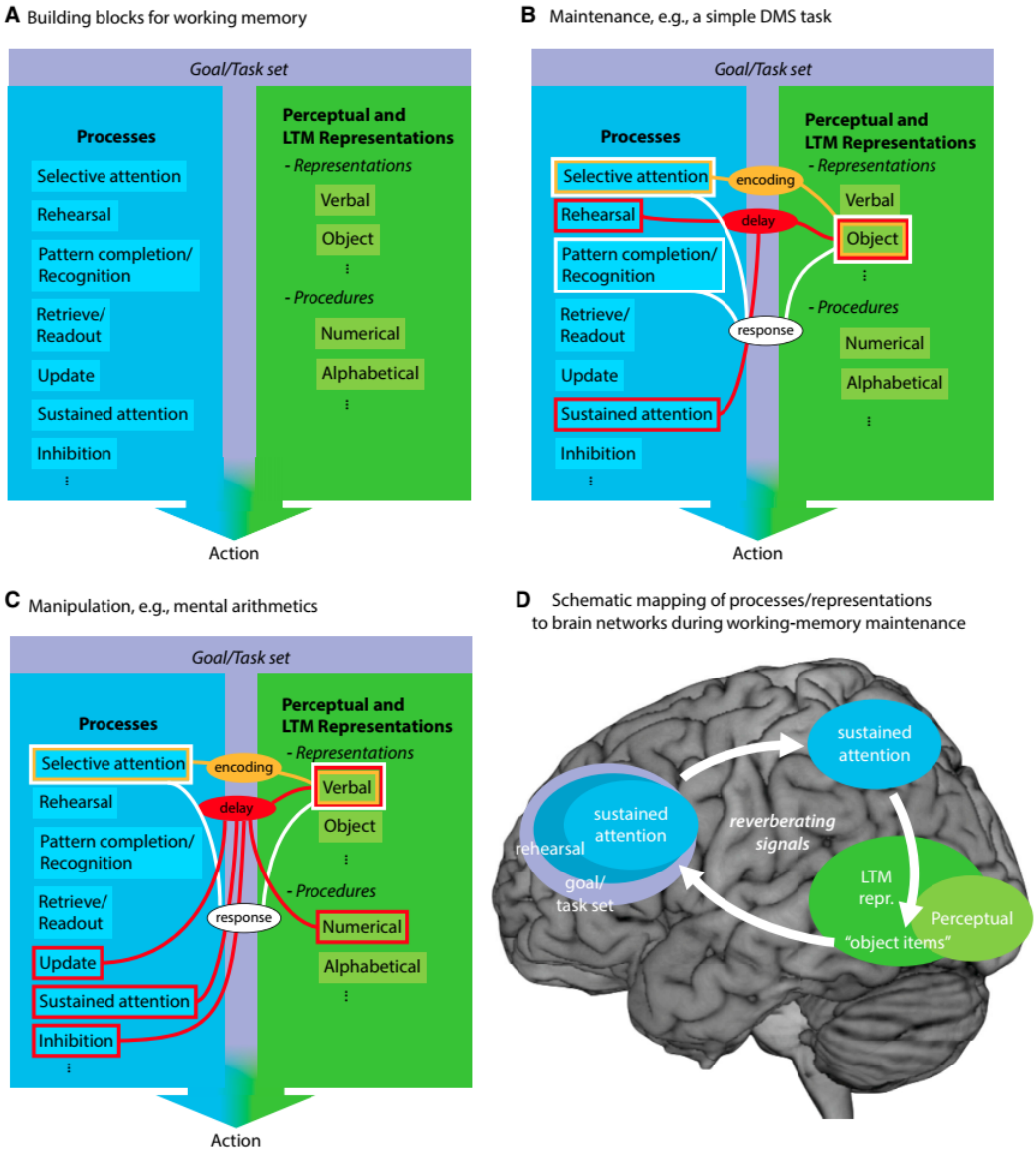

Fig. 2. 3 The Component processes view of Working Memory
A-D represent a schematic overview of different representational components, processes and their associated systems. As can be seen in B and C, different processes are active depending on the nature and progression of the task. D is a schematic mapping of the "delay" phase of the DMS task shown in B with the purpose of demonstrating the distributed nature of processes. Adapted from Eriksson et. al., (2015)

manipulation of the memory, the frontoparietal cortical regions were found to play a role in key processes though the exact mechanism of involvement has not yet been clarified (Eriksson *et al*., 2015). The prefrontal cortex (PFC) in particular has been suggested as a critical region for WM maintenance. Likely, the left ventral PFC is more involved in verbal WM while right dorsal PFC is more involved in spatial WM. The medial temporal lobe was also found to play a role in WM particularly for binding/relational processing (Allen *et al*., 2014) and possibly also involved when a WM task exceeds the WM capacity (Jeneson & Squire, 2011).

2.3. Long term memory

2.3.1. Semantic Memory

If a memory passes the selection processes of STM, it is ushered into long term memory (LTM) where it is stored for an indefinite amount of time. As depicted in **Fig 2. 1**, long term memory can be largely divided into two classes; declarative and non-declarative memory. Non-declarative memory is a largely heterogeneous combination of stored abilities, habits, skills and some kinds of classical conditioning. It is implicit and thus occurs mostly without a basis of conscious recognition. Since this class of memories is represented within the motor and premotor cortex, cerebellum and basal ganglia without any requirements for the hippocampus as an auxiliary processing mechanism (Nadeau, 2008), going into further detail about non-declarative memory is beyond the scope of this study.

The other branch of LTM is declarative memory which is again split into two; semantic and episodic memory (EM). Semantic memory (SM) is the knowledge that we have in storage, sort of like a dictionary or a thesaurus, while episodic memory (EM) is the memory of specific events; ones we can recall the context and dimensions of, such as the actual happenings, the time and place of an event. As Balota & Coane (2008) exemplify, SM of the word ‘dog’ would entail its spelling, pronunciation, grammatical usage, the general appearance, behaviour and sound of a dog, how it feels like while petting a dog and much more. On the other hand, an EM would be the recollection of seeing a cute puppy alone in the rain a day ago, the image of the dog, the smell of the air and the memory of the feeling of sadness. While the distinction of the two types of memories appears clear cut, there still is some controversy regarding where one ends and the other one starts. In the classic case of HM (Scoville & Milner, 1957), the patient had a bilateral surgical resection of two thirds

of his hippocampus, parahippocampal cortex, entorhinal cortex (EC), piriform cortex and amygdala, in an attempt to cure his epilepsy. As a side-effect of the procedure, HM suffered from severe anterograde amnesia, meaning he could not form new memories, and temporally graded retrograde amnesia, meaning he forgot some memories up to a certain time in his life. While severe, the condition appeared to only impact EM with little to no impact on other classes of memory including SM. This was, at the time, taken as a sign of the clear distinction between the two types of memories down to their structural bases. This conclusion, however, did not come without disagreements. Since the publication by Ebbinghaus in 1885 (English translation: (Ebbinghaus (1885), 2013)), researchers have been concerned about the influence of semantics on EM and have been trying to counteract this during memory tasks ever since. It is in itself a question of what episodic storage is in the total absence of meaningful information.

It is now widely accepted that semantics play a crucial role in the remembrance of experiential information. The DRM paradigm is one first addressed by Deese (1959) and (Roediger & McDermott, 1995), that shows how strong pre-existing semantic memories can totally overwhelm episodic experience. This is also apparent in false memory research performed by Roediger III and colleagues (2001). As mentioned earlier, episodic memories are contextualised lessons including properties pertaining to the situation such as the time and place, and to the personal dimensions such as feelings and emotions. It has been postulated that semantic memories could simply be episodic memories which have lost their context over time (Balota & Coane, 2008). With further studies on the neural basis of declarative memory formation it was found that damages to the medial temporal lobe (MTL) including the hippocampal region, the Cornu Ammonis (CA), the Dentate Gyrus (DG) and the Subiculum (SUB)) results not only in impaired acquisition of EM but also in the detriment of SM (Manns *et al*., 2003; Verfaellie *et al*., 2000). The role of the hippocampus in semantic memory however, is still questioned as some argue that the surrounding neocortical structures are sufficient (Squire & Zola, 1998). One argument in favour of the latter is the fact that developmental amnesia from a damaged hippocampus before or at early childhood results in unaltered semantic memory while EM is impaired (Vargha-Khadem *et al*., 1997).

In a review by Martin & Simmons (2008) it is suggested that semantic memory is not localised in a single brain region but rather particular object concepts are represented within discrete networks of cortical regions. The most relevant information or knowledge related

to the experiential interactions with an object is stored within the sensorimotor region which is active when that information is acquired. The findings in the review support the embodied cognition theory for knowledge representation, claiming that "conceptual property information is stored in the perceptual and motor systems active when that property information is learned". As for the processing of SM, three regions are consistently identified as responsible; the left ventrolateral prefrontal cortex (VLPFC) and the ventral and lateral regions of the posterior temporal lobes. Both neuroimaging and neuropsychological findings point to VLPFC as the top-down control centre for SM, functioning in the guidance of retrieval and postretrieval selection of concept property information stowed in other brain regions (Bookheimer, 2002; Thompson-Schill, 2003; Thompson-Schill *et al*., 1998). The ventral and lateral regions of the posterior temporal cortex on the other hand are mostly important for the conceptual processing of pictures and words. Neuroimaging studies showed that the higher the semantic comprehension the higher the activity in these brain areas (Martin, 2007).

2.3.2. Episodic Memory

Ultimately, EM is the type of memory most relevant to the topic of this study. Tulving (2002) describes EM as a type of memory that is past-oriented, has only recently evolved and is possibly unique to humans. Tulving also noted that this memory develops late and deteriorates early as it is more vulnerable than other memory systems to neuronal dysfunction. This is probably due to the wide array of brain regions involved. As hinted earlier, EM, while going beyond other memory systems including SM, is still sub-served and is closely related to them (Nyberg, 2008).

EM can be broken down to three broad stages; encoding, consolidation and retrieval. The first is the conversion of sensed information into a construct or an engram that can be processed by the brain. While it is not clear what is the selection process for encoding of memories, studies point towards more attention-capturing and more novel episodes as being preferably encoded (Nyberg, 2008). The sensory memory passes through STM before proceeding to the hippocampus for the next step, consolidation. Within STM, the information is fragile and is easily disrupted by various modes of interferences such as behavioural, pharmaceutical and electrical. Consolidation is the process of stabilization of this freshly forming LTM starting at the synaptic level, then cellular level and ultimately

Table 1. Neuronal basis of episodic memory.

Region(s)	Proposed function	Reference
Hippocampus	A bottle neck structure which integrates the regions that jointly define EM. It also consolidates and distributes memories to their allocated regions.	Markowitsch, (1995); Moscovitch, (1992)
Perirhinal cortex	Could contribute to EM with top down contribution from frontal cortex.	Brown and Aggleton, (2001)
Amygdala	May influence encoding and consolidation but is specifically related to retrieval as it gives emotional flavouring to memory. Emotion is also a powerful retrieval cue.	Markowitsch, (1995); Sharot *et al*., (2004)
Frontal lobe	Probably responsible for the control and optimization of encoding and retrieval. It is unlikely that it participates in storage of memory. Specific regions seem to be responsible for monitoring of the fate of retrieval success thus it critically contributes to explicit memory. The prefrontal cortex, particularly Brodmann Area 10 is the region that likely gives us the ability of mental time travel.	Fletcher and Henson, (2001); Tulving *et al*., (1994); Tulving, (2002)
Parietal lobe and diencephalon	There are likely anatomical connections between regions of the Parietal Lobe, dorsomedial nucleus of thalamus, mamillary bodies and Medial Temporal Lobe (MTL) that underlie various mnemonic processes. Also, due to the exhibition of similar activation patterns in attention, WM, EM retrieval and conscious perception when exposed to visual stimuli, the parieto-frontal region was suggested as an integration centre for different memory systems.	Nyberg, (2008); Wagner *et al*., (2005)
Basal ganglia	Lesions in basal ganglia result in similar patterns of amnesia reminiscent of Frontal Lobe damage. This is probably due to the strong anatomical interactions between the Frontal Lobe and the limbic and associative network.	Yin and Knowlton, (2006)
Cerebellum	Possibly forms part of the network that initiates and monitors the conscious retrieval of episodic memories. The right cerebellum and the Lateral Frontal Cortex are commonly recruited for both SM and EM	Andreasen *et al*., (1999)
Modality specific cortical areas	Specific modalities activate tend to activate the same regions both during their encoding and retrieval. These areas are suggested to be the distributed sites of memory storage of their respective modality. E.g.: Parietal cortex → spatial information Occipital cortex → visual information Motor cortex → activity-related information	Nyberg, (2002)

proceeds to a broader redistribution of memory to the systems level. Consolidation is a process that mainly occurs within the hippocampus and for several years, the memories remain dependent on the region. After that, they transition to a hippocampal-independent state with elevated stability (Alberini *et al.*, 2013). Retrieval of memories, which in itself is an umbrella term of a set of subprocesses, necessitates two components. The first being that the system needs to be in retrieval mode which is a state that is ready to for the conscious recollection of information, and the second is the presentation of an appropriate cue which could come in various modes, both from external sources such as a question or internally such as a particular thought or sensation. If retrieval is successful, it results in conscious recollection. Strictly defined, EM retrieval involves reexperiencing, through autonoetic awareness, a previous experience.

Several brain regions are involved in the episodic memory system. A brief summery is presented in **Table 1** above. While these regions contribute to EM in their respective ways, they do not function independently of other regions. All aspects of memory are arguably viewed as the activation of their respective network which is in turn defined by the pattern of increased firing of neuronal ensembles. Nyberg (2008) highlighted the main connections that most likely contribute to EM (**Fig. 2. 4**), however, he cautioned against individual variability, state-dependent variability and external validity. Connections:

- Between different MTL regions
- Between hippocampus and amygdala
- Between MTL and:
    - LTL
    - Parietal Lobe
    - Modality specific cortices
    - Diencephalon
- Between frontal regions and cortical and subcortical areas and:
    - Temporal cortex
    - Basal ganglia
    - Cerebellum

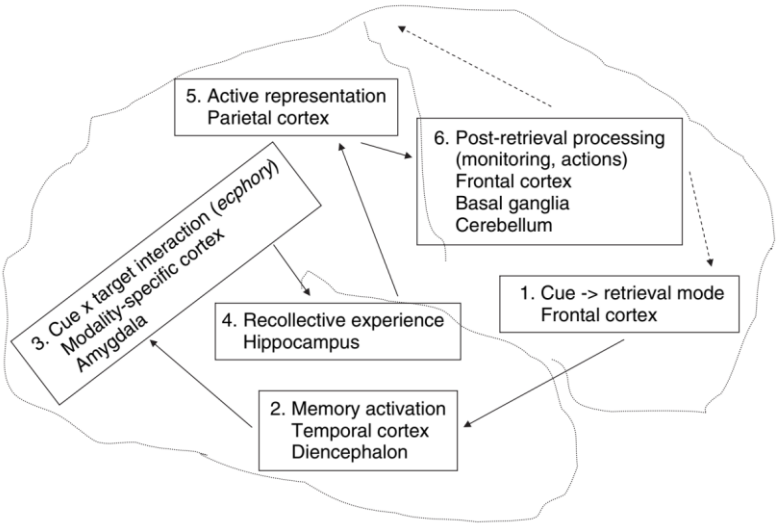

Fig. 2. 4 A schematic diagram of a tentative episodic retrieval network.
Diagram indicates both processes and regions with arrows denoting connections and information flow. As adapted from Nyberg, (2008)

3. The Hippocampus

3.1. Overview

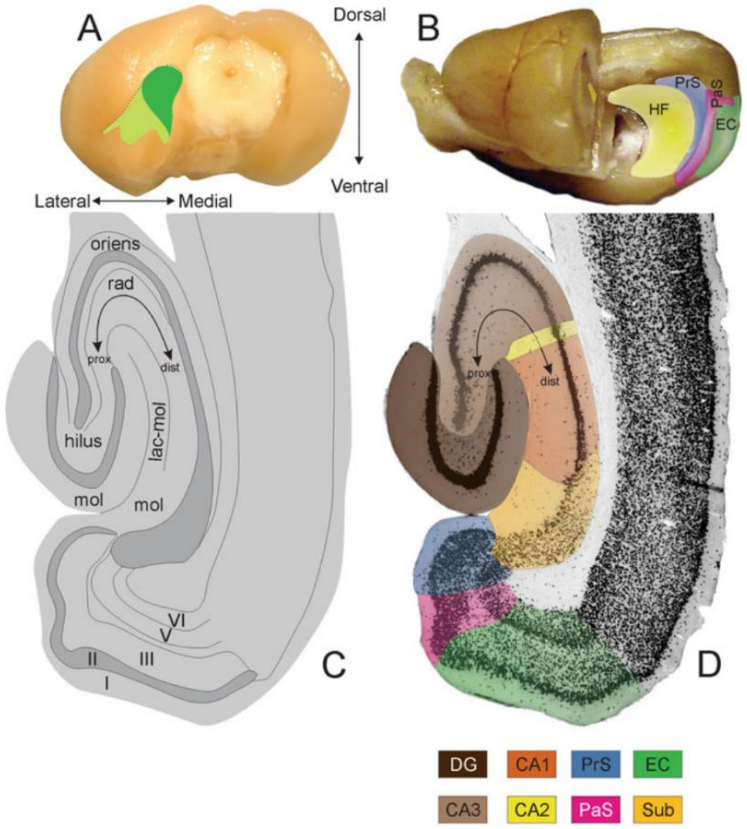

Fig. 3. 1 View of hippocampal formation and EC in the rat.
A: Posterior view of brain. LEC shown in light green and MEC shown in dark green. B: Lateral view of partially dissected brain showing the hippocampal structures and EC. Note the associated dorsoventral axis. C: schematic diagram of D showing the strata and the proximodistal axis. D: Horizontal cross-section of the hippocampal formation and EC, showing the color-coded sub divisions. Stained with NeuN. As adapted from Witter, (2010)

As already mentioned, the hippocampus is a brain structure of major importance for the consolidation and retention of information in our brain and ever since the case study of H.M., it has been at the forefront of research into the neurobiological bases of memory. This has led to the discovery of long-term potentiation and depression which is the basis of plasticity, a significant breakthrough in memory research. Also, studies into the rodent hippocampal formation have facilitated the detection of place cells, head direction cells and grid cells which strongly point towards the hippocampus as the bases of a spatiotemporal framework within which the various sensory, emotional and cognitive components of an experience can be integrated together (Knierim, 2015).

The hippocampus or more specifically the hippocampal formation, is a seahorse-shaped part of the medial temporal lobe, one in each hemisphere. The cross-section in **Fig. 3. 1** exhibits the folded arrangement of its constituent regions; the hippocampus proper (in turn partitioned into three parts, CA1, CA2 and CA3), the subiculum and the Dentate Gyrus (DG) (**Fig. 3. 3**). The hippocampal formation is closely connected with the entorhinal cortex (EC); an adjacent structure which is easily differentiated due to the dissimilar stratification arrangement (**Fig. 3. 1 and 3. 2**).

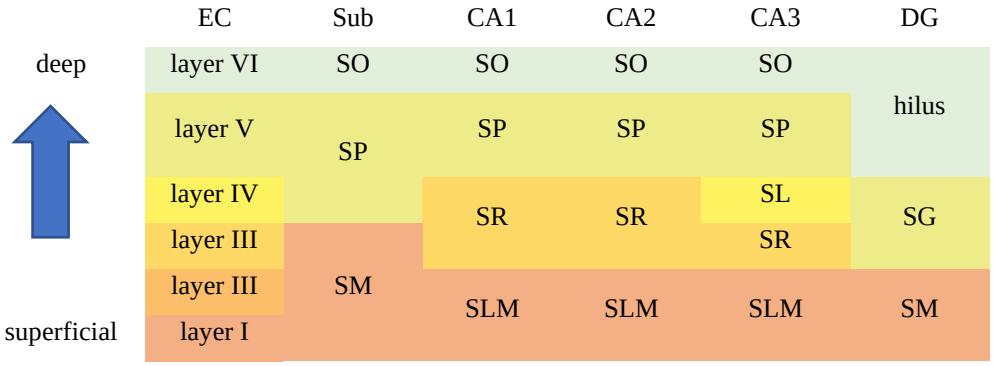

Fig. 3. 2 Distribution of strata within the hippocampus and EC.

SO	*stratum oriens*	SM	*stratum moleculare*
SP	*stratum pyramidale*	SG	*stratum granulosum*
SL	*stratum lucidum*	EC	entorhinal cortex
SR	*stratum radiatum*	DG	dentate gyrus
SLM	*stratum lacunosum-moleculare*	Sub	subiculum

The EC is often further divided into lateral (LEC) and medial (MEC) parts. It is also important to note the relevant axes used with regards to the hippocampus: the long axis (for rodent – dorsal to ventral); the transverse or proximodistal axis, which runs parallel to the cellular layers, starting at the DG; and the superficial-to-deep or radial axis which is demonstrated in **Fig. 3. 2**. The darker layers visible in figures 5C and 5D represent the cellular layers – meaning they host the cell bodies or somata of the principal cells which are the most abundant cell types in their sections. Within the hippocampal formation and the subiculum, the principal cells are known as pyramidal cells (PC) due to their characteristic pyramidal-shaped somata. They are generally taken as being excitatory glutamatergic neurons which are radially oriented within the layers. The layers superficial to the cellular layer host their apical dendrites and the majority of axons that supply the inputs to PCs together with the cell bodies of some interneurons while the deep layers contain their basal

dendrites and a mixture of afferent and efferent fibres and more interneurons (Witter, 2010). In the DG the principal excitatory cells are granule cells and their somata are found within the granule layer with their dendrites projecting throughout *stratum moleculare* (SM) ending at the hippocampal fissure or the ventricular surface. The inhibitory GABAergic, neurons are known as interneurons and they generally serve to modulate the connectivity in neural circuits.

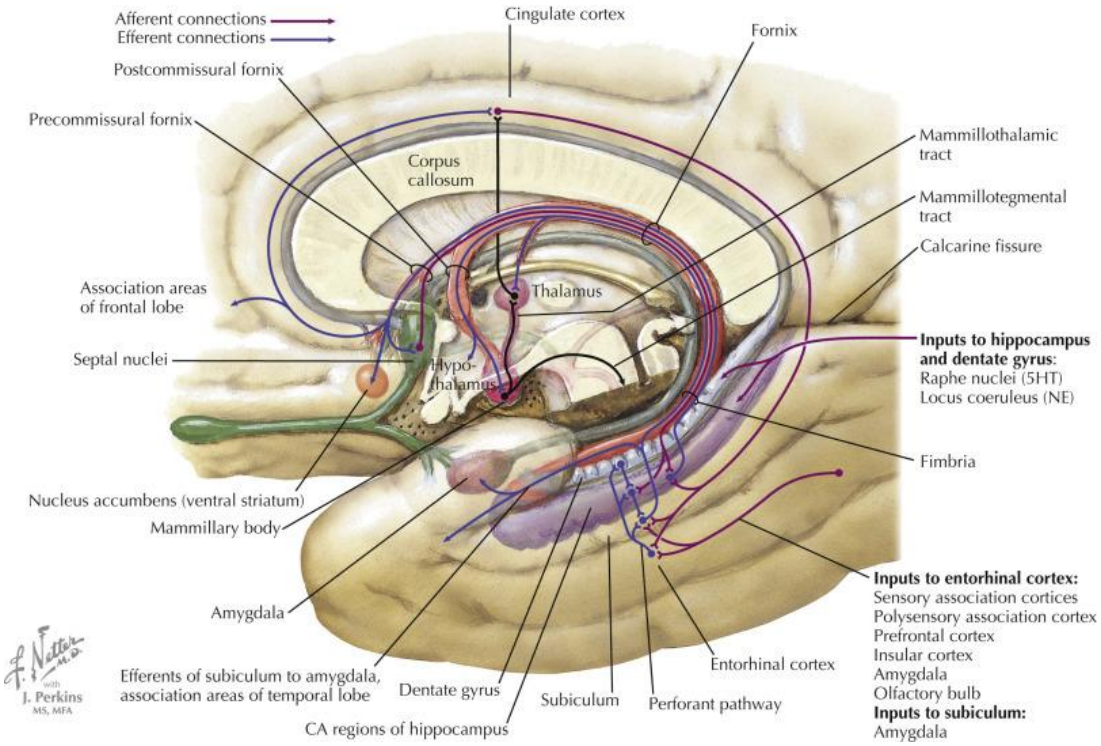

Fig. 3. 3 The limbic system.
A diagram of the limbic system of the human brain showing the structures which are closely connected to the hippocampal formation during memory encoding and consolidation. The afferent connections represent the flow of input information while the efferent connections represent the output. As adapted from: Rubin and Safdieh, (2016)

3.2. Regions and pathways of the hippocampus.

The standard view of entorhinal-hippocampal connections (**Fig. 3. 4 and 3. 5**) summarises the input-output network of the EC and hippocampal formation starting with the neocortical inputs that eventually reach the EC. The schematic network comprises of the activity flow mainly through excitatory paths conducted by principal cells. Two parallel projections stem from the LEC and MEC leading to differing routes. The Perforant Pathway (PP) projects out from the EC to all subregions of the hippocampus. As illustrated in **Fig. 3. 5**, EC layer II leads to DG, CA3 and CA2 while EC layer III leads to CA1 and subiculum. The name of the PP stems from the fact that EC axons perforate the SP of the subiculum. From SM of

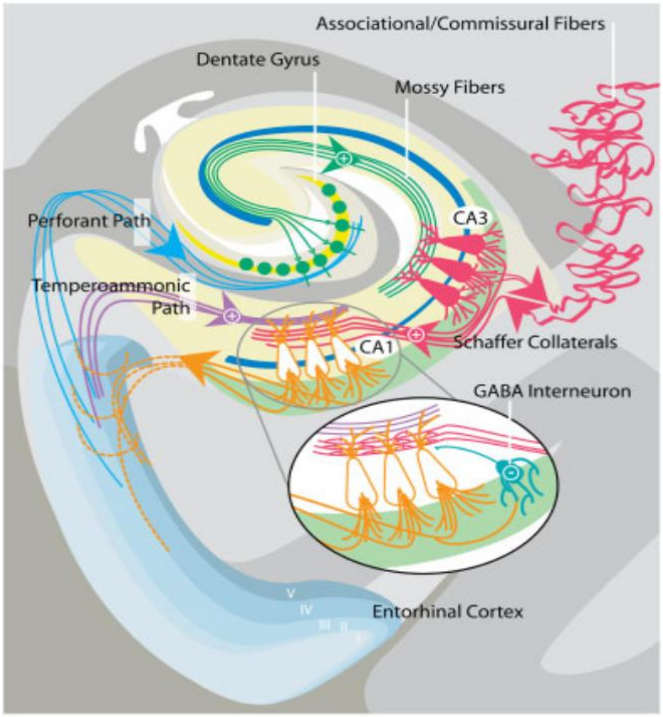

Fig. 3. 4 A schematic view of the basic circuitry within the hippocampus and EC.
As adapted from Thomas, (2009)

the subiculum, axons either cross the hippocampal fissure into DG or take the temperoammonic route through SLM of CA1, CA2 and CA3 synapsing both principal cells and interneurons on their way to entering the tip of SM in DG. Axons from EC can alternatively follow the temporo-alvear tract (not sown in **Fig. 3. 4**). These axons do not perforate the *stratum pyramidale* (SP) of the subiculum, rather they run through the alveus and *stratum oriens* (SO) in the subiculum, CA1, CA2 and CA3, only to pierce the SP at specific points in the hippocampus proper and terminating in stratum *lacunosum moleculare* (SLM). The axons target both basal and apical PC dendrites and interneurons in SO, SP and *stratum radiatum* (SR). In the rat, most fibres are likely excitatory and target mostly

principal cells but a small proportion is probably inhibitory and targets principal cells and interneurons more or less equally. Return projections only get back to EC after Layer I and Layer II EC projections are combined in CA1 and the subiculum. When considering both transverse and longitudinal axes, it emerges that these return projections are point-to-point reciprocal with EC inputs to these areas (Witter, 2010).

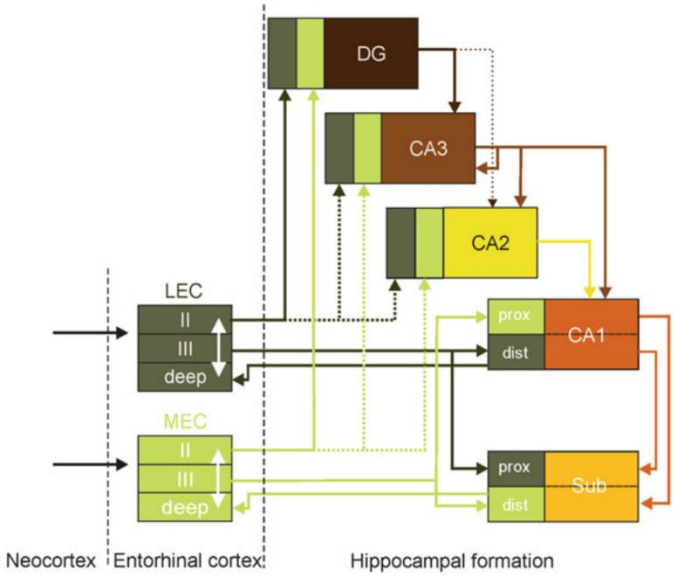

Fig. 3. 5 An extended standard view of the entorhinal-hippocampal network.
Network follows neocortical input. Arrows show excitatory pathways. As adapted from: Witter, 2010.

Projecting from the dentate granule cells through, and terminating in, the superficial layers of CA3, are mossy fibres which mainly target CA3 PCs. On their route, the axons contact mossy cells in the hilus and also source collaterals which target several types of interneurons. While most studies picture DG-CA3 connections as unidirectional, there is now evidence that proximal CA3 PCs have hilar-reaching collaterals and in the ventral hippocampus they are known to even reach inner sites of DG (Witter, 2010). These back-projecting axons source not only from principal cells but also from interneurons (Jinno *et al*., 2007).

A characteristic feature of the CA3 is the strong autoassociative network; the associational/commissural system. This is formed by CA3 axon collaterals (likely excitatory) synapsing with other local principal cells and interneurons. Axon fibres form CA3 principal cells also target CA1 neurons through a pathway dubbed the Schaffer Collaterals and they distribute in SR and SO of the CA1. Dorsally, these collaterals tend to be found deeper within these two strata as opposed to the more superficial orientation within the ventral part of the hippocampus. As for excitatory back-projection from CA1 to CA3, none has yet been described (Witter, 2010).

Within the CA1 itself there are also some recurrent connections, however, principal cells in CA1 mostly project towards the PCs of the subiculum, targeting both proximal and distal apical dendrites (Fink *et al*., 2007). Apart from the connections mentioned above, the hippocampus proper also receives inputs from other sources such as the nucleus reuniens (NR) in the thalamus which terminates in SLM and the amygdala whose collaterals are found in deeper layers like SO (Klausberger, 2009). **Fig. 3. 6** below, further elaborates on the standard connection view of the hippocampus by outlining the type of information that is flowing through the circuit according to a schematic by Knierim (2015).

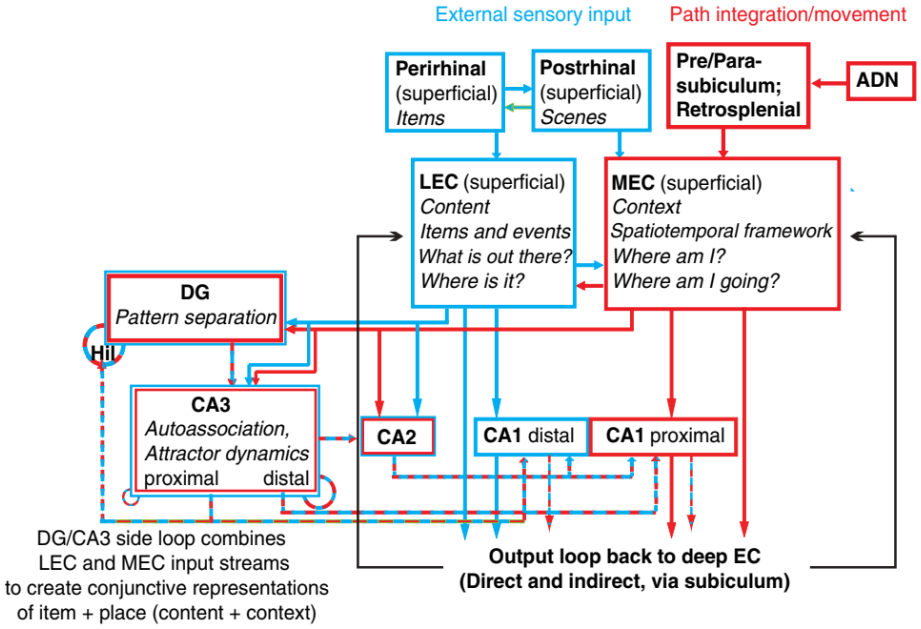

Fig. 3. 6 Memory-related flow of information through the hippocampal system.
The blue pathway signals the information sourcing from LEC which processes mainly sensory input. The red pathway is the information sourced mainly from MEC which receives input about scenes and information about proprioception. Information particularly about head-direction arrives via the anterior dorsal nucleus (ADN) of the thalamus. The CA3 and DG combine the input from both LEC and MEC allowing for the storage of a holistic representation the experience within its spatiotemporal context. The output from DG/CA3, proceeds to CA1 either through or bypassing CA2 where it is compared with direct input from EC. From CA1, information is either sent to deep EC for distribution to other neocortical areas or it is sent to superficial EC where it has the ability of influencing the next stage of memory processing. As adapted from Knierim, (2015).

4. Project purpose and description

4.1. Purpose

On our quest for trying to bridge the gap between mind and brain and understanding human consciousness and its components, in this case, conscious recollection, several projects have taken the bottom up approach (e.g. Markram *et al*., 2015); attempting to explore from molecular structures and electrophysiology up to the systems level, explaining each node and each process in the meantime. Computation and simulation neurosciences are very important fields that support this seemingly impossible task by building models and simulations of brain regions attempting to explain the phenomenon of memory.

Thus, understanding the circuitry involved in memory formation, processing and storage is a very important feat. With implications in several fields like psychology, psychiatry, neuroscience, philosophy and even machine learning and cybernetics. Clearly, ideally, we would focus on the human brain and try to answer the big questions of what makes us us. However, direct research on the human brain has its limitations.

In vivo studies carried out to observe the network structure and function in living tissue are met with obvious ethical challenges so most research is performed either *in vitro* or through behavioural studies. This is very often not ideal as external validity might not be very high. A second significant limitation is simply the size and intricacy of the human brain which is beyond the complexity of any other known organism. An alternative to *in vivo* and *in vitro* studies are *in silico* ones which are simulated regions or processes model the processes of the brain. Theoretically, if perfected, these simulations could replace the need of experimentation on real tissue though in practice, any real-life experiment still overcomes any data obtained by computation. It also necessitates both computational power and often copious amounts of data. Frequently, both a limiting. Nonetheless, computational neuroscience still has enormous potential. On comparing it with *in vivo*, *in silico* experimentation rids us of most ethical dilemmas but still faces the issue of the vast complexity of the brain which in turn necessitates vast amounts of data and, if the simulated region is relatively large, an enormous amount of computational power. It is for this reason, among others, that this study focuses on supplying data for the rodent brain, particularly the mouse.

Mice are mammals with a structurally smaller and simpler brain than humans but is still sufficiently similar that it could shed considerable light on processes relevant to the human

brain. Mice are also relatively easy to work with for behavioural, anatomical and physiological studies and while they do come with their own set of ethical boundaries, leniency is much higher for mouse studies. Moreover, they have high reproduction rates and are easy to manipulate genetically, making them ideal candidates for experimentation. Consequently, there is a flood of mouse data, but unfortunately still no mouse brain model with full anatomical features. The main reason is probably due to the sparsity and lack of standardisation of data which is often obtained though different techniques by different research groups and with different experimental objectives. The aim of this study, therefore is to streamline, classify and quantify, based on existing empirical data, the cell types present in the CA1 section of the mouse hippocampus to serve both as a knowledge base for future computational work and as an indication of any knowledge gaps so as to focus future experimental research onto the necessary paths.

4.2. Human vs rodent.

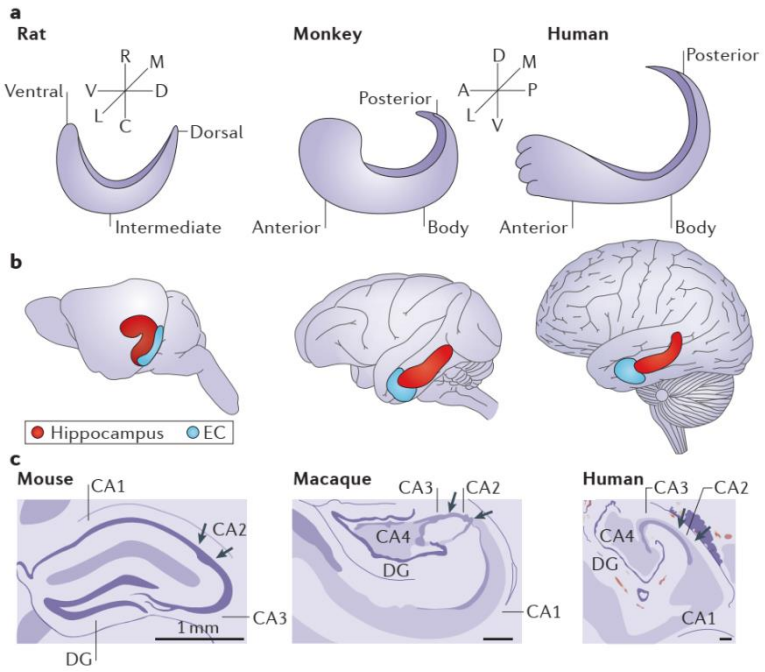

Fig. 4. 1 A cross-species hippocampal anatomy comparison.
A comparison between rodent, non-human primate and human. a: demonstrates the general shape and the orientation of the long axis of the hippocampus of a rat, monkey and human. The rat hippocampus requires a 90º rotation so as to align with those of the primates. b: The position of the hippocampus (red) and EC (blue) is displayed within the rat, macaque monkey and human. The full long axis is visible. c: Diagrams of Nissl cross-sections of the mouse, rhesus monkey and human hippocampi. A, anterior; C, caudal; D, dorsal; DG, dentate gyrus; L, lateral; M, medial; P, posterior; R, rostral; V, ventral. As adapted from Strange *et al*., (2014).

The facts that the hippocampus proper is one of the simplest cortical regions in the mammalian brain and is evolutionarily very old, are signs that the structure is probably stable making its anatomical and physiological findings likely translatable between species. (Cembrowski & Spruston, 2019). Nonetheless we tried to identify the major differences between rodent and human. As seen from **Fig. 4. 1**, while the rodent hippocampus to brain size ratio is larger than that of the human, the general anatomy is very similar. Non-human primates are arguably much more similar to humans, however, the issue of the complexity and limited access to brain tissue still persists. The long axis of the rodent brain lies on a different orientation from that of primates, probably due to the majority of the dorsal hippocampus residing below the corpus callosum in the rodent.

The ventral hippocampus in humans appears to have been forced into the anterior temporal lobe, thus changing its orientation. A second difference the and limited access to brain tissue still persists. The expansion of the anterior hippocampus in primates whereas rodents have a relatively uniform cross-sectional area throughout the long axis. This size discrepancy could be blamed again on the shifting and enlargement of the EC which could have resulted in a subsequent growth and disproportionation of the anterior hippocampus.

It is not yet known whether this skewed version of the hippocampus has had any functional repercussions. This hippocampal torsion can also be observed during primate development as up until the 14-week stage, the human hippocampus has a dorso-ventral orientation, similar to that of the rodents, but the dorsal part is later involuted and the ventral part forms the length of the human hippocampus. Ultimately, even though on the macro-scale, human and rodent hippocampus appear different, anatomical connectivity studies have posed evidence that the primate and rodent hippocampus may in fact be mostly homologous. Considering the torsion, input connectivity from EC and output connectivity towards subcortical areas follow analogous graded mapping in rodents and primates (Strange *et al*., 2014)

On a cellular morphology level, while still being similar, the dendritic and axonal morphologies of human pyramidal cells (PC) are both larger and show some structural differences compared to those in the mouse, indicating that the human cells are not a stretched-out version of the mouse cells. Therefore while some morphological parameters are kept, others were found to be species specific (Benavides-Piccione *et al*., 2019). Moreover, morphological differences on CA1 PCs were found between different strains of

mice (Routh *et al*., 2009). It is due to this specificity that we chose to, whenever possible, limit our data mining to one strain of mice: C57Bl/6.

Nonetheless, considering all the differences, rodents hippocampi can still be considered homologous to human ones thus circumstantially justifying the mouse as an alternative to human for *in silico* hippocampal simulations. From now on, unless otherwise specified, all references to hippocampal anatomy will be done in relation to rodents and during quantification, mice will be specifically considered. **Table 2** below specifies which rodent strains are used for particular calculations.

Table 2

Animals used for the quantifications.

Reference	Species	Strain(s)	Sex	Age	Weight	Sample No.
Lee *et al*., (2014)	mouse	C57BL/6J	both	2-3 months	-	-
Yamada & Jinno, (2017)	mouse	C57BL/6	male	2 months	-	27
Somogyi *et al*., (2004)	rat	Winstar	male	-	150-250	-
Kim *et al*., (2017)	mouse	C57Bl/6J	both	8-10 weeks	-	3
Jinno & Kosaka, (2006)	mouse	C57Bl/6J	male	8-10 weeks	20-25g	
Jinno & Kosaka, (2002b)	mouse	C57Bl/6J	male	8-11 weeks	22-25g	19
Jinno *et al*., (2007)	rat	Sprague Dawley	male	-	250-350g	9
Jinno *et al*., (1998)	mouse	C57Bl/6J	male	11	22-25g	16
Chittajallu *et al*., (2013)	mouse	C57BL/6	both	30 days	-	-
Jinno & Kosaka, (2002a)	mouse	C57Bl/6J	male	8-11 weeks	22-25g	44
Tricoire *et al*., (2010)	mouse	wild-type Swiss Webster	-	3-4 weeks	-	-
Somogyi *et al*., (2012)	rat	Sprague-Dawley	male	3-4 weeks	-	-

5. Neuronal classification and quantifications of the CA1 of a mouse hippocampus.

The for ease of reference, frequently used abbreviations are collectively presented in the tables below (See **Table 3** and **4**).

Table 3. Abbreviations of markers and other proteins

Abbreviation	Full name
PV	Parvalbumin
CR	Calretinin
CB	Calbindin
NPY	Neuropeptide - Y
SST	Somatostatin
CCK	Cholecystokinin
VIP	Vasoactive intestinal polypeptide
NOS	Neuronal nitric oxide synthase
ENK	Enkephalin
Calb2	Calbindin 2
M2R	Muscarinic acetylcholine receptor M2
SATB1	Goat polyclonal anti-special AT-rich sequence-binding protein-1
NADPH	Nicotinamide adenine dinucleotide phosphate
$GABA_A$-α1	Alpha-1 subunit of $GABA_A$ receptors
GABA	Gamma-Aminobutyric acid
Kir3	Effector channels of $GABA_B$
ErbB4	Protein Coding gene Erb-B2 Receptor Tyrosine Kinase 4
μOR	M-Opioid-Receptor
NMDAR	N-methyl-d-aspartic acid receptor
VGLuT3	Vesicular glutamate transporter 3
5-HT3A	5-hydroxytryptamine receptor 3A
ACAN	core protein of aggrecan

Table 4. Abbreviations of cell types

Abbreviation	Full name
PC	Pyramidal Cells
BPC	Backprojection Cells
PV BC	Parvalbumin Basket Cells
CCK BC	Cholecystokinin Basket Cells
AAC	Parvalbumin Axo-Axonic Cells
BSC	Bistratified Cell
SCI	Schaffer Collateral Associated Cells
PPA	Perforant Path Associated Cells
ADI	Apical Dendritic Associated Cells
NGF	Neurogliaform Cells
Ivy	Ivy Cells
O-LM	Oriens-Lacunosum Moleculare Cells
DPC	Double Projecting Cells
O-BI	Oriens Bistratified
IS-I	Interneuron-Specific Type 1
IS-III	Interneuron-Specific Type 2
IS-III	Interneuron-Specific Type 3

5.1. Principal cells

5.1.1. Morphology

The principal cells found in the CA1 area of the hippocampus are pyramidal neurons. They are the most common cell type and the main projection neurons in the region, making them responsible for the transmission of most of the processed information in CA1. Unlike interneurons, their axons are the main source of excitatory glutamatergic synapses both within and projecting out of CA1. Their spiny dendritic also mainly receive excitatory synapses (Benavides-Piccione *et al.*, 2019). The activity in these cells is largely modulated by inhibitory interneurons which in turn are also excited by the PCs. The quantity and quality of this relationship largely depends on the type and position of both the CA1 PC and the interneuron. This will be further elaborated on below. PCs are radially oriented with their soma within SP and their apical dendrites emerge from the upper pole of the soma towards SR and SLM giving off a number of oblique collaterals terminating in an apical tuft.

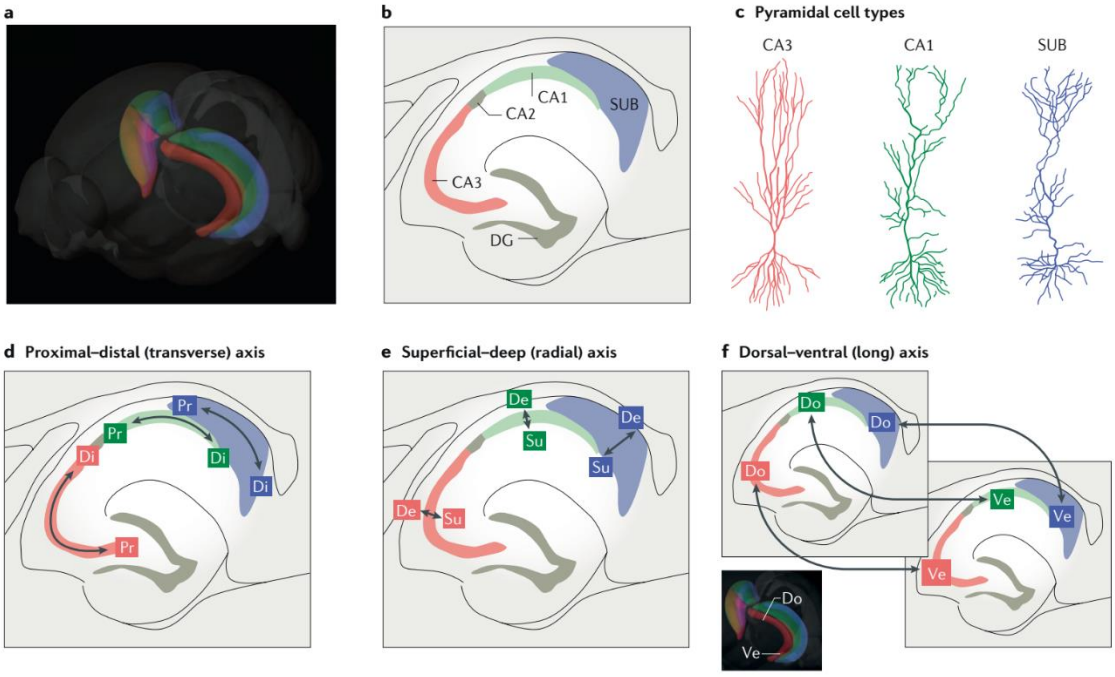

Fig. 5. 1 An overview of the axes of the mouse hippocampus and its characteristic PCs.
a: A 3D render of the mouse brain prepared with the Allen Brain Explorer 2 showing the CA3 in red, CA1 in green and the subiculum (SUB) in blue. b: A cross section of the hippocampal long axis with labelled regions. c: characteristic CA1, CA3 and SUB cells illustrating the morphological differences between the three types. d-f: schematic illustrations of the three hippocampal spatial axes; d: proximal-distal (Pr-Di), e: superficial-deep (Su-De) and f: dorso-ventral (Do-Ve). As adapted from Cembrowski and Spruston, (2019)

The basal dendrites protrude from the base of the soma and travel horizontally or radially within SP and SO. The axon either arises from the base of the cell or from the origin of the basal dendrite, normally giving off several collaterals (DeFelipe & Fariñas, 1992). As mentioned earlier, CA1 PCs mainly interact with input synapses from CA3 and EC while their axons primarily target the subiculum. These circuits are in accordance to the "lamellar hypothesis" which suggests that the hippocampus is an organized stack of parallel trisynaptic circuits (→DG →CA3→CA1→) (Andersen *et al*., 1971). However, a single longitudinally oriented branch was also identified, originating from the thick proximal axon. This axon collateral not only defies this hypothesis but also, since it connects with other CA1 PCs, indicates an associational and interlamellar network among CA1 PCs (Yang *et al*., 2014). CA1 PCs, have their characteristic shape which differs even from PCs in other regions of the hippocampus as seen in **Fig. 5. 1**, as well as characteristic genetic markers, *Calb1* and *Nov* (Zeisel *et al*., 2015).

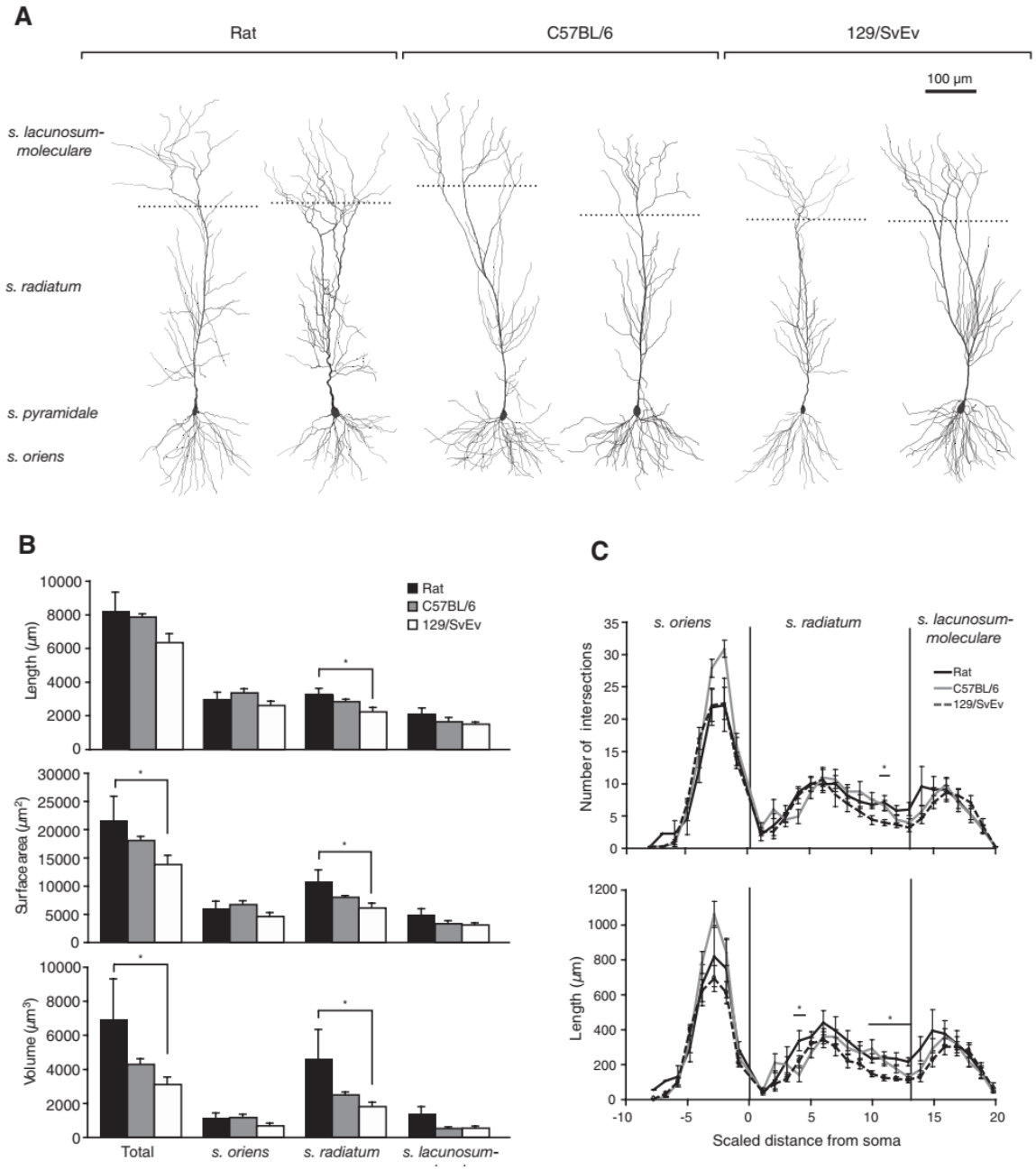

Fig. 5. 2 Morphology comparison of CA1 PCs of rats, C57Bl/6 and 129/SvEv mice.
A: representative reconstructions of neurons from rats and two mice strains. The dotted lines show the SR-SLM borders for each cell. B: Plots showing the average dendritic length, membrane surface area and volume within different CA1 strata. **P*<0.05. C: Sholl analyses of intersections and dendritic lengths within different strata. The scaled distance represents the number of Sholl spheres going incrementally from 1 to 20 with increasing distance from the soma. The negative distances refer to the basal dendrites found within SO. **P*<0.05. Rat vs. 129/SvEv mice: difference in intersections at Sholl distance 11 and in dendritic length at Sholl distances 11–13. Rat vs. C57BL/6 mice: difference in dendritic length at Sholl distances 4 and 13. C57BL/6 vs. 129/SvEv: differences in dendritic length at Sholl distances 10–11. *n* 5 rats, 6 C57BL/6 mice, and 8 129/SvEv mice. As adapted from Routh *et al*., (2009).

It is also noteworthy, as illustrated in **Fig. 5. 2**, that CA1 PCs differ morphologically both between species and between different strains. Average morphological parameters, with those of C57Bl/6 being the most relevant for this study, are also presented in the figure. However, even though they have traditionally been clustered within one cell type with one set of characteristics, it is becoming increasingly clear that CA1 PCs can differ significantly also between themselves. Arguably, cells from opposite ends of CA1 dorso-ventral axis are qualitatively as diverse as PCs between different regions (Cembrowski & Spruston, 2019). This heterogeneity probably allows for the simple structure of the hippocampus to perform complex processes involving the passage of time, fear, stress, anxiety and the processing of both spatial and non-spatial environments. As these cells repeat across space along the dorso-ventral axis, the concurrent execution of distinct computations through the same apparent circuitry could be facilitated (Cembrowski & Spruston, 2019). **Table 5** summarises the differing characteristics over the length of the long axis, transverse axis and radial axis. The variations are present on all levels, from molecular to behavioural. There is evidence that this heterogeneity is not discrete but continuous and is thus more indicative of gradients rather than of clear-cut variations as evidenced by studies including recent transcriptomics (Habib *et al*., 2016), anatomical connectivity (Kishi *et al*., 2006) and *ex vivo* electrophysiological recordings (Milior *et al*., 2016).

Table 5: Heterogeneity of CA1 pyramidal cells across the long, transverse and radial axes.

Heterogeneous feature	**Axes**	**Showing Variation in:**
Molecular scale		
Gene expression	Long:	Wfs1 and Grp*
	Transv:	Crtac1
	Radial:	Col11a1
Protein products	Long:	WFS1
	Transv:	Unknown
	Radial:	CALB1
Cellular scale		
Electrophysiology ex vivo	Long:	Resting membrane potential
	Transv:	Burstiness
	Radial:	Burstiness
Morphology	Long:	Dendritic surface area
	Transv:	Abundance of axon-carrying dendrites
	Radial:	Spine density
Circuit scale		
Extrahippocampal inputs	Long:	Distribution of inputs from amygdala
	Transv:	Distribution of inputs from entorhinal cortex
	Radial:	Distribution of inputs from entorhinal cortex
Extrahippocampal outputs	Long:	Distribution of outputs to amygdala
	Transv:	Unknown
	Radial:	Unknown
Intrahippocampal connectivity	Long:	Distribution of connections with CA3
	Transv:	Distribution of connections with CA3
	Radial:	Distribution of connections with CA3 and number of PV BC input and output synapses on PC**
Neuromodulation	Long:	Unknown
	Transv:	Degree of dopaminergic modulation
	Radial:	Degree of cannabinoidergic modulation
Systems and/or behavioural scale		
Electrophysiology *in vivo*	Long:	Place field size
	Transv:	Spatial selectivity
	Radial:	Excitability
Optophysiology *in vivo*	Long:	Unknown
	Transv:	Unknown
	Radial:	Landmark-specific firing
IEG-basted functional activity	Long:	Activation by spatial exploration
	Transv:	Activation by spatial exploration
	Radial:	Unknown
Effects of perturbation	Long:	Disrupted fear memory
	Transv:	Disrupted fear memory
	Radial:	Disrupted olfactory associative learning

As adapted with permission from Cembrowski and Spruston, (2019)
*(Zeisel *et al*., 2015) **(Lee *et al*., 2014)

5.1.2. Electrophysiology

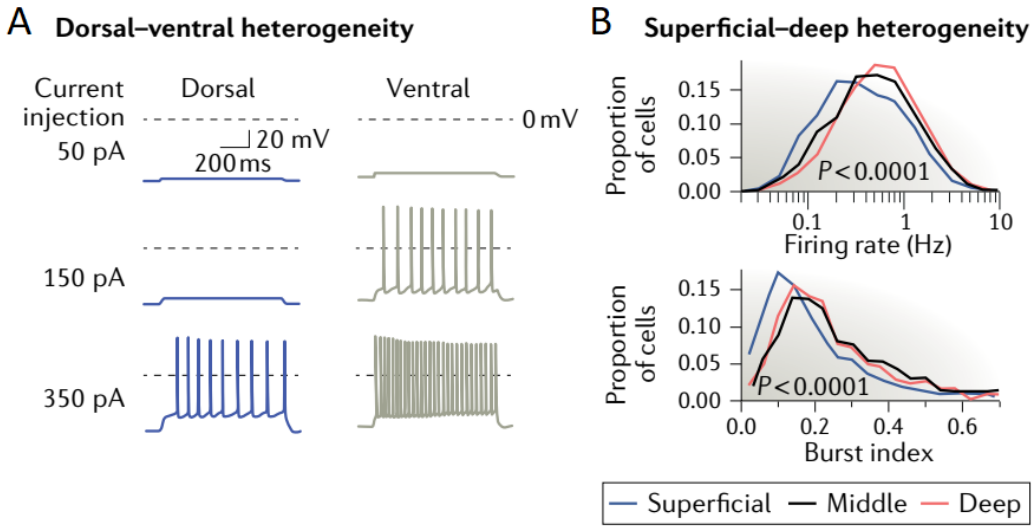

Fig. 5. 3 Heterogeneity within the rat CA1 pyramidal cell type.
A: Showing representative voltage responses in ex vivo brain slices from dorsal and ventral CA1cells following current injections of 50pA (top), 150pA (middle) and 350pA (bottom). Recordings were performed in rat brain slices ex vivo. B: Comparison of firing rate (top) and burst index (bottom) from the superficial, middle and deep layers. The burst index id defined as the fraction of spikes with <6ms interspike intervals. These *in vivo* measurements were taken during running. *P* values depict comparison between superficial and deep layers. As adapted from Cembrowski & Spruston, (2019).

Generally, all CA1 cells exhibit regular spiking behaviour when subjected to direct somatic injection (Staff *et al.*, 2000), however due to the heterogeneity within this cell type, excitability of the cells is significantly higher than that of dorsal cells (**Fig. 5. 3**) and deep PCs were much more excitable and prone to bursting (Cembrowski & Spruston, 2019)

5.1.3. Cell quantifications

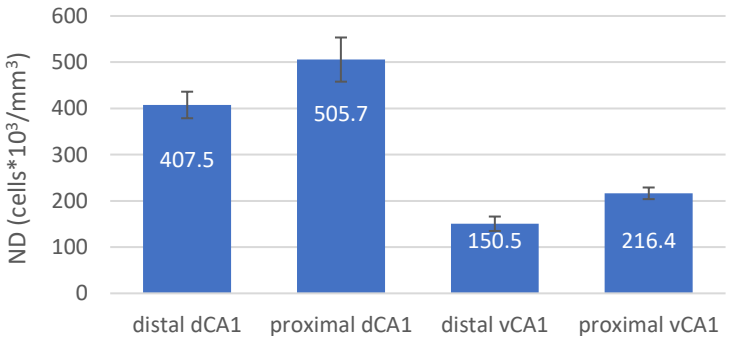

Fig. 5. 4 Numerical densities of pyramidal cells in CA1.
Bar graph showing the numerical densities (ND) of pyramidal cells in the proximal and distal parts of the dorsal and ventral CA1 of the mouse. Values and standard deviations from Jinno & Kosaka (2010)

Jinno & Kosaka (2010) estimated the numerical density of glutamatergic principal neurons in the mouse CA1 hippocampus in four areas; the proximal and distal parts of both the dorsal and ventral hippocampus. As can be seen from the values in **Fig. 5. 4**, there are significant differences between the CA1 sub-regions which is an indication of further heterogeneity which is present not only on the cellular level but also on the organisational level of CA1.

5.2. Interneurons

Interneurons are inhibiting GABAergic neurons responsible for the modulation of circuitry in CA1. Below is a classification based on the type and location of their target cells and their target morphology sites. Whenever possible, alternative names, origin, markers, morphology and electrophysiology will be elaborated on together with their sources and targets. In this report, cells having majorly the same morphology, immunocytochemistry and electrophysiology will be considered as a cell type. Sometimes these cell types can be grouped together into cell families by common characteristics and at other times, minor variations such as developmental origin can divide these types into subtypes. Please note that calculated values will be typed in blue for better differentiation from values obtained directly from the literature. Values which were mined from plotted data using the online value extraction software WebPlotDigitizer (https://apps.automeris.io/wpd/) will be typed in yellow.

5.2.1. Perisomatic Inhibitory neurons

5.2.1.1. Parvalbumin Basket Cells

Other names: Fast-spiking basket cells

Origin: MGE (Tricoire *et al*., 2011)

Markers: Highly immunopositive for PV and SATB1. Also positive for NADPH, GABAAα1+, KV3.1b, ErbB4, M2R, μOR+ and NR2D (Yamada and Jinno, 2017, Vida *et al*., 2018)

Morphology: Parvalbumin basket cells (PV BC) have a general laminar distribution similar to that of PCs, though the total length of the dendrites appears to be shorter. The soma of most of the PV BCs is situated in SP, however a small percentage can also be found in SO and even in SR (Vida *et al*., 2018). The actual percentage of distribution of somas within the different layers is not known but it is generally assumed that PV BCs fully reside in SP when considered for quantification (Baude *et al*., 2007; Yamada & Jinno, 2017). PV BCs are characterized by their axon which terminates in and near SP. Dendrites, that normally span all layers, contain no spines and are radially oriented. Moreover, Yamada and Jinno (2017) observed that over 88% of ventral and over 99% of dorsal putative PVBCs in CA1 were surrounded by ACAN+ perineuronal nets which are specialized structures of extracellular matrix, enriched with CS-bearing proteoglycans (Giamanco & Matthews, 2012) and have been shown to play a critical role in the regulation of neural plasticity (Wang & Fawcett, 2012). The axon on the other hand terminates in a circular or ellipsoid area of the SP and cradles PC somata within it; hence the term basket cell. Booker and colleagues (2017) additionally described a putative PV BC with horizontal dendrites exclusively in SO, suggesting divergent dendritic morphologies.

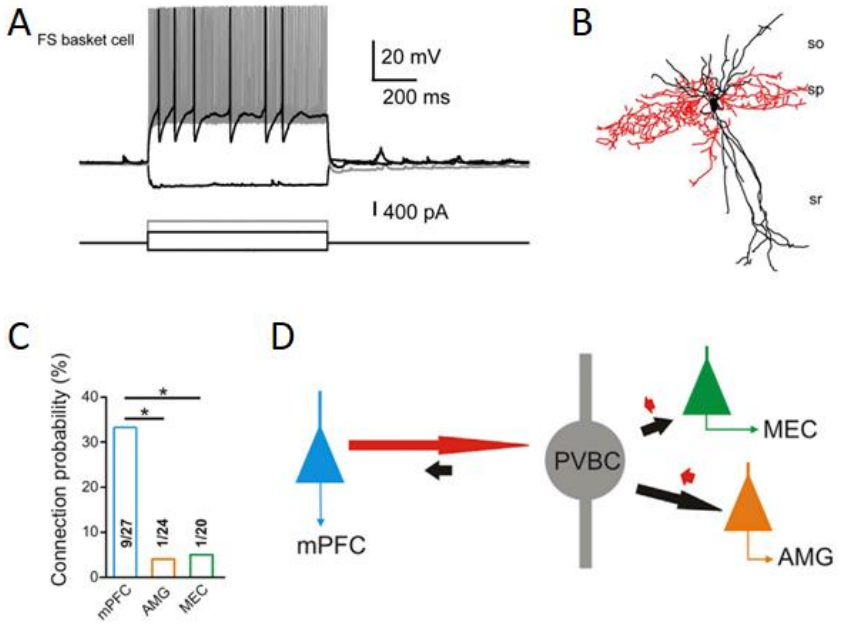

Fig. 5. 5 Parvalbumin Basket Cell profiles.
A: Electrophysiological profile of mouse PV BC. B: Morphological profile of mouse PV BC. so, *stratum oriens*, sp, *stratum pyramidale*, sr, *stratum radiatum*. As adapted from Tricoire *et al*., (2011). C: Summary of connection probabilities with medial Prefrontal Cortex (mPFC), Amygdala (AMG) and medial Entorhinal Cortex (MEC). D: Schematic representation of inputs and outputs to and from PV BCs. The length of the red and black arrows is proportional to mean eul/EPSC amplitudes times connection probability. As adapted from Lee *et al*., (2014).

Sources and Targets: Both the dendritic shafts and the perisomatic domain receive excitatory and inhibitory synaptic inputs, however, inhibitory inputs show a preference towards the soma, with about 17% of synapses (in the rat) converging there (Vida *et al*., 2018). As documented by (Gulyás *et al*., 1999) also for the rat, about 28% and 70% of inhibitory synapses on the dendrites and the soma respectively are PV+, indicating a high interconnectivity within the PV interneurons themselves. Gap junctions are also concentrated at dendritic locations mainly between basal dendrites at SO-alveus border. The duality of this connectivity is hypothesized to aid in the synchronization of interneural network activity patters such as gamma oscillations. (Vida *et al*., 2018)

PV BCs form multiple synaptic contacts on somata and proximal dendrites of their target PCs which make up approximately 10% of the PCs within their axonal cloud (Bezaire & Soltesz, 2013 - rat). Lee and colleagues (2014) investigated the possible predispositions in PV BC – PC connections in CA1 depending on the location of the PC and its role within the network. From **Fig. S1** (Lee *et al*., 2014), it could be calculated that within the superficial layer of SP (closer to SR), one PVBC innervates one PC via 3.97 boutons with a connection probability of 50%. PVBCs were calculated to have a convergence of about 50.6 cells on one superficial PC. In contrast, in the deep sublayer, one PVBC innervates one PC via 8.68 boutons. PVBCs have a convergence of about 41.1 cells on one deep PC. The average connection probability from PVBCs and deep PCs is of 46.8%. This preferential innervation is not brought about by unequal bouton densities along the axon of the interneurons but by a significantly larger proportion of PVBC axon being present in the deeper layer (**Fig.S2**; Lee *et al*.,2014). It is also noteworthy that Földy *et al*. (2010) found a distinctly different ratio of PV+ boutons innervating the PC soma to those innervating proximal dendrites (1.12:1) compared to Lee *et al*., (2014) (0.38:1) PV BCs are also more likely to innervate PCs leading to the amygdala than the MEC or the mPFC (Fig. PVBC1). PVBCs also form synapses with other interneurons particularly other PV+ interneurons (Vida *et al*., 2018).

Electrophysiology: PV BCs are fast spiking cells (Tricoire *et al*., 2011) (**Fig. 5. 5A**)

5.2.1.2. Cholecystokinin Basket Cells

Other names: non-fast spiking basket cells.

Origin: CGE (Tricoire *et al*., 2011)

Markers: Very immunopositive for CCK and CB1. Also positive for ErB4. Selective expression of VIP and VGLut3. Consistently PV- (Bezaire & Soltesz, 2013; Vida *et al*., 2018)

Morphology: CCK BCs are not only heterogeneous in terms of their molecular profiles as shown in the "markers" section above and in the "quantifications" section below, but also show variation in their distribution and morphologies. The cell bodies of CCK BCs are found throughout all strata. In the rat, higher concentrations of soma appear in SR (Bezaire & Soltesz, 2013), however our calculations for the mouse point towards a higher concentration of somas in SP. This is especially comparable since the classifying criteria used for CCK+ interneurons are the same as those used by Bezaire and Soltesz (2013). This heterogeneity is also reflected in the dendrites. While most are radially oriented bitufted or multipolar, spanning all layers, a small percentage of cells limit their dendrites to SO or SR. The defining feature of this cell type is the axon morphology within SP. Similar to PV BCs, the axon surrounds the soma and proximal dendrites of PCs. The axon can also sometimes invade the borders of SO and SR. Their defining molecular characteristic is the neuropeptide CCK-8, found throughout the soma, dendrites and axon (Pelkey *et al*., 2017).

Sources and targets: CCK BCs innervate the soma and proximal dendrites of PCs within the CA1. Unlike PV BCs, however they do not differentiate between superficial and deep PCs. There is a uniform average connection probability of 42% with PCs throughout their axonal arbors and each CCK BC connects to a PC via about 7-8 boutons. Interestingly however, PCs do not appear to innervate CCK BCs at all (Lee *et al*, 2014). Their terminals are heavily impregnated with CB1 type receptors which are responsible for depressing their GABAergic output in response to endogenous and exogenous cannabinoids. In contrast with PV BCs, they also selectively possess $GABA_B$ receptors (I. Katona *et al*., 1999).

Electrophysiology: CCK BCs are known to be non-fast spiking in comparison to the fast spiking PV BCs. The electrophysiological profile can be observed in **Fig. 5. 6**.

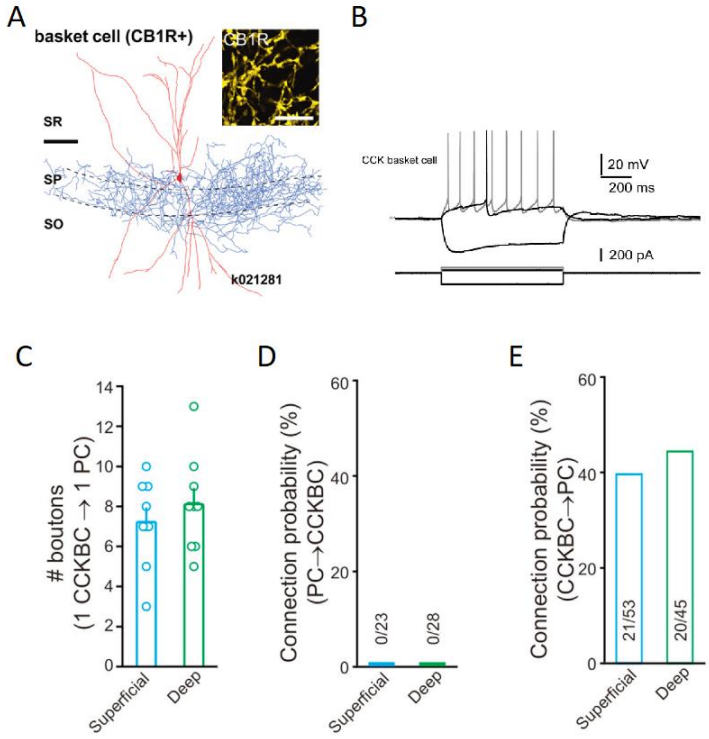

Fig. 5. 6 Cholecystokinin basket cell profiles.
A: Morphological profile of a rat CCK BC (scale bar, 100µm). Inset shows CB1R immunofluorescence (scale bar, 10µm). SR, stratum radiatum, SP, stratum pyramidale, SO, stratum oriens. As adapted from (Nissen *et al*., 2010). B: Electrophysiological profile of non-fast spiking basket cell. As adapted from Tricoire *et al*., 2011. C: Number of putative synaptic terminals of one CCK BC onto either superficial or deep PCs. D: Excitatory connection probability from superficial and deep PCs to CCKBCs. E: Inhibitory connection probability from CCKBCs to superficial and deep PCs. As adapted from Lee *et al*., (2014).

5.2.1.3. Axo-axonic Cells

Other names: Chandelier Cells, Horizontal Axo-axonic cells (subset having soma in SO)

Markers: Highly immunopositive to PV, Immunopositive to M2R, µOR and in contrast to PV BCs, they express low a level of $GABA_A$-α1 and no SATB1 (Yamada and Jinno, 2017, Vida *et al*., 2018).

Origin: MGE (Tricoire *et al*., 2011)

Morphology: The somata of axo-axonic cells (AAC) are mostly found in SP, less often in SO and rarely in other layers. Most AACs have radially oriented, mostly aspiny dendrites spanning all layers with an extensive dendritic tuft in SLM (Freund & Buzsáki, 1996; Klausberger *et al*., 2003), however, some display horizontal dendrites restricted to SO

(Ganter *et al*., 2004). The axon, which originates either from the soma or a primary dendrite, forms a dense arbor within SP and superficial SO. The structure of the axon is responsible for their characteristic "chandelier" appearance as the main branches orient horizontally along the SP-SO border and in turn subdivide into perpendicular or oblique collaterals towards SP. Each row of terminals innervates a single PC postsynaptic axon initial segment (Pelkey *et al*., 2017).

Sources and Targets: Their radially oriented dendritic tree predicts an input from all major afferent pathways namely, thalamic, entorhinal, CA1 and CA3 pyramidal glutamatergic inputs. For AACs with horizontal dendrites however, it is possible that their input is

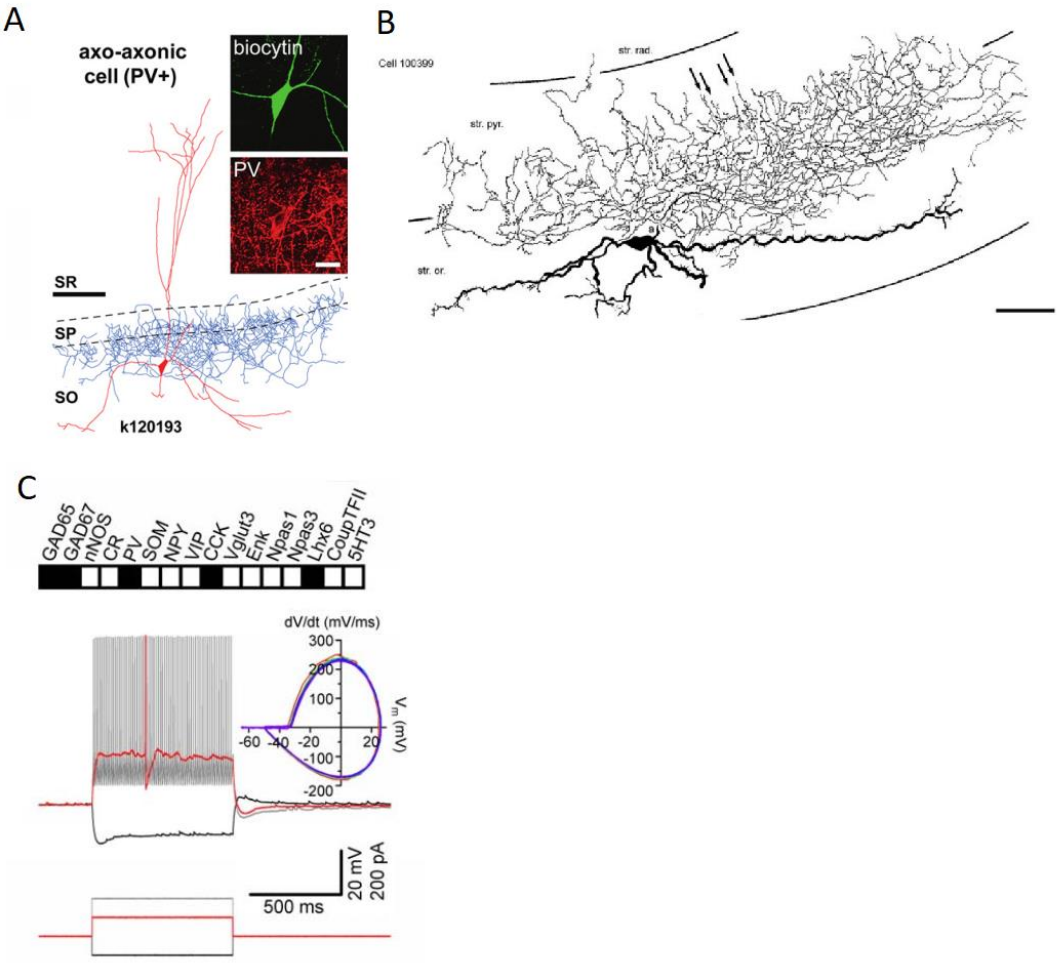

Fig. 5. 7 Axo-axonic cell profiles.
A: morphology profile of radially oriented AAC in rat. Dendrites and soma (red) axon (blue) (scale bar, 100µm) Insets show the expression of biocytin in the soma and PV in the dendrites. Scale bar, 20µm. SO, *stratum oriens*, SP, *stratum pyramidale*, SR, *stratum radiatum.* As adapted from Nissen *et al*., (2010). B: Morphology profile of horizontal AAC in rat with characteristic radial axon terminals (arrows) (scale bar, 50µm). str. or., *stratum oriens*, str. pyr., *stratum pyramidale*, str. rad., *stratum radiatum*. Dendrites and soma (bold). As adapted from Ganter *et al*, 2004. C: PCR molecular profile, bottom: electrophysiological profile of AAC showing response to square current from -60mV. Pulses = near threshold and 2x threshold stimulation. Inset: Phase plot of 2x threshold stimulation. As adapted from Tricoire *et al*., (2011).

restricted to local sources (Vida *et al*., 2018, Ganter *et al*., 2004). Recurrent excitatory inputs from PCs has also been observed (Ganter *et al*., 2004; Li *et al*., 1992). Additionally, this cell type possibly participates in the PV interneuron network coupled by gap junctions in a way that it receives but does not contribute inhibitory synapses to the network (Fukuda & Kosaka, 2000). AACs almost exclusively target local PC axon initial segments through their characteristic radially oriented axon terminals as mentioned above.

Electrophysiology: As characteristic to PV+ interneurons, AACs are fast-spiking cells (Tricoire *et al*.,2011). See **Fig. 5. 7**.

5.2.2. Dendritic inhibitory neurons

5.2.2.1. Bistratified cells

Origin: MGE (Tricoire *et al*., 2011)

Markers: Highly immunopositive for PV, SATB1 and NPY. Also positive for M2R, μOR+ and GABAA-α1 (Baude *et al*., 2007; Klausberger *et al*., 2004).

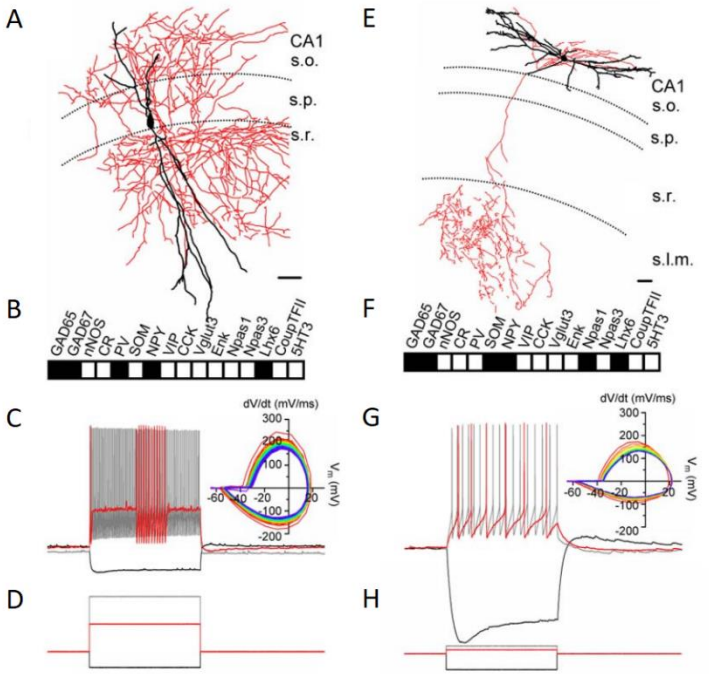

Fig. 5. 8 Bistratified cell and O-LM cell profiles.
A, E: Morphological profile of BSC (left) and O-LM (right) from mice. Dendrites and soma (black) axon (red). Scale bar: 100μm. Dashed lines indicate borders between strata. so, *stratum oriens*, sp, *stratum pyramidale*, sr, *stratum radiatum*, s.l.m, *stratum lacunosum moleculare.* B, F: single-cell PCR molecular profiles of cells above. Filled boxes indicate transcripts detected. C, D, G, H: electrophysiological profile of above cells showing response to square current (D, H) from -60mV. Pulses = near threshold and 2x threshold stimulation. Inset: Phase plot of 2x threshold stimulation. A-D: BSC profiles, E-H: O-LM profiles. As adapted from Tricoire *et al*., (2011).

Morphology: Bistratified cells (BSC), not to be confused with Oriens-Bistratified cells (O-Bi) which are hippocamposeptal (HS) cells, are PV+ cells with the somata usually situated in SP. Their smooth and multipolar dendritic arbours are radially oriented along the SO to SR axis (Klausberger *et al*., 2004; Tricoire *et al*., 2011). Their axons are their distinguishing feature as their collaterals split above and below SP thus innervating both the basoslateral and apical dendrites of PCs in equal proportions while avoiding the somatic and perisomatic region (Pelkey *et al*., 2017).

Sources and Targets: The dendritic distributions and electrophysiological data indicate a primary activation via Schaffer Collaterals (SC) and a possibly recurrent excitatory input from local PC axons in SO. Perforant path (PP) inputs are generally missing (Vida *et al*., 2018). Their targets on the other hand are mostly local PC shafts and, to a lesser extent, spines of small-calibre dendrites. Very rarely do they target main apical dendrites or somata. A very small percentage of synapses are aimed towards interneurons and they likely participate in the mutual inhibitory network of PV+ interneurons connected by gap junctions (Klausberger *et al*., 2004)

Electrophysiology: BSC are generally fast-spiking neurons (Tricoire *et al*., 2011)

5.2.2.2. Oriens-Lacunosum Moleculare cells

Other names: The equivalent of Oriens-Lacunosum Moleculare (O-LM) cells in the dentate gyrus are called hilar performant path associated cells (HIPP) while in the neocortex they are called Martinotti cells.

Origin: Probably both MGE and CGE (Chittajallu *et al*., 2013)

Markers: Highly immunopositive for SST and the metabotropic glutamate receptor mGluR1α. Selectively also PV+ and NPY+. Additionally, specifically in the CA1, O-LM cells are positive for nicotinic receptor α4. (Vida *et al*., 2018)

Morphology: The soma of O-LM cells is always found in SO, often bordering the alveus. The dendritic tree is horizontally oriented within SO and alveus and is densely crowded with long and thin spines. The axon is their defining feature; projecting from a main dendrite in SO, right through SO and SR, where they often bifurcate, then branching out into a dense arbor within SLM (**Fig. 5. 8E-H**). An additional, less extensive, arbor within SO has also been observed in some cells (Tricoire *et al*., 2011, Vida *et al*., 2018). While the axon is

concentrated in SLM, it does not cross the hippocampal fissure into the DG as seen in several other cell types (Katona *et al*., 2017).

Although the general morphology and the presence of SST appears to be constant within this cell type, there seems to be a parsing according to 5-HT3A expression. Chittajallu and colleagues (2013) claim that the presence of these receptors in a subpopulation of O-LM cells is indicative of a CGE origin, while its absence, together with the selective presence of PV, indicates an MGE origin. The two subtypes were also found to differ in their participation in network gamma oscillations. Consequently, serotonergic tone may preferentially recruit CGE derived O-LM cells over MGE derived ones. Interestingly however, Overstreet-Wadiche and McBain, (2015) documented the presence of ionotropic 5-HT3A in NGF cells originating from both MGE and CGE. Also, since the Chittajallu and colleagues claim both groups are SST+, their results are not in agreement with those by Tricoire *et al*. (2011) which show a completely MGE derived SST+ interneuron subpopulation. While the actual origin of O-LM cells calls for further digging, in this study we still proceeded to quantifying the two subtyped independently as, even though the origin might ultimately be homogeneous, there are still minor differences between the two subtypes.

Sources and targets: In the rat, O-LM cells have four times more afferent excitatory synapses than inhibitory ones and the majority of excitatory synapses appear to originate from local PCs rather than from the Schaffer collateral pathway which terminates within reach of their dendrites (Blasco-Ibáñez & Freund, 1995). They receive inhibitory synapses from CR-containing interneurons (Tyan *et al*., 2014) but they themselves also mediate the inhibition of NGF cells and possibly also other interneurons. Primarily, however, they target the dendritic shafts of PCs and less frequently their spines (Elfant *et al*., 2008).

Electrophysiology: Basic spiking patterns do not distinguish between CGE and MGE derived subsets of O-LM cells. Compared to MGE-derived interneurons, they are more slowly accommodating and show a more pronounced membrane sag upon hyper polarisation. They are regarded as regular spiking neurons (**Fig. 5. 8 E-H**).

5.2.2.3. Schaffer Collateral-associated and Apical Dendritic-Innervating interneurons

Origin: CGE (Tricoire *et al*., 2011)

Markers: Highly immunopositive for CCK. Selectively positive for CB (Bezaire & Soltesz, 2013).

Morphology: The somata of Schaffer Collateral-associated (SCA) cells are found predominantly in SR and their dendrites run radially across all layers. Their multipolar axons ramify almost exclusively in SR and SO, overlapping with Schaffer Collateral and Commissural pathway PCs originating from CA3 (Cope *et al*., 2002). Apical dendritic-innervating (ADI) cells have a very similar morphology (Klausberger & Somogyi, 2008)

Sources and Targets: The axons of SCAs target predominantly the oblique and basal dendrites of the PCs that they co-align with while ADIs preferentially innervate the main apical shaft (Klausberger *et al*., 2005). Their dendrites on the other hand, span all layers and could therefore possibly receive inputs from all afferent pathways. Since SCAs and ADIs selectively express CB, they are likely targeted by IS cells though multiple contacts in a climbing up pattern along both their soma and dendrites (Pelkey *et al*., 2017). They are possibly also inhibited by O-LM cells (Elfant *et al*., 2008).

Electrophysiology: These cells exhibit considerable spike frequency adaptation that limits their maximal firing frequency. They generally produce a regular spiking pattern (typically <50Hz) (Tricoire *et al*., 2011, Pelkey *et al*., 2017).

5.2.2.4. Perforant Path-Associated Interneurons

Other names: They have been called Radiatum- Lacunosum Moleculare (R-LM) as they are generally found near SR while their axons innervate SLM (Hájos & Mody, 1997).

Markers: Highly immunopositive for CCK and ErbB4. Selectively positive for CB. (Vida *et al*., 2018)

Origin: CGE (Tricoire *et al*., 2011)

Morphology: The cell bodies of Perforant Path-associated (PPA) cells are most commonly found in SR and SLM, often at the border of the two layers. The radially oriented dendrites normally also restrict themselves to SR and SLM but occasionally extend into SO and alveus.

The axon is usually concentrated in SLM but often also extends collaterals across the hippocampal fissure into the DG (Klausberger *et al*., 2005; Vida *et al*., 2018)

Sources and Targets: The dendritic distribution in SR indicates probable inputs from the PP and SC pathways. Additionally, their distal dendrites in SO and alveus likely also receive their share of feedback excitation. PPA cells receive inhibition from other interneurons such as OLM cells and even IS-I cells in a similar manner as the afore-mentioned SCA cells (Klausberger *et al*., 2005; Pelkey *et al*., 2017).

Due to their axon configuration and its penetration into the DG, their synaptic targets are primarily the distal apical tufts of local PC dendrites where they overlap their inputs with excitatory ones incoming from EC and the nucleus reuniens (NR). Their secondary targets are the dendrites of DG granule cells and they are also known to target other interneurons (Klausberger *et al*., 2005, Vida *et al*., 1998)

Electrophysiology: PPA cells are regular spiking neurons similar to SCA and ADI interneurons. It is also noteworthy to point out that even though CCK+ interneurons are a heterogeneous group in CA1, they appear to have a relatively homogeneous and phase locked firing behaviour during theta rhythms (Klausberger *et al*., 2005)

5.2.2.5. Neurogliaform cells

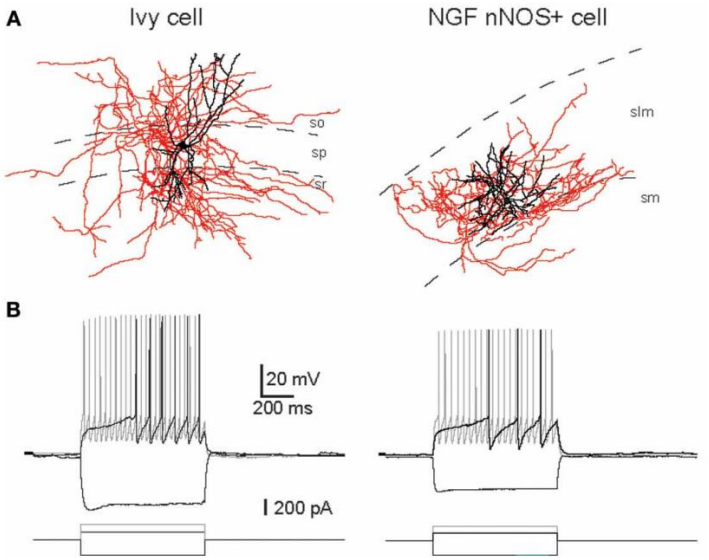

Fig. 5. 9 MGE derived Ivy and NGF cell profiles of the mouse CA1.
A: Morphological profiles of Ivy cell (left) and NGF cell (right); axon (red), dendrites and soma (black). B: Electrophysiological profile of Ivy cell (left) and NGF cell (right) showing voltage responses to 200pA, just suprathreshold and 2x suprathreshold current injections. As adapted from Tricoire and Vitalis (2012)

Origin: Both CGE and MGE (Tricoire *et al*, 2010)

Markers: The MGE derived subpopulation is very immunopositive for NPY and nNOS. It is also positive for reelin and Lhx6. The CGE derived subpopulation is very immunopositive for NPY and positive for reelin and COUP-TFII (Tricoire *et al*., 2010; Tricoire & Vitalis, 2012; Vida *et al*., 2018).

Morphology: Neurogliaform (NGF) cells together with the closely related interneuron cell type of Ivy cells (below), have been described as the most abundant family of GABAergic cell types in the CA1 area (Fuentealba *et al*., 2008a). NGF cells are characterized by a small stellate and profusely branched dendritic arbor, a very dense local axon and a relatively small, round soma. The soma is found in SR or SLM, normally close to their border and the axon densely occupies the SR and SLM layers. Small *en passant* boutons densely populate the axon and, while able to form synaptic contacts, usually these comprise of an unusually wide synaptic cleft with some even lacking an easily identifiable postsynaptic target (Armstrong *et al*., 2012; Tricoire & Vitalis, 2012; Vida *et al*., 2018). While they differ in origin and molecular markers, CGE and MGE (**Fig. 5. 9** and **5. 10**) derived NGF cells have similar morphologies and electrophysiological properties (Tricoire *et al*., 2010).

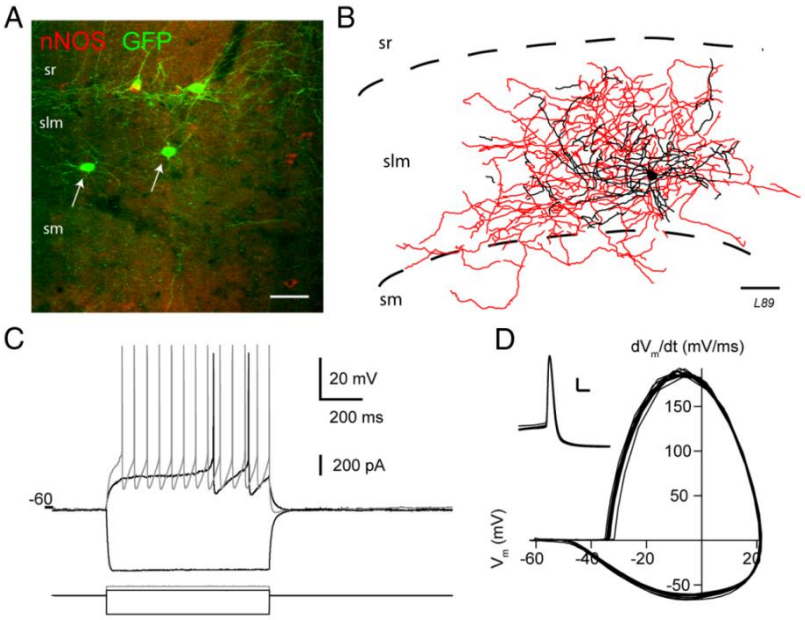

Fig. 5. 10 Profile of CGE derived NGF cells.
A: Fluorescence image showing two CGE derived cells with neurogliaform morphology and being nNOS negative. B: Neurolucida reconstruction of mouse CGE NGF cell at E12.5. dendrites and soma (black), axon (red). Scale bar: 50µm. C: Electrophysiological profile of cell in B following three current step injections (200 pA, just suprathreshold, and 2x just suprathreshold) D: phase plot of 2x just suprathreshold response shown in C. Inset illustrates overlaid action potentials; scale bar: 10 mV, 2ms. As adapted from Tricoire *et al*., (2010).

Sources and Targets: MGE and CGE NGF cells provide local feed forward inhibition mainly on the shafts but also the spines of CA1 PCs' distal dendrites (Vida *et al*., 1998) thus modulating both temporoammonic and thalamic input. Both cell types are also rich in ionotropic 5-HT3A and can be activated by the co-released serotonin and glutamate from the raphe nucleus' subcortical fibres. They in turn direct the activity onto the distal dendrites of local PCs in SLM by inhibition volume transmission. This syphoning of temporoammonic excitation inputs allows the domination of CA1 PCs by CA3 SC inputs (Overstreet-Wadiche & McBain, 2015). NGF cells are able to induce a biphasic current in the post-synaptic cell that involves both a $GABA_A$-mediated (slow) and a $GABA_B$-mediated component. The postsynaptic $GABA_B$ response is generated even by a single neurogliaform action potential. Their unique axonal arrangement allows them to mediate GABAergic volume transmission practically anywhere within their axonal plexus (Armstrong *et al*.,2012, Vida *et al*., 2018). Furthermore, Price and colleagues, (2005) indicated that NGF cells are excited both by SC and also by the PP and are inhibited by O-LM while also participating in mutual inhibition. NGF cells are broadly coupled by gap junctions within themselves and with other interneurons (Vida *et al*., 2018).

Electrophysiology: NGF cells show a persistent regular spiking pattern which continues for several seconds after the stimulus has stopped (Armstrong *et al*., 2012).

5.2.2.6. Ivy cells.

Origin: So far only MGE derived Ivy cells have been confirmed however a possibly CGE derived subpopulation of Ivy cells which is genetically similar but lacks MGE-related markers such as nNOS and reelin has been suggested (Harris *et al*., 2018).

Markers: Highly immunopositive for NPY and nNOS (Tricoire *et al*., 2011)

Morphology: Ivy cells are part of the Neurogliaform family of cells and are estimated to be the largest cohort of hippocampal interneurons. The somata of Ivy cells are most commonly found in SP but have also been observed in SO and SR (Fuentealba *et al*., 2008). Their ivy-like axon is what gives them their name. They extensively branch close to their origin and terminate in fine collaterals densely covered in small *en passant* boutons. Their smooth dendrites are multipolar but less compact than those of NGF cells. They branch into SO and SR (**Fig. 5.9**) and generally span further out then the axon (Fuentealba *et al*., 2008). It has

been suggested that Ivy and NGF cells form more of a gradient of cells rather than two distinct cell types. This has been proposed both on the basis of morphology (Traub *et al*., 1996) and genetics (Harris *et al*., 2018).

Sources and Targets: In contrast to NGF cells, Ivy cells target more proximal oblique basal CA1 PC dendrites. The configuration of their dendrites in SO and SP positions them for feedforward recruitment by CA3 SC inputs and for feedback recruitment by CA1 PC collaterals (Pelkey *et al*., 2017).

Electrophysiology: Ivy terminals are dramatically inhibited by μOR activation. They display persistent regular firing which is however inhibited by μOR activation (Krook-Magnuson *et al*., 2011). **Fig. 5.9** displays the morphological profile of an Ivy cell.

5.2.3. Interneuron-Specific Interneurons

5.2.3.1. Interneuron-specific type 1

Other names: interneuron selective type 1

Origin: CGE (Tricoire *et al*., 2011)

Markers: Highly immunopositive for CR (Besaire and Soltesz, 2013)

Morphology: Interneuron specific type 1 (IS-I) is the first of three currently recognised subgroups of interneurons that preferentially target other interneurons, as opposed to glutamatergic principal cells. The somata of these cells have been observed in all layers of the CA1, however they have most often been spotted in SO, SP and SR (Vida *et al*., 2018). The spiny dendrites of IS-I cells form extensive arbors typically within SR but can also penetrate all other strata. This cell type reveals a unique phenomenon of entangled "braids" with each constituent dendrite sourced from 2-7 separate IS-I cells. Frequently, additional varicose axons sourced from similar interneurons are also included. These dendritic junctions are usually more than 100μm long and likely function as synchronisation nodes to coordinate the electrical and synaptic activities of about 15-cell IS-I clusters (Gulyás *et al*., 1996).

The axons characteristically ramify within SR and SP and less often within SO. The distribution of terminals along the axons is highly uneven and appears to be dependent on the proximity of the axon collateral to appropriate GABAergic postsynaptic elements. The

closer the collaterals are to suitable contacts, the higher the bouton density (Pelkey *et al*., 2017).

Sources and Targets: IS-Is preferentially target CB+ dendrite targeting interneurons such as PPC and SCA cells as well as VIP+ CCK BCs. They are also mutually connected with other IS-Is within their special dendritic junctions. They, however, appear to avoid PV+ interneurons and principal cells. Individual axons of IS-Is connect to the dendrites and soma of their post-synaptic targets via multiple contacts within a close range of each other. The wide-spread radial dendrites allow for several excitatory inputs sourcing from SC, EC, NR or even local PCs which are ultimately expected to result in disinhibition of CA1 PC dendrites particularly the apical ones that fall within the SC termination zone (Pelkey *et al*., 2017).

Electrophysiology:

IS cells have been found to exhibit various spiking phenotypes including irregular spiking, bursting and stuttering. During irregular spiking, spikes with highly variable inter-spike intervals are generated throughout a sustained suprathreshold current injection. During bursting, 3-5 spikes are rapidly discharged at the initiation of the depolarizing pulse followed by single spikes of variable inter-spike intervals. Stuttering is the name given to a spiking phenotype characterised by clusters of generated spikes separated by unpredictable inter-spike intervals (Pelkey *et al*., 2017).

5.2.3.2. Interneuron-specific type 2

Other names: interneuron-selective type 2

Origin: CGE (Tricoire *et al*., 2011)

Markers: Highly immunopositive for VIP (Bezaire and Soltesz, 2013)

Morphology: The cell bodies of this IS subset are also found within all layers but with higher frequencies at the SR-SLM border (Acsády *et al*., 1996a; Acsády *et al*., 1996b). The dendrites, which are mostly restricted to a tuft within SLM, are mostly smooth but occasionally sparsely spiny. The axons ramify radially within SR, ending in uneven terminal distributions along thin collaterals similar to IS-Is.

A subpopulation, usually classified within IS-II, however, has bipolar dendrites running radially through all layers which is more commonly an IS-I characteristic and frequently expresses both CR and VIP which is typical of IS-III cells (Pelkey *et al*., 2017). This indicates a possible gradual change rather a clean separation between the IS family of interneurons.

Sources and Targets: Similarly to IS-Is, IS-IIs preferentially target CB+ dendrite inhibiting interneurons via multi-synapse connections as the axons contact post synaptic cells in a climbing-fibre manner. They also inhibit VIP+ interneurons which includes VIP+ CCK BCs and VIP+ IS cells that they can approach within SR. Also similar to IS-Is, they avoid PV+ interneurons and PCs. The position of their dendrites suggests a major input from EC and NR. Excitation of IS-IIs by these networks will likely ultimately result in the disinhibition of CA1 PC apical dendrites within the CA3 SC termination zone (Pelkey *et al*., 2017).

Electrophysiology: As mentioned in IS-I, IS cells generally exhibit either irregular, bursting or stuttering spiking phenotypes.

5.2.3.3. Interneuron Specific interneurons Type 3

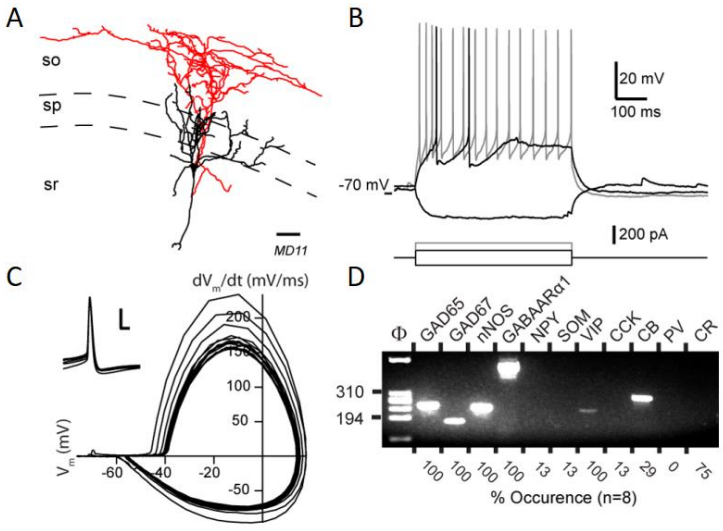

Fig. 5. 11 Profile of CGE-derived nNOS+ IS interneuron.
A: Morphological profile from mouse. Soma and dendrites (black) axon (red) Scale bar: 25µm. B: electrophysiological profile following 3 different current step injections (-80pA, just suprathreshold and twice suprathreshold stimulation). C: 2x suprathreshold current injection response represented in a phase plot. Inset denotes overlaid action potential; scale bar 10mV, 2ms. D: Single-cell RT-PCR analysis. As adapted from Tricoire *et al*., (2010)

Other names: interneuron selective type 3

Origin: CGE and possibly the lateral ganglionic eminence (LGE) (Tricoire and Vitalis, 2012)

Markers: Highly immunopositive for both CR and VIP though 25% of nNOS+ bipolar cells were found to be CR-. Also positive for nNOS (Harris *et al*., 2018).

Morphology: The somata of interneuron specific type 3 (IS-III) cells have a fusiform shape and are more concentrated within SP and SR than within the other layers (Acsády *et al*., 1996a, Acsády *et al*., 1996b). The majority of cells display bipolar dendrites spanning all strata and a horizontally oriented tuft within SLM. These bipolar cells are known to be nNOS+ (Tricoire and Vitalis, 2012). On the contrary to other nNOS+ interneurons such as Ivy and NGF cells, these bipolar cells appear to be derived from the CGE (Tricoire *et al*., 2011). In other IS-IIIs, all of their primary dendrites descend towards SLM (Tyan *et al*., 2014). The axon is mostly concentrated within SO where it ramifies horizontally while also extending into the alveus where it co-aligns with horizontal dendrites of other interneurons in SO (Gulyás *et al*., 1996; Tricoire & Vitalis, 2012).

Sources and Targets: As already established, IS interneurons target predominantly if not exclusively other GABAergic neurons. In the case if IS-IIIs, their axonal morphology allows for them to target SO residing dendrites, mainly the SST+ OLM interneurons via multiple synaptic contacts as is typical of IS cells. Less frequently, however, they also target BSCs and PV BCs (Chamberland *et al*., 2010; Tyan *et al*., 2014).

The concentration of dendrites within SLM suggests a major input from the thalamus and EC, however, those neurons whose dendrites span all layers are most likely to be recruited by all afferent excitatory networks including CA1 PCs. They are in turn inhibited by at least IS-II interneurons. Their morphology overall suggests that their role in the network is to disinhibit the OLM mediated feedback inhibition of the CA1 PCs' apical dendrites within the termination zone of EC and NR afferent input (Pelkey *et al*., 2017).

Electrophysiology: When depolarized with current injection, IS-III bipolar cells exhibit an irregular firing pattern (**Fig. 5. 11**) (Tricoire and Vitalis, 2012).

5.2.4. Projection interneurons

5.2.4.1. Hippocamposeptal cells

Origin: At least the M2R+ subset is probably CGE derived (Tricoire *et al*., 2011).

Markers: Highly immunopositive for SST. Also positive for PV, NPY, M2R, mGluR1α, CB, ENK and a very small percentage also being CR+ (Jinno *et al*., 2007; Jinno, 2009).

Morphology: Hippocamposeptal (HS) interneurons are a heterogeneous group of cells which project into the medial septum. Identification of these cells is mostly done through retrograde labelling from the septum. In the CA1, the somata of these cells are majorly concentrated within SO (Jinno *et al*., 2007) and usually exhibit a basket cell morphology (Jinno, 2009). The axons can be divided into a local axon which targets local CA1 PCs and long-range axonal branches which target either the medial septum alone or more commonly, both the septum and retrohippocampal areas. One well described subset of HS cells is the SST+/CB+/mGluR1α+ double projection cells (DPC).

DPCs make up a distinct cell type which is known to innervate both the medial septum and retrohippocampal areas. The soma and dendrites are both found within SO. The axon branches out into a rostral and caudal part aiming towards the septum and the subiculum respectively. These axons travel through SO to their destinations while the local axon ramifies into SO and SR. The rostral axon enters the triangular septum through the lateral septum while the caudal branch enters the presubiculum through the corpus callosum (Jinno *et al*., 2007). Roughly a quarter and a third of DPCs in the rat are NPY+ and PV+ respectively (Jinno *et al*., 2007). Since a third of our calculated numerical density of DPC is almost the same as the PV+ HS numerical density measured by Yamada and Jinno (2017), it is possible that the only HS cells that are PV+, are DPCs.

Sources and Targets: Within CA1, HS cells target small diameter dendrites of PC and also other interneurons. However, the ratio of the two is still unclear due to conflicting results. (Gulyás *et al*., 2003; Jinno *et al*., 2007; Jinno, 2009). Further research is necessary. The main postsynaptic targets in the medial septum are PV+ interneurons and to a lesser extent cholinergic neurons. Since the dendrites are in SO, they are most likely targeted by the Schaffer Collaterals coming from CA3.

Electrophysiology: These interneurons fire at (like DBC) or shortly after the through of theta oscillations and show an increase in firing rate during sharp wave-associated ripple oscillations (Jinno *et al*., 2007).

5.2.4.2. Hippocamposubicular interneurons

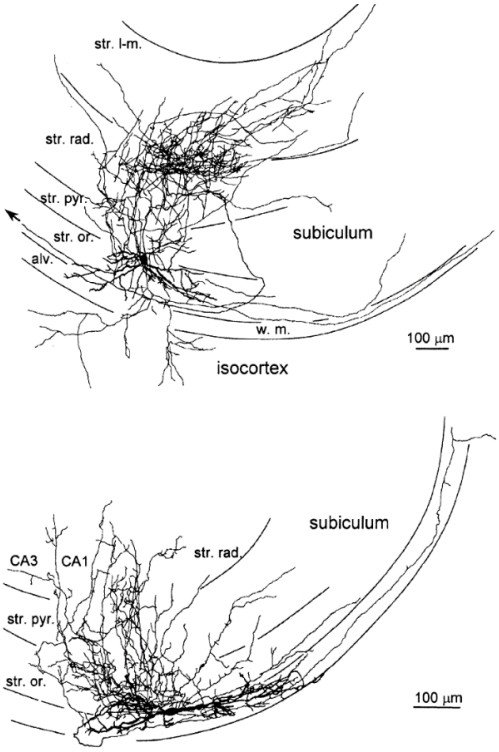

Fig. 5. 12 Two of the morphologies of O-Bi cells.
Top one showing dendrites (bold lines) restricted to SO and an extensive axon (narrow lines) in all CA1 layers. Also, there are projections to the isocortex, subiculum and a main axon leading to the fimbria and CA3 area (arrow). Bottom: the soma is at the border of SO and alveus with dendritic ramifications in both layers. The axon ramifies in SP, SP and SR and collaterals reach both towards CA3 and the subiculum. str. or., stratum oriens, str. pry., *stratum pyramidale*, str. rad., *stratum radiatum*, str. l-m., *stratum lacunosum moleculare*, alv., alveus, w.m., white matter. As adapted from Losonczy *et al*., (2002).

Origin: At least the M2R+ subset is probably CGE derived (Tricoire *et al*., 2011).

Markers: Positive for M2R and mGluR1α (Jinno *et al*., 2007).

Morphology: This is a heterogeneous population of cells that predominantly projects towards the subiculum. While most HS interneurons also project to the subiculum, in this section we are including those interneurons that do not normally project to the medial septum. Contrarily to HS cell somata's confinement to SO, H-Sub somata occupy all strata. Generally, there were large horizontal cells in SO and small to medium-sized bipolar and

multipolar cells in SR and SLM (Jinno, 2009). There are a few identified types of H-Sub interneurons though both their immunocytochemistries and morphologies tend to overlap thus making their quantification a difficult one.

Oriens-retrohippocampal projection neurons (O-RH), which are probably the same as Oriens-Bistratified (O-Bi) cells (Jinno *et al*., 2007; Losonczy *et al*., 2002) are a heterogeneous cell population (probably made up of a few different cell types) have horizontally elongated somas found in SO while the horizontal dendrites are similarly restricted to SO and alveus. The local axon mainly innervates SO and SR, secondarily SP and very rarely SLM. The long-range axon collaterals on the other hand ramify though SLM into SP of the subiculum and onto the presubiculum (Jinno *et al*., 2007). 47% of cells have axonal varicose branches extending into the isocortex. Additionally, 73%, 47% and 40% of O-RH cells innervate the CA3, subiculum or both respectively (Losonczy *et al*., 2002). O-RH cells appear to be immunochemically very heterogeneous (Losonczy *et al*., 2002), thus quantification based on this criterion was not attempted. According to Jinno and colleagues (2007), these cells fire around the trough of theta oscillations.

Radiatum-retrohippocampal projection neurons (R-RH) cells are another subgroup of H-Sub interneurons. They innervate the subiculum, presubiculum, retrosplenial cortex and *indusium griseum*. The somata are concentrated at the border of SR and SLM with multipolar dendrites shortly extending radially into SR and SLM. The local axon consists of only a few relatively short collaterals while the long-range axon ramifies caudally towards the molecular layer of the subiculum and presubiculum where it further ramifies into more caudal and rostral branches. *In vivo* firing patterns demonstrate firing at the descending phase of extracellular theta oscillations (Jinno *et al*., 2007) and the cells possibly show a regular spiking pattern (Tricoire *et al*., 2011).

Trilaminar cells are strongly M2R+, have their soma in SO and their axon in SO, SP and SR. Their local axon innervates CA1 PC dendrites and to a lesser extent their soma. Their long-range axon projects towards the subiculum (Klausberger, 2009). They are fast spiking neurons (Gloveli *et al*., 2018).

Sources and Targets: Since the dendrites of this heterogeneous group are found in different strata, their inputs depend on the afferent networks that reach them. Locally, most cells target mainly the dendritic shafts of PCs while a subgroup of ENK+ neurons seems to target both interneurons and PCs in all layers except the alveus. In both the alveus and the

subiculum, these ENK+ cells targeted exclusively interneurons (Jinno, 2009). The common characteristic that brings H-Sub interneurons together is their long projecting axons to the subicular area. Further research needs to be directed to investigating the synaptic targets of H-Sub cells.

5.2.4.3. Backprojection cells

Other names: SST+/nNOS+ cells (Jinno & Kosaka, 2004)

Markers: Highly immunopositive for SST, nNOS and NPY. Positive for PENK, CHRM2, GRM1 and PCP4 (Harris *et al*., 2018; Sik *et al*., 1994).

Origin: Likely MGE as most of nNOS is MGE derived (Tricoire *et al*., 2011)

Morphology: Backprojection cells (BPC) are an easily identified cell type due to their unique combination of SST and nNOS immunopositivity. The somata of BPC are confined within SO and so are their horizontal bipolar dendrites which are covered in long, thin spines. In the rat, 59% of the axon length remains in CA1 where they synapse with local PC dendrites and occasionally somata, while 41% projects back to the CA3 and hilus, hence the term "backprojection" (Sik *et al*.,1994). It has been suggested that these cells are the same as ENK+ interneurons introduced by Fuentealba and colleagues (2008b) (Harris *et al*., 2018), making them part of H-Sub. However, none of H-Sub were found to be nNOS+ so this is therefore unlikely (Jinno *et al*., 2007).

Sources and targets: Due to their positioning of their dendrites within SO, it is likely that they receive input from the SC pathway and also from local PCs. Their targets are local and CA3 pyramidal cells, however the exact proportion is not yet known nor is the extent of inhibition towards and from other interneurons.

Electrophysiology: BPC are very strongly modulated to gamma oscillations which implies their function as gamma-frequency coordinators across hippocampal subregions (Craig & McBain, 2015; Gloveli *et al*., 2018).

5.2.5. Interneuron quantifications.

5.2.5.1. Parvalbumin positive interneurons

Numerical densities (ND) for PV BCs, AACs, BSCs and PV+ O-LM and HS interneurons in their main strata were directly extracted from plots (Yamada & Jinno, 2017 Fig. 2B) using WebPlotDigitizer (See **Table S1**). The authors considered the PV+/SATB1+/NPY- cells in SP as PV+ basket cells, PV+/SATB1-/NPY- cells in SP as Axo-Axonic cells (AAC), PV+/SATB+/NPY+ cells in SP as Bistratified cells (BSC), PV+/SST+/FG- in SO as PV+ Oriens-Lacunosum Moleculare (O-LM) cells and PV+/SST+/FG+ cells in SO as PV+ Hippocampo-Septal (HS) cells.

The total PV NDs were taken from Jinno and Kosaka (2006). The NDs of the PV+ O-LM and PV+ HS cells from Yamada and Jinno were deducted from the total PV NDs of SO. The remaining unclaimed numbers were allocated to the known cell types following the method used by Bezaire and Soltesz (2013). The densities in SO, SR and SLM were divided between AACs, BSCs and PV BCs in the same ratio these same cell types were found in SP (**Table 6**). The full amount of O-LM and HS cells is calculated in the SST+ interneuron sections as they are largely SST immunopositive.

The values may in reality be a little lower as Jinno *et al.* (2007) mentioned a very small amount (about 3% in SO and SR for rat) of H-Sub interneurons being PV+. This amount, being so small and also from a different species, was not considered in the calculation of the mouse PV+ cell classes. Additionally, the authors could not determine the percentage of PV+ H-Sub interneurons in SP due to a difficulty in differentiating them from retrogradely labelled pyramidal cells in the same layer. It is therefore possible that the remaining unclaimed PV+ interneurons in SP belong to this group of cells. Note that the NDs of PV BCs, AACs and BSCs are the final NDs of the cell types. The PV+ O-LM and HS cells are subtypes of O-LM and HS cell types respectively.

Table 6

Calculated numerical densities of PV+ interneuron classes and subclasses

		Hippocampal CA1 strata							
		dSO	vSO	dSP	vSP	dSR	vSR	dSLM	vSLM
Jinno & Kosaka (2006)	PV ND (cells*1000/mm^3)	1.340	2.680	5.730	3.830	0.230	0.040	0.060	0
PV+ interneurons ND (cells*1000/mm^3)	PV BC	**0.249**	**1.132**	**3.380**	**2.900**	**0.152**	**0.031**	**0.040**	**0**
	AAC	**0.055**	**0.212**	**0.749**	**0.545**	**0.034**	**0.006**	**0.009**	**0**
	BSC	**0.073**	**0.104**	**0.989**	**0.266**	**0.044**	**0.003**	**0.012**	**0**
	PV+ O-LM	0.522	0.712	0	0	0	0	0	0
	PV+ HS	0.441	0.520	0	0	0	0	0	0
	Other PV+	0	0	0.612	0.119	0	0	0	0

Assumptions:

- The ratio of PV BCs, AACs and BSCs within SO, SR and SLM followed the same ratio of the same cells within SP due to lack of information on such ratio in these layers.

5.2.5.2. Cholecystokinin Positive Interneurons

A similar reasoning to Bezaire and Soltesz (2013) for the rat was also used for the quantification of CCK+ interneurons. In their quantification, the authors used the colocalization percentages of vGluT3, CB and VIP with CCK from Somogyi and colleagues (2004) (rat) to quantify CCK+/vGluT3+, CCK+/CB+ and CCK+/VIP+ interneurons respectively (See **Table S2**). However, a calculation simply using the percentages from Somogyi, applied as percentages to the Jinno and Kosaka (2006) CCK+ ND measurements resulted in a significant difference in the CCK+/VIP+ numerical density calculations of SO and SP when compared to the measurements of CCK+/VIP+ colocalization ND of Kim *et al*. (2017) in the mouse. This is possibly due to species variabilities and/or a difference in measurement techniques. The Kim *et al*. (2017) measurements were therefore calculated as a percentage of the Jinno and Kosaka (2006) CCK+ measurements, accounting

proportionally for the dorso-ventral variation and was then substituted with the Somogyi *et al*. (2004) CCK+/VIP+ percentage, evenly distributing the difference in CCK+/VIP+ values between the other three categories, CCK only, CCK+/vGluT3+ and CCK+/CB+ (**Table S3**). The same assumptions (See Assumptions below) made by Bezaire and Soltesz (2013) were then applied for the categorisation of the calculated numerical densities (**Table S3**) into CCK BC, SCA, ADI and PPA interneuron types. **Table 7** illustrates the NDs of cell types CCK BCs, SCA, ADI, and PPA cells in bold while their subtypes are categorised by one or none of VIP, vGluT3 or CB colocalised with CCK.

Table 7

Calculated numerical densities of CCK+ interneuron classes and subclasses

		Hippocampal CA1 strata							
		dSO	vSO	dSP	vSP	dSR	vSR	dSLM	vSLM
CCK+ interneurons ND (cells*1000/mm^3)	CCK BC total	**0.173**	**0.334**	**0.616**	**0.875**	**0.183**	**0.313**	**0.078**	**0.301**
	VIP+ CCK BC	0.003	0.007	0.016	0.022	0.01	0.018	0.007	0.025
	vGluT3+ CCK BC	0.061	0.118	0.173	0.246	0.173	0.295	0.071	0.276
	CCK only CCK BC	0.109	0.21	0.426	0.606	0	0	0	0
	SCA total	**0**	**0**	**0**	**0**	**0.113**	**0.194**	**0**	**0**
	CB+ SCA	0	0	0	0	0.054	0.093	0	0
	CCK only SCA	0	0	0	0	0.059	0.101	0	0
	ADI total	**0**	**0**	**0**	**0**	**0.113**	**0.194**	**0**	**0**
	CB+ ADI	0	0	0	0	0.054	0.093	0	0
	CCK only ADI	0	0	0	0	0.059	0.101	0	0
	PPA total	**0**	**0**	**0**	**0**	**0**	**0**	**0.092**	**0.359**
	CB+ PPA	0	0	0	0	0	0	0.044	0.172
	CCK only PPA	0	0	0	0	0	0	0.048	0.187
	CCK/CB other	0.117	0.226	0.144	0.205	0	0	0	0

Assumptions:

- CCK BCs are found in all CA1 strata (Vida *et al*.,1998)
- SCA and ADI interneurons are restricted to SR. All CCK+ interneurons in SR that are not CCK BCs are equally divided between SCA and ADI
- PPA cells are restricted to SLM and therefore all CCK+ interneurons in SLM that are not CCK BCs were deemed PPA cells. In reality, PPA cells are sometimes also present in SR and even more rarely in SO (Hájos & Mody, 1997; Klausberger *et al*., 2005).
- Even though an undefined percentage of ADI cells are vGluT3+ (Klausberger *et al*., 2005), it was assumed that all CCK+/VIP+ and CCK+/vGluT3+ interneurons in CA1 were CCK BCs.
- None of the CCK+/CB+ interneurons are CCK BCs since there have been no known instances of CCK BCs which were found to be CB+.
- Interneurons in SO and SP that are CCK+/CB- are CCK BCs.
- Due to the lack of research on lesser known CCK+ cell types, probably due to their very low numbers, it was assumed that the remaining unclaimed numbers in SO and SP were the sums of these lesser known CCK+ interneurons.

5.2.5.3. Somatostatin positive interneurons

5.2.5.3.1. Backprojection cells

Harris and colleagues (2018) came across a highly distinct SST/nNOS immunopositive cell class which they identified as BPC. Since this was the only class with these distinct characteristics, we relied on the colocalization of nNOS and SST for the quantification of this cell class. Measurements of SST/nNOS colocalization from Kim *et al*. (2017) were disregarded for a calculation based on Jinno and Kosaka (2004) and Jinno and Kosaka (2006) measurements for the sake of consistency, since most other calculations in this project were founded on results of the same authors.

The numbers of SST+ and nNOS+ cells in each sublayer were calculated by multiplying the numerical densities of the markers from Jinno and Kosaka (2006) with the layer volumes from Kim *et al*. 2017. The percentage of nNOS+ SST+ interneurons and the percentage of SST+ nNOS+ interneurons were obtained from Jinno and Kosaka (2004) (**Table S4**). The average cell numbers of nNOS:SST and SST:nNOS were then converted back to numerical

densities. The final NDs of BPCs in the respective sublayers of CA1 are denoted in **Table 7** below.

Table 7

Laminar distribution of Backprojection cells.

	Hippocampal regions							
	dSO	vSO	dSP	vSP	dSR	vSR	dSLM	vSLM
ND of BPCs (cells*1000/mm^3)	**0.13**	**0.06**	**0**	**0.07**	**0.01**	**0.24**	**0.01**	**0**

5.2.5.3.2. Oriens-Lacunosum Moleculare Cells

O-LM cells have generally so far been considered a homogeneous interneuron class due to their largely uniform neurochemical, anatomical and electrical features. However, Chittajallu *et al*. (2013) revealed a separation of two subpopulations depending on their origins; either MGE (5-HT3AR-) or CGE (5-HT3AR+) derived. To determine the numerical density of CGE O-LM interneurons, the percentage (31.5%) of CGE-derived cells in SO was extracted from a plot by Chittajallu *et al*. (2013) using WebPlotDigitizer. This was used, together with the total ND of GABAergic neurons in SO from Jinno *et al*. (1998), the percentage of SST+ CGE interneurons in SO and the ratio of O-LM neurons in CGE SST+ SO interneurons (Chittajallu *et al*., 2013) to calculate the ND of CGE-derived O-LM cells (**Table S4**). The MGE portion of O-LM interneurons was calculated by the addition of PV+ O-LM cells (calculated in PV+ interneurons section) as all PV+ O-LM cells are MGE derived (Chittajallu *et al*., 2013), and the ND of SST+ interneurons which remained unclaimed in SO after all other SST+ cell types and subtypes were considered (**Table S5** and **S6**). While in the rat the estimated percentage of SST+ cells in SO that are O-LM cells was about 40% (Ferraguti *et al*., 2004), our estimation for the mouse was somewhat lower (29.4% in dSO and 24.6% in vSO). This could be due to species variations or The ND of O-LM cells within SO, the only layer in which they reside, is presented in **Table 8** below together with the ND of its constituent subtypes; CGE O-LM and MGE O-LM cells.

Table 8

Laminar distribution of O-LM cells

	Hippocampal CA1 strata	
	dSO	vSO
ND of CGE O-LM (cells*1000/mm^3)	0.220	0.356
ND of MGE O-LM (cells*1000/mm^3)	0.689	1.066
Total ND of O-LM cells (cells*1000/mm^3)	**0.908**	**1.421**

Assumptions:

- 5-HT3AR- O-LM cells are MGE derived while 5-HT3AR+ O-LM cells are CGE derived.
- SST+ cells other than BSC, BPC, HS cells, PV+ and CGE derived O-LM cells are MGE derived O-LM cells.

5.2.5.3.3. Hippocampo-Septal Cells

As almost all reported HS cells in CA1 were confined to SO, we assumed that all HS cells in CA1 are found in SO (Jinno, 2009; Jinno *et al*., 2007; Jinno & Kosaka, 2002b). PV+ HS (ND calculated in PV+ interneurons section) only make up a small percentage of the total HS population in CA1. From Jinno and Kosaka (2002b) 2.5% and 22.6% of total PV+ and SST+ subpopulations of GABAergic neurons respectively in the CA1 projected to the medial septum. Since these measurements were taken by retrograde labelling using Fluoro-Gold, the authors caution that these percentages are minimum values.

For the finding of the ND of HS cells, therefore, we started by calculating the ND of 2.5% of PV+ GABAergic neurons which as suspected was lower than the already known value of PV+ HS cells from Yamada and Jinno (2017). Let's say that the latter value was "X" times larger. The ND of 22.6% of SST+ interneurons was then calculated and multiplied by "X" to obtain the real value of SST+ HS cells (**Table S7**). This value was then distributed between dorsal and ventral SO following the same distribution ratio of the currently unclaimed SST+ SO interneurons.

Unclaimed SST+ SO interneurons = (total SST+) – (CGE O-LM) – (PV+ O-LM) – (BSC) – (BPC)

We estimated 1980 and 4210 SST+ HS cells/mm^3 for dSO and vSO respectively (**Table S8**). Finally, the total HS value was calculated based on the findings of Jinno and Kosaka (2002b) that only 95.5% of HS cells are SST+. The total HS ND was estimated at 2070 and 4410 cells/mm^3 for dSO and vSO respectively (**Table 9** and **S8**).

5.2.5.3.4. Double projection cells

Since double projection cells are known to express CB and SST together (Jinno *et al*., 2007; Tóth & Freund, 1992, both in rats), we assumed that all CB+/SST+ HS cells were double projection cells. Jinno and Kosaka (2002b) found a minimum of 19% of all CB+ interneurons in CA1 projected to the septum. However, using the same reasoning for CB+ HS cells as for PV+ and SST+ above, did not give realistic results as the resultant ND was higher than the unclaimed SST+ interneurons. The same authors also estimated that 57.1% of HS interneurons in SO were CB positive. Using this percentage, we got a DPC ND of 1180 and 2520 cells/mm^3 for dSO and vSO respectively (**Table S8**). Also at least 21% of HS interneurons, which are SST+/M2R+/mGluR1α- and which may or may not be double projection cells were found to project exclusively towards the medial septum and not towards the subiculum (Jinno *et al*., 2007, data for rats) (**Table S9).**

Table 9
Laminar distribution of total HS and DPC

	Hippocampal regions	
	dSO	vSO
Total HS ND (cells*1000/mm^3)	**2.07**	**4.41**
DPC ND	**1.18**	**2.52**

Assumptions:

- All HS cells in CA1 are in SO. Very few cells in CA1 were found to project to the medial septum from strata other than SO (Jinno *et al*., 2007, Jinno and Kosaka, and Jinno 2009).
- All CB+/SST+ HS cells are double projection cells.

5.2.5.3.5. Hippocampo-subicular interneurons

Due to the information in **Table S9** which was reproduced from the supplementary material of Jinno *et al*. (2007), together with the fact that the same authors mentioned a major overlap between cells that project to the septum and those that project to the subiculum, we assumed that SST+/mGluR1α+/M2R- that projected from SO to the subiculum were exactly the same cells that projected from SO to the medial septum. Therefore 43% of H-Sub in SO are equal to 50% of HS in SO (**Table S9** - data from rats). This gave a ND of 1036 and 2204 cells/mm^3 for dSO and vSO respectively. Knowing this amount, the rest of the H-Sub interneurons with different molecular profiles could be calculated (**Table 10 and S10**).

Table 10
Numerical densities of H-Sub subtypes within CA1 SO.

Molecular profiles	ND of H-Sub dSO (cells*1000/mm^3)	ND of H-Sub vSO (cells*1000/mm^3)
SST-/mGluR1α-/M2R+	0.70	1.49
SST-/mGluR1α-/M2R-	0.24	0.51
SST-/mGluR1α+/M2R-	0.12	0.26
Total ND of interneurons projecting only to subiculum *	**1.06**	**2.26**
Total ND of H-Sub	**2.46**	**5.23**

* This includes SST-/mGluR1α-/M2R+, SST-/mGluR1α-/M2R- and SST-/mGluR1α+/M2R-. This is the minimum value as it is possible that other molecular profiles also include a percentage of cells which only project to the subiculum.

Unlike HS interneurons which are confined to SO in CA1, H-Sub interneurons were found within all the strata (Jinno *et al*, 2007). While it is not the most accurate type of measurement, the sample cell number taken in each stratum was used for calculating the ratio of H-Sub cells within CA1. The authors measured the number of cells within slices of specific volumes that included all strata in a slice. These numbers should therefore correspond to an adequate ratio of cells between the strata. This ratio was used to calculate the ND in SR and SLM, also taking in consideration the difference in volume of the strata. The NDs within SP could not be calculated due to the difficulty in distinguishing interneurons from retrogradely labelled pyramidal cells within the layer. The total ND of H-Sub interneurons was calculated to be 2460 and 5230 cells/mm^3 in dSO and vSO respectively (Table S10) and 1820 and 1020 cells/mm^3 for SR and SLM respectively (**Table**

11). Considering only the neurons which exclusively target the subiculum, the NDs of dSO and vSO are reduced to 1060 and 2260 cells/mm^3 respectively since only 44% of H-Sub cells in SO project exclusively to the Subiculum, while the ND of SR and SLM remain the same.

Table 11

Calculating ND of H-Sub interneurons in other strata

		Hippocampal CA1 strata			
		SO	SP*	SR	SLM
Kim *et al*. (2017)	Volume or ROI (mm^3)	1.83	N/A	2.83	2.33
Jinno *et al*. (2007)	Sampled cells	139	N/A	102	47
ND (cells*1000/mm^3)	Total H-Sub	**3.84**	**N/A**	**1.82**	**1.02**
	interneurons projecting only to Subiculum	**1.66**	**N/A**	**1.82**	**1.02**

* ND in SP could not be estimated since retrogradely labelled interneurons in SP could not be distinguished from pyramidal cells in the layer (Jinno *et al*., 2007).

Assumptions:

- The same SST+/mGluR1α+/M2R- interneurons that project to the medial septum, also project to the subiculum.

5.2.5.4. Interneuron-specific interneurons

The same assumptions as in Bezaire and Soltesz (2013) for the quantification of the rat hippocampal interneurons were followed in our quantification. We assumed that all IS interneurons are either CR+ or VIP+ or both and all interneurons that express any combination of the markers with the exception of VIP+ CCK BCs and CR+ HS cells are interneurons specific. These two markers are generally limited to interneuron specific interneurons, though with some known exceptions as listed above (Gulyás *et al*., 1996; P. Somogyi & Klausberger, 2005; Tricoire *et al*., 2010). The classes of IS cells were determined by the various combinations of these two markers.

The quantification of IS cells was initiated with IS-III. IS-III interneurons were all assumed be immunopositive for both CR and VIP with the exception of 25% of IS-III bipolar cells which are CR- (Tricoire *et al*., 2010). The authors found that these bipolar cells were all immunopositive for VIP and nNOS but only about 75% were immunopositive for CR. CR+/nNOS+ interneurons calculated from the average of percentages of CR+ nNOS+ cells and nNOS+ CR+ cells (Jinno & Kosaka, 2002a, 2006) (**Table S11**) were therefore taken as 75% of the total ND of IS-III bipolar cells (**Table S12**). As for the total IS-III cells, the colocalization of VIP and CR by Kim *et al*., (2017) was utilised. Since the laminar distribution of the measurements were not divided into dorsal and ventral, an average of the distribution ratios of the yet unclaimed densities of CR and VIP was used to calculate the dorsal and ventral values in all the strata. Ultimately, the NDs of the CR- IS-III bipolar cells were added to obtain the total densities of IS-III cells. The NDs of IS-III were then subtracted from the NDs of the unclaimed VIP+ interneurons to give the NDs of IS-II cells which were assumed to be all VIP+/CR- cells except VIP+ CCK BCs and the abovementioned CR- IS-III cells. Finally, the NDs of the dorso-ventrally distributed CR+/VIP+ cells were deducted from the unclaimed CR+ interneurons to obtain the ND of IS-I cells which were assumed to be all CR+/VIP- interneurons other than 6% of HS cells (Jinno *et al*., 2007 – data from rat) (**Table S12**). **Table 12** below shows the laminar distributions of the IS-I, IS-II and IS-III cell types (bold) together with that of the nNOS+ subtype IS-III bipolar cells.

Table 12

Laminar distribution of IS interneurons.

	Hippocampal CA1 strata							
	dSO	vSO	dSP	vSP	dSR	vSR	dSLM	vSLM
IS-III bipolar ND (cells*1000/mm^3)	0.00	0.06	0.95	1.38	0.12	0.32	0.16	0.65
IS-III ND (cells*1000/mm^3)	**0.05**	**0.10**	**0.46**	**0.52**	**0.12**	**0.20**	**0.09**	**0.28**
IS-II ND (cells*1000/mm^3)	**0.18**	**0.35**	**2.31**	**1.84**	**0.24**	**0.36**	**0.34**	**1.01**
IS-I ND (cells*1000/mm^3)	**0.17**	**0.22**	**2.46**	**1.75**	**0.38**	**0.40**	**0.58**	**1.06**

Assumptions:

- All IS interneurons are either CR+ or VIP+ or both and all interneurons that express any combination of the markers with the exception of VIP+ CCK BCs and CR+ HS cells are interneurons specific.
- All VIP+/CR- interneurons except VIP+ CCK BCs and CR- IS-III bipolar cells are IS-II.
- All CR+/VIP- interneurons other than CR+ HS cells are IS-I.
- All CR+/VIP+ interneurons other than CR- IS-III bipolar cells are IS-III.

5.2.5.5. Neurogliaform family cells

The Neurogliaform family is made up of Ivy cells and Neurogliaform (NGF) cells. According to Tricoire and Vitalis (2012), nNOS in the CA1 is confined to Ivy cells, MGE derived NGF cells as well as IS-III bipolar subtype. However, there is also a very distinct group of SST+/nNOS+ interneurons, identified as backprojection cells (BPC) (Harris *et al*., 2018; Sik *et al*., 1994). Harris and colleagues, using single cell transcriptomics also revealed that nNOS is only found in this handful of neuron classes and we therefore felt confident that subtracting the numerical densities of BPCs and IS-III bipolar cells from the total nNOS numerical densities by Jinno and Kosaka (2006), would leave us with the collective numerical densities of the Ivy cells and MGE derived NGF cells.

It is known that Ivy cells are NPY+/nNOS+ cells in SO, SP and SR while MGE NGF cells are NPY+/nNOS+ cells on the SR/SLM border (Fuentealba *et al*., 2010; Tricoire *et al*., 2010; Tricoire & Vitalis, 2012). Therefore, we assumed that all the unclaimed nNOS+ interneurons in SO and SP were Ivy cells and those in SLM were NGF cells. The distribution in SR was decided by the observation of 80% Reelin expression in SR by J. Somogyi and colleagues (2012) (rat). Since reelin is only present in Ivy cells, we divided the ND in SR as 80% Ivy and 20% NGF (**Table S13**).

A dual origin of NGF cells has been suggested (Tricoire *et al*., 2010), with nNOS- NGF cells being CGE derived but still NPY positive. We therefore aimed to find the still unclaimed NPY ND. Harris *et al*. (2018), showed the presence of NPY in BPC, HS, H-Sub, BSC, Ivy, NGF and also trace amounts in CCK+ cells. It was also found in a cluster of unidentified SST+/Reelin+/NPY+ cells. The percentage of NPY in CCK+ cells is unknown, however,

since the ND of CCK+ cells in SR and SLM is already low, we determined that their contribution to NPY in those layers would be negligible. For the other cell classes however, the percentage of NPY is known.

Due to the nature of the measurement by Yamada and Jinno (2017), all BSC are NPY+. All BPC are also NPY+ (Harris *et al*.,2018). We assumed that all NPY+ HS cells were included in the total H-Sub. Then according to Jinno *et al*. (2007), 36%, 10% and 0% of H-Sub in SO, SR and SLM respectively are NPY+ (data from rat).

Unfortunately, there is no data from SP, however, NGF cells are not known to be present in SP. As for the unidentified cluster of cells, we had no further information about it and speculate it might be part of HS or H-Sub. The NDs of all these NPY+ interneurons were deducted from the total ND of NPY (Jinno & Kosaka, 2006) and the unclaimed difference in SR and SLM was taken as CGE derived NGF. Surprisingly, there was only a significant surplus in SO and SP but not in SR and SLM. This indicates a higher percentage of NPY actually present in the above-mentioned cell classes with the major culprit probably being H-Sub and HS both due to the fact that the percentages used from Jinno *et al*. (2007) were from the rat and the because we took the minimum amount and assumed that all NPY in HS and H-Sub overlapped within SO. Only 80 cells/mm^3 in dorsal SR were left over for CGE NGF cells (**Table S14**). **Table 13** below shows the laminar distribution of the cell types Ivy and NGF cells in bold and the subtypes MGE and CGE derived NGF cells.

Table 13

Calculation of CGE NGF cells

		Hippocampal CA1 strata							
		dSO	vSO	dSP	vSP	dSR	vSR	dSLM	vSLM
interneuron ND (cells*1000/mm^3)	Ivy	**1.04**	**0.65**	**3.28**	**0.99**	**0.45**	**0.16**	**0.00**	**0.00**
	Total NGF	**0.00**	**0.00**	**0.00**	**0.00**	**0.19**	**0.04**	**1.79**	**1.19**
	MGE NGF	0.00	0.00	0.00	0.00	0.11	0.04	1.79	1.19
	CGE NGF	0.00	0.00	0.00	0.00	0.08	0.00	0.00	0.00

Assumptions:

- All MGE derived NGF cells and Ivy cells are NPY+/nNOS+.
- nNOS is only present in BPC, IS-III bipolar cells, Ivy cells and MGE derived NGF cells.
- All NPY+/nNOS+ cells other than BPC in SO and SP are Ivy cells while those in SLM are NGF. In SR both cell types are present.
- All NPY+ NS cells also project to the subiculum.
- NPY is only present in BPC, H-Sub, BSC, Ivy and NGF cells.

5.2.5.6. Summary:

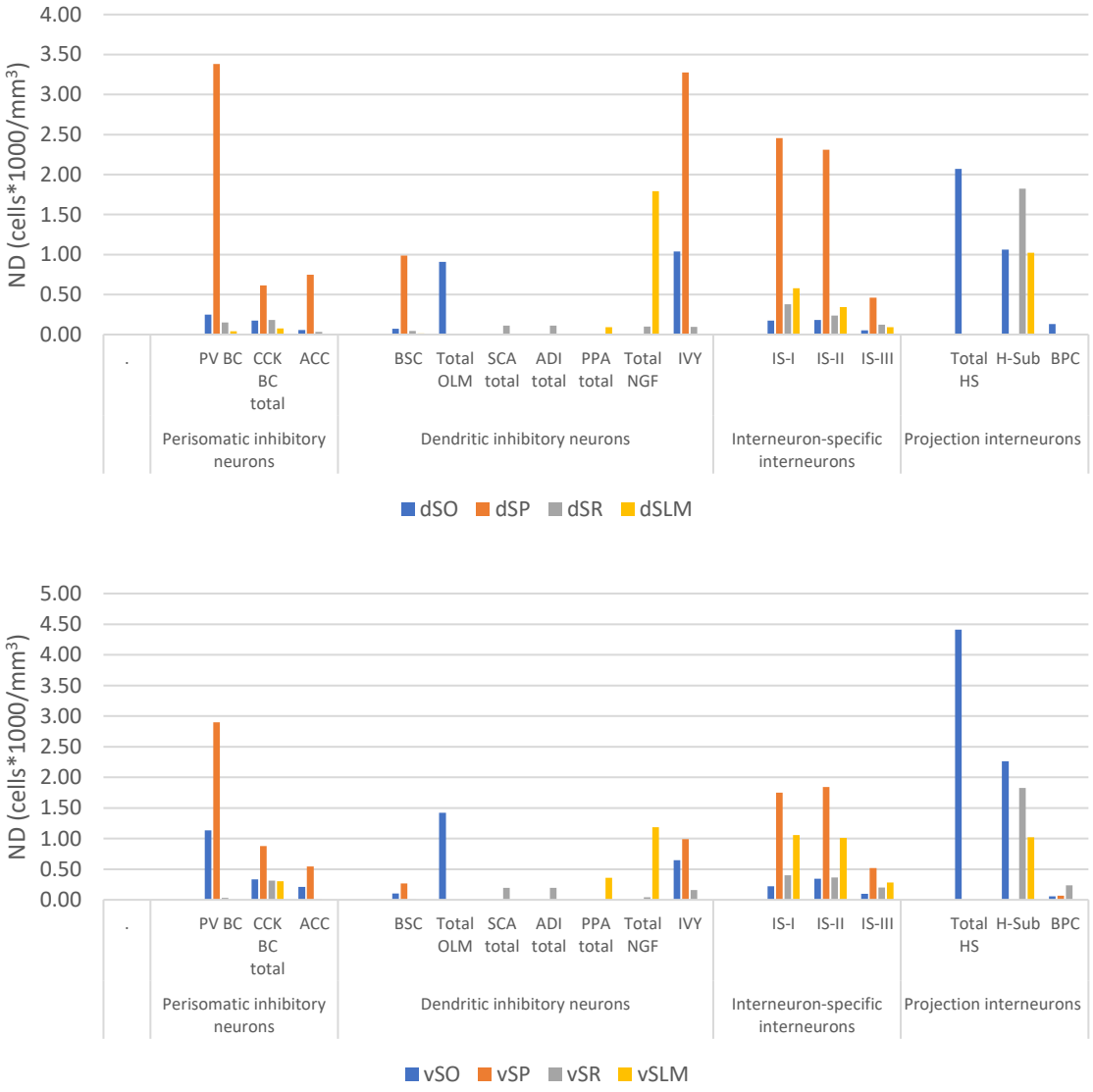

Fig. 5. 13 Interneuron ND laminar distribution within CA1 of the mouse hippocampus. Dorsal (top) and ventral (bottom).

Table 14

Summary of CA1 cell class quantifications.

	ND in hippocampal CA1 strata (cells*1000/mm3)							
	dSO	vSO	dSP	vSP	dSR	vSR	dSLM	vSLM
Total GABAergic neurons (Jinno *et al*., 1998)	6.48 ± 0.45	10.50 ± 0.62	13.52 ± 0.93	10.13 ± 1.55	3.2 ± 0.8	4.26 ± 0.53	8.42 ± 0.88	8.82 ± 1.05
Perisomatic inhibitory neurons								
PV BC	0.25	1.13	3.38	2.90	0.15	0.03	0.04	0.00
CCK BC total	0.17	0.33	0.62	0.88	0.18	0.31	0.08	0.30
ACC	0.06	0.21	0.75	0.55	0.03	0.01	0.01	0.00
Dendritic inhibitory neurons								
BSC	0.07	0.10	0.99	0.27	0.04	0.00	0.01	0.00
Total OLM	0.91	1.42	0	0	0	0	0	0
SCA total	0.00	0.00	0.00	0.00	0.11	0.19	0.00	0.00
ADI total	0.00	0.00	0.00	0.00	0.11	0.19	0.00	0.00
PPA total	0.00	0.00	0.00	0.00	0.00	0.00	0.09	0.36
Total NGF	0.00	0.00	0.00	0.00	0.10	0.04	1.79	1.19
IVY	1.04	0.65	3.28	0.99	0.10	0.16	0.00	0.00
Interneuron-specific interneurons								
IS-I	0.17	0.22	2.46	1.75	0.38	0.40	0.58	1.06
IS-II	0.18	0.35	2.31	1.84	0.24	0.36	0.34	1.01
IS-III	0.05	0.10	0.46	0.52	0.12	0.20	0.09	0.28
Projection interneurons								
Total HS	2.07	4.41	0.00	0.00	0.00	0.00	0.00	0.00
H-Sub	1.06	2.26	-	-	1.82	1.82	1.02	1.02
BPC	0.13	0.06	0.00	0.07	0.01	0.24	0.01	0.00
Remaining GABAergic interneurons	0.31	-0.74	-0.72	0.38	-0.21	0.29	4.35	3.60

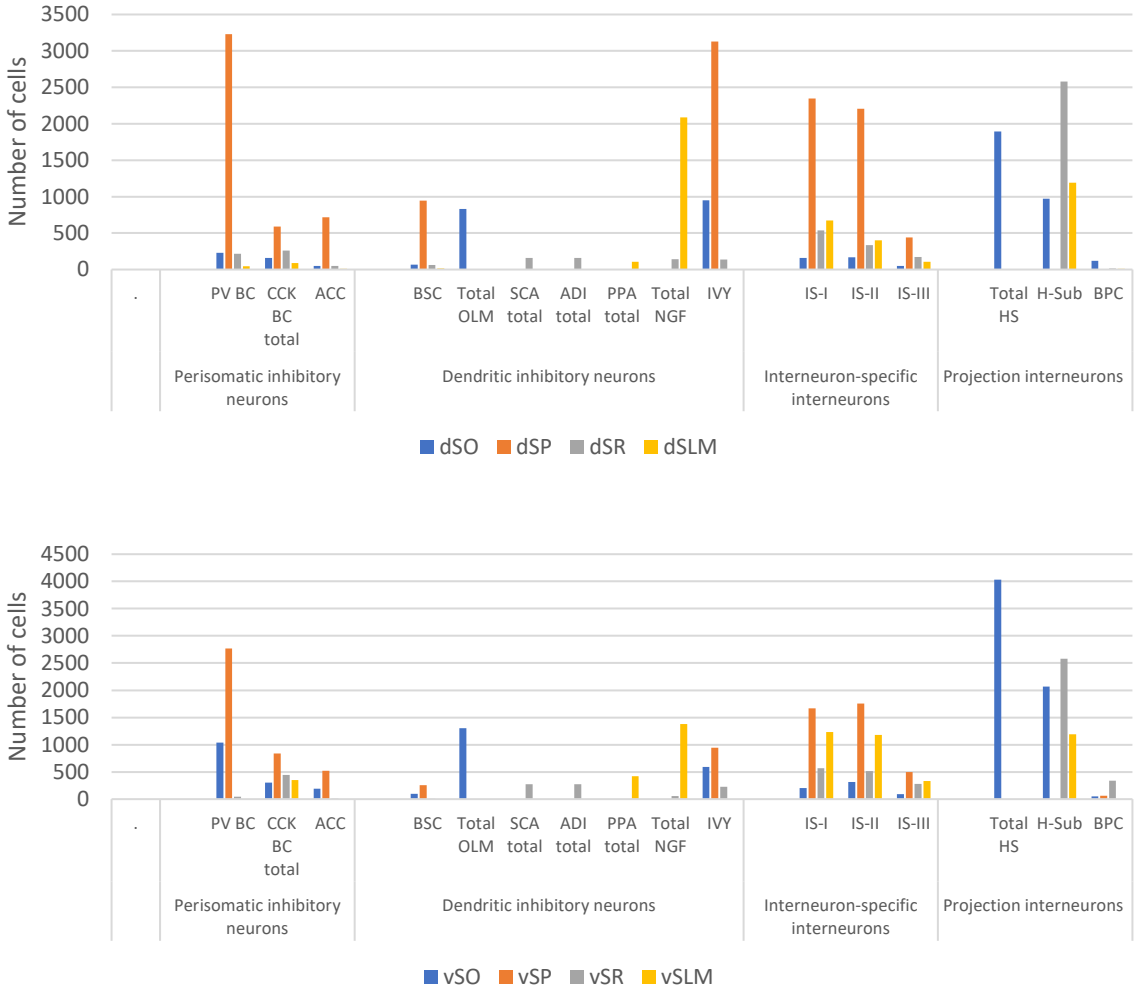

Fig. 5. 14 Interneuron numbers laminar distribution within CA1 of the mouse hippocampus. Dorsal (top) and ventral (bottom).

A summary of the NDs of the cell types or cell groups accounted for in this study is presented in table format in **Table 14** and in the bar-graphs separated according to dorsal and ventral distribution in **Fig. 5. 13**. The NDs of all the cell types were deducted from the total number of GABAergic neurons (Jinno *et al*., 1998) to check for accuracy of calculations. The total interneuron counts in SO, SP and SR came very close to the total values of Jinno and colleagues. However, 4350 and 3600 cells/mm^3 in dSLM and vSLM respectively remained unaccounted for. This accounts for 5073 and 4193 cells in dSLM and vSLM respectively, assuming equal volumes of dorsal and ventral SLM subregions. The volumes of the CA1 layers (Kim *et al*., 2017) were multiplied by the NDs to obtain the actual numbers of the interneuron types. It was again assumed that dorsal and ventral subregions of the strata occupied the same volume. The cell numbers are presented in **Fig. 5. 14** and **Tables S15** and **S16**.

6. Discussion

As first mentioned by Aristotle and later incorporated in the Gestalt principles (Wertheimer, 1923), "the whole is greater than the sum of its parts". This refers to the concept of emergence where adding together the properties of the constituents of the whole, in the right amount and configuration, will not simply give a heap of parts and properties but will give rise to a whole with a new set of properties. As an example, having two wheels, some metal rods, a seat and a chain will not help you get to another place unless you use those parts to construct a bicycle which has the added properties that allow you to use it as a means of transport. It is on this principle that this study becomes a relevant one. Obtaining all the individual quantities of cell types does not provide us with significant information if the potential of emergent properties from such data is not considered.

6.1. Results discussion

In this study, a total of 18 cell types were identified, of which 15 were independently quantified. The reason for the discrepancy is due to the difficulty discerning between cell types of HS and H-Sub groups simply on the available immunocytochemical data. In other cases, however, further quantification down to the subtype level was possible. NGF and O-LM subtypes were quantified according to their origin and subtypes of CCK+ cells were quantified according to their varied immunoreactivities.

Our results suggest that PV BCs have the highest density in general among interneuron cell types both in the dorsal and ventral CA1 with NDs of 3380 and 2900 cells/mm^3 respectively. It is closely followed by Ivy cells in the dorsal region with a ND of 3280 cells/mm3, also in SP. in the dorsal part of SP while the second densest in the ventral side are the HS cell type DPCs with 2520cells/mm3 in SO (**Fig. 5.13**, **Table 9**). PV BCs also dominated when considering cell numbers. They showed a total population (considering all layers and regions) of 7566 cells followed by IS-I, IS-II and Ivy cells at 7390, 6877 and 5980 cells respectively. While Ivy cells and NGF cells show high numbers and densities in the dorsal hippocampus, their total populations in both the dorsal and ventral regions were surpassed by the total IS cells and projection neurons (sum of HS and H-Sub). This contradicts previous research (Fuentealba *et al*., 2008a) where it was suggested that the Neurogliaform family of cells is the most abundant interneuron type in CA1. This could have been concluded due to

the heterogeneity of H-Sub, HS and IS cells which show significant heterogeneity within themselves, possibly leading to their constituent cell types not being grouped together.

Considering the total GABAergic neuron densities, we are confident that cell types within SO, SP and SR have been quantitatively accounted for as the estimated interneuron totals came within the standard deviations of the total GABAergic NDs given by Jinno and colleagues (1998). The total of vSO fell just outside the standard deviation range, however, our calculated values, though the mined data did not allow for an estimation of standard deviations, inevitably, still come with an error margin. We are confident that this undefined error margin would cover the difference of 120 cells/mm^3 between our total and that of Jinno and colleagues in vSO. This indicates that within these layers, any cell types within this layers that have either not yet been identified or could not be quantified within these layers, either are present in very low amounts or are included within the quantifications of cell groups considered here.

Interestingly, 5073 and 4193 cells in dSLM and vSLM respectively have remained unassigned to any cell type or family and all the common markers (PV, CR, SOM, CCK, VIP, nNOS and NPY) quantified by Jinno and Kosaka (2006) have been accounted for within this layer. Only a small CB ND has remained unaccounted for and it still does not come close to the above numbers. It is possible that these cells could make part of already established cell types, but lack the main markers for the quantification. It is also possible that entire cell types have gone undetected due to their lack of immunostaining by the above-mentioned common markers. Further research should surely be focused on this numerical discrepancy as this is a rather large gap that needs to be accounted for. This research has shed light on the largely non-uniform and unstandardized lack of data and the amount and content of the assumptions considered for the quantifications is a great indicator of what and how much still needs to be clarified. The review by Pelkey and colleagues (2017) is a good source of reference for currently advisable driver mice to be used for the identification and quantification of specific hippocampal interneuron classes. Overall, a very different histological profile has emerged between dorsal and ventral parts of the CA1 and this is further evidence of the divergent circuitry and functions between the two regions. A significant role is surely played in the resultant behavioural responses that emerge from the separate regions; the dorsal region being mainly responsible for cognitive functions such as spatial and declarative memory processing while the ventral is more dominant in emotional responses (Milior *et al*., 2016).

Further to this, it is evident that, even though GABAergic neurons are varied and give a significant contribution to circuit modulation, principal cells are orders of magnitude more abundant than interneurons and show variations along all three spatial axes in both the quantity and the quality of the cells. The density varies from lowest in the distal ventral CA1 region at 150.5cells*10^3/mm^3 to the highest in the proximal dorsal CA1 at 505.7cells*10^3/mm^3. The gradients in pyramidal cells have been directly linked to functional differences as exemplified in **Table 5** above and in conjunction with GABAergic interneurons give rise to emergent functions such as the encoding and consolidation of episodic memory, mood and emotion modulation and both spatial and non-spatial information processing (Pelkey *et al*., 2017). Here we will discuss how these emergent properties are approached by science and how they can affect different aspects of behaviour.

6.2. Behavioural implications.

To date, most computational models have been built upon the assumption of a largely homogeneous cell type connected via random synapses, which, as recently evidenced, is not the case (Soltesz & Losonczy, 2018). It is crucial that the heterogeneity gradients listed in **Table 5** are considered together with the numerical densities of PCs and interneurons for an accurate and representative circuit build. It is well established that spatial and non-spatial information is mostly segregated within the hippocampus however, the computational modules within these streams are less known. It has been suggested that they are non-uniform implying non-identical transformations of the non-identical incoming signals (from different parts of EC).

This makes it possible for the various dimensions of the different process domains to be processed independently and in parallel. Taking just the spatial aspect of episodic memory as an example, the hippocampus is able to support the spatial, temporal, associative and contextual learning processes within the contexts of encoding, consolidation and memory retrieval depending on intrinsic and extrinsic information (Soltesz & Losonczy, 2018).

Unfortunately, in this study, only densities in the dorsal and ventral CA1 could be estimated due to very scarce data along the other axes. Though the values given suggest a discrete segregation, densities should be taken as a gradient along the dorso-ventral axis. Radial variation for interneuron quantification is usually available as laminar distributions. It would be interesting to find out whether interneurons of the same cell types that reside in multiple

layers or deep or superficial within the same layer, have differential targets depending on their somatic locations and what would be the functional implications behind it. It has been observed that certain interneuron cell types have certain target preferences for subclasses of CA1 PCs, for example the discrete preferential inhibition of PVBCs towards deep over superficial ones. Deep CA1PCs were found to be more active, have the ability to change their firing-phase according to brain state and are more likely to form place fields compared to superficial cells (Mizuseki *et al*., 2011). They also have distinct extra-hippocampal projection targets (Lee *et al*., 2014). This preferential innervation likely has implications in spatial mapping. This supports the notion of differentiated CA1 circuits possibly modulated by different interneurons. Additionally, early-born PV BCs preferentially target superficial PCs and play a role in learning associations while late-born PV BCs preferentially target deep PCs and promote enhanced acquisition in learning (Donato *et al*., 2015).

Together with PCs being place cells and contributing to encoding of spatial memories, some interneurons are known to participate in the task. Interneurons, likely perisomatic targeting ones, were found to not just be driven by PCs but they actively take part in the shaping of place fields through disinhibition of PCs. Modulation of the spike timing of place cells is affected by PV+ cells while their firing rates are controlled by SST+ interneurons (Pelkey *et al*., 2017).

Unfortunately, little is yet known on other interneuron functions such as CCK+ cells. Further research needs so be conducted on their source and target specificities and their implications.

6.3. Interneuron-related neurological disorders.

Several studies have shed light onto how interneurons could contribute to developmental, neurological and psychiatric disorders. This shows an additional motive as to how these numbers, applied within models could shed light on the exact mechanisms of specific hippocampal abnormalities and possibly point towards more efficient treatments.

Developmental: Multiple genes have been implicated in the cause of autistic spectrum disorder (ASD) whose ethology is still greatly unknown and the complexity of this range of developmental disorders is still to be unravelled. Mutations or deletions of the implicated genes in animal models, shed light on anatomical and physiological abnormalities at circuit levels in CA1. The deletion of the *Tsc1* gene from CA1 PCs causes a reduction in inhibitory

input making the network hyperexcitable (Bateup *et al*., 2013). Deleting the same gene from MGE interneurons disrupts their developmental migration and results in loss of interneurons thus further contributing to hyperexcitability (Fu *et al*., 2012). Mutations in *Shank1* disturb the excitatory input into PV+ interneurons offsetting the excitation-inhibition balance (Mao *et al*., 2015) and a deletion of CNTNAP2 in mice also resulted in hyperexcitability, impaired neuron migrations and a reduction in PV+, NPY+ and CR+ interneurons (Peñagarikano *et al*., 2011). These mutations resulted in autistic phenotypes of hyperactivity, rigid behaviour, ASD stereotypic movements and impaired social interactions. Additional Autism-related disorders such as Fragile X syndrome and Rett syndrome and other developmental disorders such as schizophrenia also have hippocampal interneurons implicated as one of their root abnormalities (Pelkey *et al*., 2017).

Neurological: Neurological disorders, including some viral infections that manage to penetrate the blood-brain barrier such as the herpes simplex virus 1 and the human immunodeficiency virus also result in selective loss of interneurons (Pelkey *et al*., 2017). Epilepsy is one such condition, being an umbrella term for disorders causing recurrent seizures, stereotypically involving an abnormal rhythmic firing of large neuronal ensembles. While causes vary, atrophy in the human CA1 region is present with high incidence in temporal lobe epilepsy patients (Babb *et al*., 1989), while in animal models, the DG and CA1 have been confirmed as the most vulnerable regions (Freund *et al*., 1992). A rat pilocarpine model disclosed a decrease in SST+ or PV+ CA1 interneurons in SO but not SST+/PV+ cells (Dinh *et al*., 2002) such as double projection cells. The same model also showed a loss of inhibition from CCK BCs resulting in seizures (Wyeth *et al*., 2010). Traumatic brain injuries and Alzheimer's disease are additional neurological disorders impacted by CA1 interneuron loss or abnormalities.

Psychological: Given the circuitry the hippocampus shares with the amygdala which is the hub of emotion generation in the brain and its consequential role, particularly that of the ventral part, in mood modulation, it comes to no surprise that its cellular composition effects also psychiatric diseases and disorders. In chronic stress, mechanisms involving PV and CCK interneurons affect the activity of CA1 PCs (Hu *et al*., 2010) and in rat models, stress resulted in a loss of PV+, NPY+, SST+ and CR+ interneurons. Reduction in immunostaining in the latter two was associated with a pathological change (Czéh *et al*., 2015). Other psychological conditions showing an involvement of interneurons are anxiety, addiction and mood disorders such as bipolar disorders.

6.4. Implications for computational neuroscience and cybernetics.

As already mentioned, a knowledge of the classification and quantification of neuronal classes in the hippocampus allows more holistic computational models and simulations of the brain region both in healthy and pathological scenarios. As evidenced above, several conditions are rooted in anatomical and physiological abnormalities of the hippocampus, including if not exclusively, the CA1 region. Variations in the number of neurons have major implications in the development of mental disorders and diseases. Having a thorough knowledge of the constitution of a healthy brain can therefore turn out to be a significant asset in assessing such conditions. Modifications of cell numbers could shed light on yet undiscovered disorder neurological basis and emergent properties from neuronal ensembles could be translatable to other brain regions thus broadening the current knowledge of the brain in general. Nonetheless, there is as much to gain in simulating a healthy brain as there is an abnormal one and there can be huge consequences in the discovery of components and configurations responsible for specific brain functions or behaviours.

Accurately simulating a whole brain section also opens doors for *in silico* studies of brain simulation techniques which could have huge implications in the cognitive sciences. So far, most brain stimulation practices are performed with very little knowledge of the exact response in brain tissue thus this technology could highly benefit this field of research. Furthermore there has been research on the possibility of replicating, for the purpose of creating a memory prosthesis for possible functional substitution of the human hippocampus (Song *et al*., 2018). This, and similar technologies could have a huge potential in future manipulation of cognitive function both for clinical and healthy individuals. So far however, it seems that these technologies are taking a top down approach which ultimately gives very little information as to what is actually happening on the cellular and molecular level. Due to this, manipulation is unlikely to be fine-tuned. Having the ability to have *in silico* models of brain structures with data similar to that mined in this study is surely of great value to test and help build more accurate prosthetics in the future.

7. Conclusion

This study has shed light on the cellular composition of the CA1 region of the mouse hippocampus. It is to serve as a knowledge-base for future computational modelling, offering laminar distributions and dorso-ventral variations of currently identified GABAergic neurons together with distribution of principal cells along all axis of the CA1 pyramidal layer. Several assumptions with regards to the quantifications needed to be considered for the fulfilment of this task, highlighting the numerous limitations and possible resultant knowledge-gaps due to unavailable and/or unstandardized data. Further research on both the heterogeneity of principal cells and on various aspects of interneurons is therefore necessary for generation of higher quality data and the resultant computational models.

8. References

Acsády, L., Arabadzisz, D., & Freund, T. F. (1996). Correlated morphological and neurochemical features identify different subsets of vasoactive intestinal polypeptide-immunoreactive interneurons in rat hippocampus. *Neuroscience*, *73*(2), 299–315. https://doi.org/10.1016/0306-4522(95)00610-9

Acsády, L., Görcs, T. J., & Freund, T. F. (1996). Different populations of vasoactive intestinal polypeptide-immunoreactive interneurons are specialized to control pyramidal cells or interneurons in the hippocampus. *Neuroscience*, *73*(2), 317–334. https://doi.org/10.1016/0306-4522(95)00609-5

Alberini, C. M., Johnson, S. A., & Ye, X. (2013). Chapter five - Memory Reconsolidation: Lingering Consolidation and the Dynamic Memory Trace. In C. M. Alberini (Ed.), *Memory Reconsolidation* (pp. 81–117). Academic Press. https://doi.org/10.1016/B978-0-12-386892-3.00005-6

Allen, R. J., Vargha-Khadem, F., & Baddeley, A. D. (2014). Item-location binding in working memory: Is it hippocampus-dependent? *Neuropsychologia*, *59*, 74–84. https://doi.org/10.1016/j.neuropsychologia.2014.04.013

Andersen, P., Bliss, T. V. P., & Skrede, K. K. (1971). Lamellar organization of hippocampal excitatory pathways. *Experimental Brain Research*, *13*(2), 222–238. https://doi.org/10.1007/BF00234087

Andreasen, N. C., O'Leary, D. S., Paradiso, S., Cizadlo, T., Arndt, S., Watkins, G. L., Ponto, L. L. B., & Hichwa, R. D. (1999). The cerebellum plays a role in conscious episodic memory retrieval. *Human Brain Mapping*, *8*(4), 226–234. https://doi.org/10.1002/(SICI)1097-0193(1999)8:4<226::AID-HBM6>3.0.CO;2-4

Armstrong, C., Krook-Magnuson, E., & Soltesz, I. (2012). Neurogliaform and Ivy Cells: A Major Family of nNOS Expressing GABAergic Neurons. *Frontiers in Neural Circuits*, *6*. https://doi.org/10.3389/fncir.2012.00023

Babb, T. L., Pretorius, J. K., Kupfer, W. R., & Crandall, P. H. (1989). Glutamate decarboxylase-immunoreactive neurons are preserved in human epileptic hippocampus. *Journal of Neuroscience*, *9*(7), 2562–2574. https://doi.org/10.1523/JNEUROSCI.09-07-02562.1989

Baddeley, A. (2000). The episodic buffer: A new component of working memory? *Trends in Cognitive Sciences*, *4*(11), 417–423. https://doi.org/10.1016/S1364-6613(00)01538-2

Balota, D. A., & Coane, J. H. (2008). 2.28—Semantic Memory. In J. H. Byrne (Ed.), *Learning and Memory: A Comprehensive Reference* (pp. 511–534). Academic Press. https://doi.org/10.1016/B978-012370509-9.00170-4

Bateup, H. S., Johnson, C. A., Denefrio, C. L., Saulnier, J. L., Kornacker, K., & Sabatini, B. L. (2013). Excitatory/Inhibitory Synaptic Imbalance Leads to Hippocampal

Hyperexcitability in Mouse Models of Tuberous Sclerosis. *Neuron*, *78*(3), 510–522. https://doi.org/10.1016/j.neuron.2013.03.017

Baude, A., Bleasdale, C., Dalezios, Y., Somogyi, P., & Klausberger, T. (2007). Immunoreactivity for the GABAA Receptor α1 Subunit, Somatostatin and Connexin36 Distinguishes Axoaxonic, Basket, and Bistratified Interneurons of the Rat Hippocampus. *Cerebral Cortex*, *17*(9), 2094–2107. https://doi.org/10.1093/cercor/bhl117

Benavides-Piccione, R., Regalado-Reyes, M., Fernaud-Espinosa, I., Kastanauskaite, A., Tapia-González, S., León-Espinosa, G., Rojo, C., Insausti, R., Segev, I., & DeFelipe, J. (2019). Differential Structure of Hippocampal CA1 Pyramidal Neurons in the Human and Mouse. *Cerebral Cortex*, bhz122 e16553 e41714 e1000781. https://doi.org/10.1093/cercor/bhz122

Bezaire, M. J., & Soltesz, I. (2013). Quantitative assessment of CA1 local circuits: Knowledge base for interneuron-pyramidal cell connectivity: Quantitative Assessment Of Ca1 Local Circuits. *Hippocampus*, *23*(9), 751–785. https://doi.org/10.1002/hipo.22141

Blasco-Ibáñez, J. M., & Freund, T. F. (1995). Synaptic Input of Horizontal Interneurons in Stratum Oriens of the Hippocampal CA1 Subfield: Structural Basis of Feed-back Activation. *European Journal of Neuroscience*, *7*(10), 2170–2180. https://doi.org/10.1111/j.1460-9568.1995.tb00638.x

Booker, S. A., Althof, D., Degro, C. E., Watanabe, M., Kulik, Á., & Vida, I. (2017). Differential surface density and modulatory effects of presynaptic GABAB receptors in hippocampal cholecystokinin and parvalbumin basket cells. *Brain Structure and Function*, *222*(8), 3677–3690. https://doi.org/10.1007/s00429-017-1427-x

Bookheimer, S. (2002). Functional MRI of Language: New Approaches to Understanding the Cortical Organization of Semantic Processing. *Annual Review of Neuroscience*, *25*(1), 151–188. https://doi.org/10.1146/annurev.neuro.25.112701.142946

Brown, M. W., & Aggleton, J. P. (2001). Recognition memory: What are the roles of the perirhinal cortex and hippocampus? *Nature Reviews Neuroscience*, *2*(1), 51–61. https://doi.org/10.1038/35049064

Camina, E., & Güell, F. (2017). The Neuroanatomical, Neurophysiological and Psychological Basis of Memory: Current Models and Their Origins. *Frontiers in Pharmacology*, *8*. https://doi.org/10.3389/fphar.2017.00438

Cembrowski, M. S., & Spruston, N. (2019). Heterogeneity within classical cell types is the rule: Lessons from hippocampal pyramidal neurons. *Nature Reviews Neuroscience*, *20*(4), 193–204. https://doi.org/10.1038/s41583-019-0125-5

Chamberland, S., Salesse, C., Topolnik, D., & Topolnik, L. (2010). Synapse-specific inhibitory control of hippocampal feedback inhibitory circuit. *Frontiers in Cellular Neuroscience*, *4*, 130. https://doi.org/10.3389/fncel.2010.00130

Chittajallu, R., Craig, M. T., McFarland, A., Yuan, X., Gerfen, S., Tricoire, L., Erkkila, B., Barron, S. C., Lopez, C. M., Liang, B. J., Jeffries, B. W., Pelkey, K. A., & McBain, C. J. (2013). Dual origins of functionally distinct O-LM interneurons revealed by differential 5-HT3AR expression. *Nature Neuroscience*, *16*(11), 1598–1607. https://doi.org/10.1038/nn.3538

Coltheart, M. (1983). Ecological necessity of iconic memory. *Behavioral and Brain Sciences*, *6*(1), 17–18. https://doi.org/10.1017/S0140525X00014357

Cope, D. W., Maccaferri, G., Márton, L. F., Roberts, J. D. B., Cobden, P. M., & Somogyi, P. (2002). Cholecystokinin-immunopositive basket and Schaffer collateral-associated interneurones target different domains of pyramidal cells in the CA1 area of the rat hippocampus. *Neuroscience*, *109*(1), 63–80. https://doi.org/10.1016/S0306-4522(01)00440-7

Cowan, N. (2008). Sensory Memory. In *Learning and Memory: A Comprehensive Reference* (pp. 23–32). Elsevier. https://doi.org/10.1016/B978-012370509-9.00172-8

Craig, M. T., & McBain, C. J. (2015). Fast gamma oscillations are generated intrinsically in CA1 without the involvement of fast-spiking basket cells. *The Journal of Neuroscience: The Official Journal of the Society for Neuroscience*, *35*(8), 3616–3624. https://doi.org/10.1523/JNEUROSCI.4166-14.2015

Czéh, B., Varga, Z. K. K., Henningsen, K., Kovács, G. L., Miseta, A., & Wiborg, O. (2015). Chronic stress reduces the number of GABAergic interneurons in the adult rat hippocampus, dorsal-ventral and region-specific differences. *Hippocampus*, *25*(3), 393–405. https://doi.org/10.1002/hipo.22382

Deese, J. (1959). On the prediction of occurrence of particular verbal intrusions in immediate recall. *Journal of Experimental Psychology*, *58*(1), 17–22. https://doi.org/10.1037/h0046671

DeFelipe, J., & Fariñas, I. (1992). The pyramidal neuron of the cerebral cortex: Morphological and chemical characteristics of the synaptic inputs. *Progress in Neurobiology*, *39*(6), 563–607. https://doi.org/10.1016/0301-0082(92)90015-7

Definition of INFORMATION. (n.d.). Retrieved 25 May 2020, from https://www.merriam-webster.com/dictionary/information

Di Lollo, V. (1980). Temporal integration in visual memory. *Journal of Experimental Psychology: General*, *109*(1), 75–97. https://doi.org/10.1037/0096-3445.109.1.75

Dinh, T. P., Carpenter, D., Leslie, F. M., Freund, T. F., Katona, I., Sensi, S. L., Kathuria, S., & Piomelli, D. (2002). Brain monoglyceride lipase participating in endocannabinoid inactivation. *Proceedings of the National Academy of Sciences*, *99*(16), 10819–10824. https://doi.org/10.1073/pnas.152334899

Donato, F., Chowdhury, A., Lahr, M., & Caroni, P. (2015). Early- and Late-Born Parvalbumin Basket Cell Subpopulations Exhibiting Distinct Regulation and Roles in Learning. *Neuron*, *85*(4), 770–786. https://doi.org/10.1016/j.neuron.2015.01.011

Ebbinghaus (1885), H. (2013). Memory: A Contribution to Experimental Psychology. *Annals of Neurosciences*, *20*(4), 155–156. https://doi.org/10.5214/ans.0972.7531.200408

Eichenbaum, H. (2008). Memory. *Scholarpedia*, *3*(3), 1747. https://doi.org/10.4249/scholarpedia.1747

Elfant, D., Pál, B. Z., Emptage, N., & Capogna, M. (2008). Specific inhibitory synapses shift the balance from feedforward to feedback inhibition of hippocampal CA1 pyramidal cells. *European Journal of Neuroscience*, *27*(1), 104–113. https://doi.org/10.1111/j.1460-9568.2007.06001.x

Eriksson, J., Vogel, E. K., Lansner, A., Bergström, F., & Nyberg, L. (2015). Neurocognitive Architecture of Working Memory. *Neuron*, *88*(1), 33–46. https://doi.org/10.1016/j.neuron.2015.09.020

Ferraguti, F., Cobden, P., Pollard, M., Cope, D., Shigemoto, R., Watanabe, M., & Somogyi, P. (2004). Immunolocalization of metabotropic glutamate receptor 1α (mGluR1α) in distinct classes of interneuron in the CA1 region of the rat hippocampus. *Hippocampus*, *14*(2), 193–215. https://doi.org/10.1002/hipo.10163

Fink, A. E., Sariñana, J., Gray, E. E., & O'Dell, T. J. (2007). Activity-Dependent Depression of Local Excitatory Connections in the CA1 Region of Mouse Hippocampus. *Journal of Neurophysiology*, *97*(6), 3926–3936. https://doi.org/10.1152/jn.00213.2007

Fletcher, P. C., & Henson, R. N. A. (2001). Frontal lobes and human memoryInsights from functional neuroimaging. *Brain*, *124*(5), 849–881. https://doi.org/10.1093/brain/124.5.849

Földy, C., Lee, S.-H., Morgan, R. J., & Soltesz, I. (2010). Regulation of fast-spiking basket cell synapses by the chloride channel ClC-2. *Nature Neuroscience*, *13*(9), 1047–1049. https://doi.org/10.1038/nn.2609

Freund, T. F., & Buzsáki, G. (1996). Interneurons of the hippocampus. *Hippocampus*, *6*(4), 347–470. https://doi.org/10.1002/(SICI)1098-1063(1996)6:4<347::AID-HIPO1>3.0.CO;2-I

Freund, T. F., Ylinen, A., Miettinen, R., Pitkänen, A., Lahtinen, H., Baimbridge, K. G., & Riekkinen, P. J. (1992). Pattern of neuronal death in the rat hippocampus after status epilepticus. Relationship to calcium binding protein content and ischemic vulnerability. *Brain Research Bulletin*, *28*(1), 27–38. https://doi.org/10.1016/0361-9230(92)90227-O

Fu, C., Cawthon, B., Clinkscales, W., Bruce, A., Winzenburger, P., & Ess, K. C. (2012). GABAergic Interneuron Development and Function Is Modulated by the Tsc1 Gene. *Cerebral Cortex*, *22*(9), 2111–2119. https://doi.org/10.1093/cercor/bhr300

Fuentealba, P., Begum, R., Capogna, M., Jinno, S., Márton, L. F., Csicsvari, J., Thomson, A., Somogyi, P., & Klausberger, T. (2008). Ivy cells: A population of nitric-oxide-producing, slow-spiking GABAergic neurons and their involvement in hippocampal

network activity. *Neuron*, *57*(6), 917–929. https://doi.org/10.1016/j.neuron.2008.01.034

Fuentealba, P., Klausberger, T., Karayannis, T., Suen, W. Y., Huck, J., Tomioka, R., Rockland, K., Capogna, M., Studer, M., Morales, M., & Somogyi, P. (2010). Expression of COUP-TFII Nuclear Receptor in Restricted GABAergic Neuronal Populations in the Adult Rat Hippocampus. *Journal of Neuroscience*, *30*(5), 1595–1609. https://doi.org/10.1523/JNEUROSCI.4199-09.2010

Fuentealba, P., Tomioka, R., Dalezios, Y., Márton, L. F., Studer, M., Rockland, K., Klausberger, T., & Somogyi, P. (2008). Rhythmically Active Enkephalin-Expressing GABAergic Cells in the CA1 Area of the Hippocampus Project to the Subiculum and Preferentially Innervate Interneurons. *Journal of Neuroscience*, *28*(40), 10017–10022. https://doi.org/10.1523/JNEUROSCI.2052-08.2008

Fukuda, T., & Kosaka, T. (2000). Gap Junctions Linking the Dendritic Network of GABAergic Interneurons in the Hippocampus. *Journal of Neuroscience*, *20*(4), 1519–1528. https://doi.org/10.1523/JNEUROSCI.20-04-01519.2000

Ganter, P., Szücs, P., Paulsen, O., & Somogyi, P. (2004). Properties of horizontal axo-axonic cells in stratum oriens of the hippocampal CA1 area of rats in vitro. *Hippocampus*, *14*(2), 232–243. https://doi.org/10.1002/hipo.10170

Gathercole, S. E. (2008). Working Memory. In *Learning and Memory: A Comprehensive Reference* (pp. 33–51). Elsevier. https://doi.org/10.1016/B978-012370509-9.00179-0

Giamanco, K. A., & Matthews, R. T. (2012). Deconstructing the perineuronal net: Cellular contributions and molecular composition of the neuronal extracellular matrix. *Neuroscience*, *218*, 367–384. https://doi.org/10.1016/j.neuroscience.2012.05.055

Gloveli, T., Booker, S. A., Kopell, N., & Dugladze, T. (2018). Cell Type-Specific Activity During Hippocampal Network Oscillations In Vitro. In V. Cutsuridis, B. P. Graham, S. Cobb, & I. Vida (Eds.), *Hippocampal Microcircuits: A Computational Modeler's Resource Book* (pp. 327–364). Springer International Publishing. https://doi.org/10.1007/978-3-319-99103-0_8

Gulyás, A. I., Hájos, N., & Freund, T. F. (1996). Interneurons Containing Calretinin Are Specialized to Control Other Interneurons in the Rat Hippocampus. *Journal of Neuroscience*, *16*(10), 3397–3411. https://doi.org/10.1523/JNEUROSCI.16-10-03397.1996

Gulyás, A. I., Hájos, N., Katona, I., & Freund, T. F. (2003). Interneurons are the local targets of hippocampal inhibitory cells which project to the medial septum. *European Journal of Neuroscience*, *17*(9), 1861–1872. https://doi.org/10.1046/j.1460-9568.2003.02630.x

Gulyás, A. I., Megías, M., Emri, Z., & Freund, T. F. (1999). Total Number and Ratio of Excitatory and Inhibitory Synapses Converging onto Single Interneurons of

Different Types in the CA1 Area of the Rat Hippocampus. *Journal of Neuroscience*, *19*(22), 10082–10097. https://doi.org/10.1523/JNEUROSCI.19-22-10082.1999

Habib, N., Li, Y., Heidenreich, M., Swiech, L., Avraham-Davidi, I., Trombetta, J. J., Hession, C., Zhang, F., & Regev, A. (2016). Div-Seq: Single nucleus RNA-Seq reveals dynamics of rare adult newborn neurons. *Science (New York, N.Y.)*, *353*(6302), 925–928. https://doi.org/10.1126/science.aad7038

Hájos, N., & Mody, I. (1997). Synaptic Communication among Hippocampal Interneurons: Properties of Spontaneous IPSCs in Morphologically Identified Cells. *Journal of Neuroscience*, *17*(21), 8427–8442. https://doi.org/10.1523/JNEUROSCI.17-21-08427.1997

Harris, K. D., Hochgerner, H., Skene, N. G., Magno, L., Katona, L., Bengtsson Gonzales, C., Somogyi, P., Kessaris, N., Linnarsson, S., & Hjerling-Leffler, J. (2018). Classes and continua of hippocampal CA1 inhibitory neurons revealed by single-cell transcriptomics. *PLOS Biology*, *16*(6), e2006387. https://doi.org/10.1371/journal.pbio.2006387

Hu, W., Zhang, M., Czéh, B., Flügge, G., & Zhang, W. (2010). Stress Impairs GABAergic Network Function in the Hippocampus by Activating Nongenomic Glucocorticoid Receptors and Affecting the Integrity of the Parvalbumin-Expressing Neuronal Network. *Neuropsychopharmacology*, *35*(8), 1693–1707. https://doi.org/10.1038/npp.2010.31

Jeneson, A., & Squire, L. R. (2011). Working memory, long-term memory, and medial temporal lobe function. *Learning & Memory*, *19*(1), 15–25. https://doi.org/10.1101/lm.024018.111

Jinno, S. (2009). Structural organization of long-range GABAergic projection system of the hippocampus. *Frontiers in Neuroanatomy*, *3*. https://doi.org/10.3389/neuro.05.013.2009

Jinno, S., Aika, Y., Fukuda, T., & Kosaka, T. (1998). Quantitative analysis of GABAergic neurons in the mouse hippocampus, with optical disector using confocal laser scanning microscope. *Brain Research*, *814*(1–2), 55–70. https://doi.org/10.1016/S0006-8993(98)01075-0

Jinno, S., Klausberger, T., Marton, L. F., Dalezios, Y., Roberts, J. D. B., Fuentealba, P., Bushong, E. A., Henze, D., Buzsaki, G., & Somogyi, P. (2007). Neuronal Diversity in GABAergic Long-Range Projections from the Hippocampus. *Journal of Neuroscience*, *27*(33), 8790–8804. https://doi.org/10.1523/JNEUROSCI.1847-07.2007

Jinno, S., & Kosaka, T. (2002a). Patterns of expression of calcium binding proteins and neuronal nitric oxide synthase in different populations of hippocampal GABAergic neurons in mice. *The Journal of Comparative Neurology*, *449*(1), 1–25. https://doi.org/10.1002/cne.10251

Jinno, S., & Kosaka, T. (2002b). Immunocytochemical characterization of hippocamposeptal projecting GABAergic nonprincipal neurons in the mouse brain: A retrograde labeling study. *Brain Research*, *945*(2), 219–231. https://doi.org/10.1016/S0006-8993(02)02804-4

Jinno, S., & Kosaka, T. (2004). Patterns of colocalization of neuronal nitric oxide synthase and somatostatin-like immunoreactivity in the mouse hippocampus: Quantitative analysis with optical disector. *Neuroscience*, *124*(4), 797–808. https://doi.org/10.1016/j.neuroscience.2004.01.027

Jinno, S., & Kosaka, T. (2006). Cellular architecture of the mouse hippocampus: A quantitative aspect of chemically defined GABAergic neurons with stereology. *Neuroscience Research*, *56*(3), 229–245. https://doi.org/10.1016/j.neures.2006.07.007

Jinno, S., & Kosaka, T. (2010). Stereological estimation of numerical densities of glutamatergic principal neurons in the mouse hippocampus. *Hippocampus*, *20*(7), 829–840. https://doi.org/10.1002/hipo.20685

Katona, I., Sperlágh, B., Sík, A., Käfalvi, A., Vizi, E. S., Mackie, K., & Freund, T. F. (1999). Presynaptically Located CB1 Cannabinoid Receptors Regulate GABA Release from Axon Terminals of Specific Hippocampal Interneurons. *Journal of Neuroscience*, *19*(11), 4544–4558. https://doi.org/10.1523/JNEUROSCI.19-11-04544.1999

Katona, L., Micklem, B., Borhegyi, Z., Swiejkowski, D. A., Valenti, O., Viney, T. J., Kotzadimitriou, D., Klausberger, T., & Somogyi, P. (2017). Behavior-dependent activity patterns of GABAergic long-range projecting neurons in the rat hippocampus. *Hippocampus*, *27*(4), 359–377. https://doi.org/10.1002/hipo.22696

Kim, Y., Yang, G. R., Pradhan, K., Venkataraju, K. U., Bota, M., García del Molino, L. C., Fitzgerald, G., Ram, K., He, M., Levine, J. M., Mitra, P., Huang, Z. J., Wang, X.-J., & Osten, P. (2017). Brain-wide Maps Reveal Stereotyped Cell-Type-Based Cortical Architecture and Subcortical Sexual Dimorphism. *Cell*, *171*(2), 456-469.e22. https://doi.org/10.1016/j.cell.2017.09.020

Kishi, T., Tsumori, T., Yokota, S., & Yasui, Y. (2006). Topographical projection from the hippocampal formation to the amygdala: A combined anterograde and retrograde tracing study in the rat. *Journal of Comparative Neurology*, *496*(3), 349–368. https://doi.org/10.1002/cne.20919

Klausberger, T. (2009). GABAergic interneurons targeting dendrites of pyramidal cells in the CA1 area of the hippocampus. *European Journal of Neuroscience*, *30*(6), 947–957. https://doi.org/10.1111/j.1460-9568.2009.06913.x

Klausberger, T., Magill, P. J., Márton, L. F., Roberts, J. D. B., Cobden, P. M., Buzsáki, G., & Somogyi, P. (2003). Brain-state- and cell-type-specific firing of hippocampal interneurons in vivo. *Nature*, *421*(6925), 844–848. https://doi.org/10.1038/nature01374

Klausberger, T., Márton, L. F., Baude, A., Roberts, J. D. B., Magill, P. J., & Somogyi, P. (2004). Spike timing of dendrite-targeting bistratified cells during hippocampal network oscillations in vivo. *Nature Neuroscience*, *7*(1), 41–47. https://doi.org/10.1038/nn1159

Klausberger, T., Marton, L. F., O'Neill, J., Huck, J. H. J., Dalezios, Y., Fuentealba, P., Suen, W. Y., Papp, E., Kaneko, T., Watanabe, M., Csicsvari, J., & Somogyi, P. (2005). Complementary Roles of Cholecystokinin- and Parvalbumin-Expressing GABAergic Neurons in Hippocampal Network Oscillations. *Journal of Neuroscience*, *25*(42), 9782–9793. https://doi.org/10.1523/JNEUROSCI.3269-05.2005

Klausberger, T., & Somogyi, P. (2008). Neuronal Diversity and Temporal Dynamics: The Unity of Hippocampal Circuit Operations. *Science*, *321*(5885), 53–57. https://doi.org/10.1126/science.1149381

Knierim, J. J. (2015). *The hippocampus | Elsevier Enhanced Reader*. https://doi.org/10.1016/j.cub.2015.10.049

Krook-Magnuson, E., Luu, L., Lee, S.-H., Varga, C., & Soltesz, I. (2011). Ivy and Neurogliaform Interneurons Are a Major Target of μ-Opioid Receptor Modulation. *Journal of Neuroscience*, *31*(42), 14861–14870. https://doi.org/10.1523/JNEUROSCI.2269-11.2011

Lee, S.-H., Marchionni, I., Bezaire, M., Varga, C., Danielson, N., Lovett-Barron, M., Losonczy, A., & Soltesz, I. (2014). Parvalbumin-Positive Basket Cells Differentiate among Hippocampal Pyramidal Cells. *Neuron*, *82*(5), 1129–1144. https://doi.org/10.1016/j.neuron.2014.03.034

Li, X.-G., Somogyi, P., Tepper, J. M., & Buzsáki, G. (1992). Axonal and dendritic arborization of an intracellularly labeled chandelier cell in the CA1 region of rat hippocampus. *Experimental Brain Research*, *90*(3), 519–525. https://doi.org/10.1007/BF00230934

Loftus, G. R., Duncan, J., & Gehrig, P. (1992). On the time course of perceptual information that results from a brief visual presentation. *Journal of Experimental Psychology: Human Perception and Performance*, *18*(2), 530–549. https://doi.org/10.1037/0096-1523.18.2.530

Losonczy, A., Zhang, L., Shigemoto, R., Somogyi, P., & Nusser, Z. (2002). Cell type dependence and variability in the short-term plasticity of EPSCs in identified mouse hippocampal interneurones. *The Journal of Physiology*, *542*(1), 193–210. https://doi.org/10.1113/jphysiol.2002.020024

Luck, S. J., & Vogel, E. K. (1997). The capacity of visual working memory for features and conjunctions. *Nature*, *390*(6657), 279–281. https://doi.org/10.1038/36846

Manns, J. R., Hopkins, R. O., & Squire, L. R. (2003). Semantic Memory and the Human Hippocampus. *Neuron*, *38*(1), 127–133. https://doi.org/10.1016/S0896-6273(03)00146-6

Mao, W., Watanabe, T., Cho, S., Frost, J. L., Truong, T., Zhao, X., & Futai, K. (2015). Shank1 regulates excitatory synaptic transmission in mouse hippocampal parvalbumin-expressing inhibitory interneurons. *European Journal of Neuroscience*, *41*(8), 1025–1035. https://doi.org/10.1111/ejn.12877

Markowitsch, H. J. (1995). Which brain regions are critically involved in the retrieval of old episodic memory? *Brain Research Reviews*, *21*(2), 117–127. https://doi.org/10.1016/0165-0173(95)00007-0

Markram, H., Muller, E., Ramaswamy, S., Reimann, M. W., Abdellah, M., Sanchez, C. A., Ailamaki, A., Alonso-Nanclares, L., Antille, N., Arsever, S., Kahou, G. A. A., Berger, T. K., Bilgili, A., Buncic, N., Chalimourda, A., Chindemi, G., Courcol, J.-D., Delalondre, F., Delattre, V., … Schürmann, F. (2015). Reconstruction and Simulation of Neocortical Microcircuitry. *Cell*, *163*(2), 456–492. https://doi.org/10.1016/j.cell.2015.09.029

Martin, A., & Simmons, W. K. (2008). 3.07—Structural Basis of Semantic Memory. In J. H. Byrne (Ed.), *Learning and Memory: A Comprehensive Reference* (pp. 113–130). Academic Press. https://doi.org/10.1016/B978-012370509-9.00108-X

Martin, Alex. (2007). The Representation of Object Concepts in the Brain. *Annual Review of Psychology*, *58*(1), 25–45. https://doi.org/10.1146/annurev.psych.57.102904.190143

Milior, G., Di Castro, M. A., Sciarria, L. P., Garofalo, S., Branchi, I., Ragozzino, D., Limatola, C., & Maggi, L. (2016). Electrophysiological Properties of CA1 Pyramidal Neurons along the Longitudinal Axis of the Mouse Hippocampus. *Scientific Reports*, *6*(1), 38242. https://doi.org/10.1038/srep38242

Miller, E. K., Li, L., & Desimone, R. (1993). Activity of neurons in anterior inferior temporal cortex during a short- term memory task. *Journal of Neuroscience*, *13*(4), 1460–1478. https://doi.org/10.1523/JNEUROSCI.13-04-01460.1993

Mizuseki, K., Diba, K., Pastalkova, E., & Buzsáki, G. (2011). Hippocampal CA1 pyramidal cells form functionally distinct sublayers. *Nature Neuroscience*, *14*(9), 1174–1181. https://doi.org/10.1038/nn.2894

Moscovitch, M. (1992). Memory and Working-with-Memory: A Component Process Model Based on Modules and Central Systems. *Journal of Cognitive Neuroscience*, *4*(3), 257–267. https://doi.org/10.1162/jocn.1992.4.3.257

Nadeau, S. E. (2008). CHAPTER 32—Subcortical Language Mechanisms. In B. Stemmer & H. A. Whitaker (Eds.), *Handbook of the Neuroscience of Language* (pp. 329–340). Elsevier. https://doi.org/10.1016/B978-008045352-1.00032-X

Nyberg, L. (2008). 3.06—Structural Basis of Episodic Memory. In J. H. Byrne (Ed.), *Learning and Memory: A Comprehensive Reference* (pp. 99–112). Academic Press. https://doi.org/10.1016/B978-012370509-9.00107-8

Nyberg, L. (2002). Where encoding and retrieval meet in the brain. In *Neuropsychology of memory, 3rd ed* (pp. 193–203). The Guilford Press.

Overstreet-Wadiche, L., & McBain, C. J. (2015). Neurogliaform cells in cortical circuits. *Nature Reviews. Neuroscience*, *16*(8), 458–468. https://doi.org/10.1038/nrn3969

Pelkey, K. A., Chittajallu, R., Craig, M. T., Tricoire, L., Wester, J. C., & McBain, C. J. (2017). Hippocampal GABAergic Inhibitory Interneurons. *Physiological Reviews*, *97*(4), 1619–1747. https://doi.org/10.1152/physrev.00007.2017

Peñagarikano, O., Abrahams, B. S., Herman, E. I., Winden, K. D., Gdalyahu, A., Dong, H., Sonnenblick, L. I., Gruver, R., Almajano, J., Bragin, A., Golshani, P., Trachtenberg, J. T., Peles, E., & Geschwind, D. H. (2011). Absence of CNTNAP2 Leads to Epilepsy, Neuronal Migration Abnormalities, and Core Autism-Related Deficits. *Cell*, *147*(1), 235–246. https://doi.org/10.1016/j.cell.2011.08.040

Price, C. J., Cauli, B., Kovacs, E. R., Kulik, A., Lambolez, B., Shigemoto, R., & Capogna, M. (2005). Neurogliaform Neurons Form a Novel Inhibitory Network in the Hippocampal CA1 Area. *Journal of Neuroscience*, *25*(29), 6775–6786. https://doi.org/10.1523/JNEUROSCI.1135-05.2005

Roediger, H. L., & McDermott, K. B. (1995). Creating false memories: Remembering words not presented in lists. *Journal of Experimental Psychology: Learning, Memory, and Cognition*, *21*(4), 803–814. https://doi.org/10.1037/0278-7393.21.4.803

Roediger III, H. L., Balota, D. A., & Watson, J. M. (2001). Spreading activation and arousal of false memories. In *The nature of remembering: Essays in honor of Robert G. Crowder* (pp. 95–115). American Psychological Association. https://doi.org/10.1037/10394-006

Routh, B. N., Johnston, D., Harris, K., & Chitwood, R. A. (2009). Anatomical and Electrophysiological Comparison of CA1 Pyramidal Neurons of the Rat and Mouse. *Journal of Neurophysiology*, *102*(4), 2288–2302. https://doi.org/10.1152/jn.00082.2009

Scoville, W. B., & Milner, B. (1957). LOSS OF RECENT MEMORY AFTER BILATERAL HIPPOCAMPAL LESIONS. *Journal of Neurology, Neurosurgery, and Psychiatry*, *20*(1), 11–21.

Sharot, T., Delgado, M. R., & Phelps, E. A. (2004). How emotion enhances the feeling of remembering. *Nature Neuroscience*, *7*(12), 1376–1380. https://doi.org/10.1038/nn1353

Sik, A., Ylinen, A., Penttonen, M., & Buzsaki, G. (1994). Inhibitory CA1-CA3-hilar region feedback in the hippocampus. *Science*, *265*(5179), 1722–1724. https://doi.org/10.1126/science.8085161

Soltesz, I., & Losonczy, A. (2018). CA1 pyramidal cell diversity enabling parallel information processing in the hippocampus. *Nature Neuroscience*, *21*(4), 484–493. https://doi.org/10.1038/s41593-018-0118-0

Somogyi, J., Baude, A., Omori, Y., Shimizu, H., Mestikawy, S. E., Fukaya, M., Shigemoto, R., Watanabe, M., & Somogyi, P. (2004). GABAergic basket cells expressing cholecystokinin contain vesicular glutamate transporter type 3 (VGLUT3) in their

synaptic terminals in hippocampus and isocortex of the rat. *European Journal of Neuroscience*, *19*(3), 552–569. https://doi.org/10.1111/j.0953-816X.2003.03091.x

Somogyi, J., Szabo, A., Somogyi, P., & Lamsa, K. P. (2012). Molecular analysis of ivy cells of the hippocampal CA1 stratum radiatum using spectral identification of immunofluorophores. *Frontiers in Neural Circuits*, *6*. https://doi.org/10.3389/fncir.2012.00035

Somogyi, P., & Klausberger, T. (2005). Defined types of cortical interneurone structure space and spike timing in the hippocampus. *The Journal of Physiology*, *562*(1), 9–26. https://doi.org/10.1113/jphysiol.2004.078915

Song, D., Robinson, B. S., Hampson, R. E., Marmarelis, V. Z., Deadwyler, S. A., & Berger, T. W. (2018). Sparse Large-Scale Nonlinear Dynamical Modeling of Human Hippocampus for Memory Prostheses. *IEEE Transactions on Neural Systems and Rehabilitation Engineering*, *26*(2), 272–280. https://doi.org/10.1109/TNSRE.2016.2604423

Sperling, G. (1960). The information available in brief visual presentations. *Psychological Monographs: General and Applied*, *74*(11), 1–29. https://doi.org/10.1037/h0093759

Squire, L. R., & Zola, S. M. (1998). Episodic memory, semantic memory, and amnesia. *Hippocampus*, *8*(3), 205–211. https://doi.org/10.1002/(SICI)1098-1063(1998)8:3<205::AID-HIPO3>3.0.CO;2-I

Staff, N. P., Jung, H.-Y., Thiagarajan, T., Yao, M., & Spruston, N. (2000). Resting and Active Properties of Pyramidal Neurons in Subiculum and CA1 of Rat Hippocampus. *Journal of Neurophysiology*, *84*(5), 2398–2408. https://doi.org/10.1152/jn.2000.84.5.2398

Strange, B. A., Witter, M. P., Lein, E. S., & Moser, E. I. (2014). Functional organization of the hippocampal longitudinal axis. *Nature Reviews Neuroscience*, *15*(10), 655–669. https://doi.org/10.1038/nrn3785

Thomas, B. F. (2009). Neuroanatomical basis for therapeutic applications of cannabinoid receptor 1 antagonists. *Drug Development Research*, *70*(8), 527–554. https://doi.org/10.1002/ddr.20333

Thompson-Schill, S. L. (2003). Neuroimaging studies of semantic memory: Inferring "how" from "where". *Neuropsychologia*, *41*(3), 280–292. https://doi.org/10.1016/S0028-3932(02)00161-6

Thompson-Schill, S. L., Swick, D., Farah, M. J., D'Esposito, M., Kan, I. P., & Knight, R. T. (1998). Verb generation in patients with focal frontal lesions: A neuropsychological test of neuroimaging findings. *Proceedings of the National Academy of Sciences*, *95*(26), 15855–15860. https://doi.org/10.1073/pnas.95.26.15855

Tóth, K., & Freund, T. F. (1992). Calbindin D28k-containing nonpyramidal cells in the rat hippocampus: Their immunoreactivity for GABA and projection to the medial septum. *Neuroscience*, *49*(4), 793–805. https://doi.org/10.1016/0306-4522(92)90357-8

Traub, R. D., Whittington, M. A., Colling, S. B., Buzsáki, G., & Jefferys, J. G. (1996). Analysis of gamma rhythms in the rat hippocampus in vitro and in vivo. *The Journal of Physiology*, *493 (Pt 2)*, 471–484. https://doi.org/10.1113/jphysiol.1996.sp021397

Tricoire, L., Pelkey, K. A., Daw, M. I., Sousa, V. H., Miyoshi, G., Jeffries, B., Cauli, B., Fishell, G., & McBain, C. J. (2010). Common Origins of Hippocampal Ivy and Nitric Oxide Synthase Expressing Neurogliaform Cells. *Journal of Neuroscience*, *30*(6), 2165–2176. https://doi.org/10.1523/JNEUROSCI.5123-09.2010

Tricoire, L., Pelkey, K. A., Erkkila, B. E., Jeffries, B. W., Yuan, X., & McBain, C. J. (2011). A Blueprint for the Spatiotemporal Origins of Mouse Hippocampal Interneuron Diversity. *Journal of Neuroscience*, *31*(30), 10948–10970. https://doi.org/10.1523/JNEUROSCI.0323-11.2011

Tricoire, L., & Vitalis, T. (2012). Neuronal nitric oxide synthase expressing neurons: A journey from birth to neuronal circuits. *Frontiers in Neural Circuits*, *6*. https://doi.org/10.3389/fncir.2012.00082

Tulving, E., Kapur, S., Craik, F. I., Moscovitch, M., & Houle, S. (1994). Hemispheric encoding/retrieval asymmetry in episodic memory: Positron emission tomography findings. *Proceedings of the National Academy of Sciences*, *91*(6), 2016–2020. https://doi.org/10.1073/pnas.91.6.2016

Tulving, Endel. (2002). Episodic Memory: From Mind to Brain. *Annual Review of Psychology*, *53*(1), 1–25. https://doi.org/10.1146/annurev.psych.53.100901.135114

Tyan, L., Chamberland, S., Magnin, E., Camiré, O., Francavilla, R., David, L. S., Deisseroth, K., & Topolnik, L. (2014). Dendritic Inhibition Provided by Interneuron-Specific Cells Controls the Firing Rate and Timing of the Hippocampal Feedback Inhibitory Circuitry. *Journal of Neuroscience*, *34*(13), 4534–4547. https://doi.org/10.1523/JNEUROSCI.3813-13.2014

Vargha-Khadem, F., Gadian, D. G., Watkins, K. E., Connelly, A., Paesschen, W. V., & Mishkin, M. (1997). Differential Effects of Early Hippocampal Pathology on Episodic and Semantic Memory. *Science*, *277*(5324), 376–380. https://doi.org/10.1126/science.277.5324.376

Verfaellie, M., Koseff, P., & Alexander, M. P. (2000). Acquisition of novel semantic information in amnesia: Effects of lesion location. *Neuropsychologia*, *38*(4), 484–492. https://doi.org/10.1016/S0028-3932(99)00089-5

Vida, I., Degro, C. E., & Booker, S. A. (2018). Morphology of Hippocampal Neurons. In V. Cutsuridis, B. P. Graham, S. Cobb, & I. Vida (Eds.), *Hippocampal Microcircuits: A Computational Modeler's Resource Book* (pp. 29–90). Springer International Publishing. https://doi.org/10.1007/978-3-319-99103-0_2

Vida, I., Halasy, K., Szinyei, C., Somogyi, P., & Buhl, E. H. (1998). Unitary IPSPs evoked by interneurons at the stratum radiatum-stratum lacunosum-moleculare border in the CA1 area of the rat hippocampus in vitro. *The Journal of Physiology*, *506*(Pt 3), 755–773. https://doi.org/10.1111/j.1469-7793.1998.755bv.x

Wagner, A. D., Shannon, B. J., Kahn, I., & Buckner, R. L. (2005). Parietal lobe contributions to episodic memory retrieval. *Trends in Cognitive Sciences*, *9*(9), 445–453. https://doi.org/10.1016/j.tics.2005.07.001

Wang, D., & Fawcett, J. (2012). The perineuronal net and the control of CNS plasticity. *Cell and Tissue Research*, *349*(1), 147–160. https://doi.org/10.1007/s00441-012-1375-y

Wertheimer, M. (1923). Untersuchungen zur Lehre von der Gestalt. II. *Psychologische Forschung*, *4*(1), 301–350. https://doi.org/10.1007/BF00410640

Witter, M. P. (2010). Connectivity of the Hippocampus. In V. Cutsuridis, B. Graham, S. Cobb, & I. Vida (Eds.), *Hippocampal Microcircuits: A Computational Modeler's Resource Book* (pp. 5–26). Springer. https://doi.org/10.1007/978-1-4419-0996-1_1

Wyeth, M. S., Zhang, N., Mody, I., & Houser, C. R. (2010). Selective Reduction of Cholecystokinin-Positive Basket Cell Innervation in a Model of Temporal Lobe Epilepsy. *Journal of Neuroscience*, *30*(26), 8993–9006. https://doi.org/10.1523/JNEUROSCI.1183-10.2010

Yamada, J., & Jinno, S. (2017). Molecular heterogeneity of aggrecan-based perineuronal nets around five subclasses of parvalbumin-expressing neurons in the mouse hippocampus: Aggrecan and parvalbumin in the hippocampus. *Journal of Comparative Neurology*, *525*(5), 1234–1249. https://doi.org/10.1002/cne.24132

Yang, S., Yang, S., Moreira, T., Hoffman, G., Carlson, G. C., Bender, K. J., Alger, B. E., & Tang, C.-M. (2014). Interlamellar CA1 network in the hippocampus. *Proceedings of the National Academy of Sciences*, *111*(35), 12919–12924. https://doi.org/10.1073/pnas.1405468111

Yin, H. H., & Knowlton, B. J. (2006). The role of the basal ganglia in habit formation. *Nature Reviews Neuroscience*, *7*(6), 464–476. https://doi.org/10.1038/nrn1919

Zeisel, A., Muñoz-Manchado, A. B., Codeluppi, S., Lönnerberg, P., Manno, G. L., Juréus, A., Marques, S., Munguba, H., He, L., Betsholtz, C., Rolny, C., Castelo-Branco, G., Hjerling-Leffler, J., & Linnarsson, S. (2015). Cell types in the mouse cortex and hippocampus revealed by single-cell RNA-seq. *Science*, *347*(6226), 1138–1142. https://doi.org/10.1126/science.aaa1934

9. Appendix A: Parvalbumin basket cells' bouton calculations.

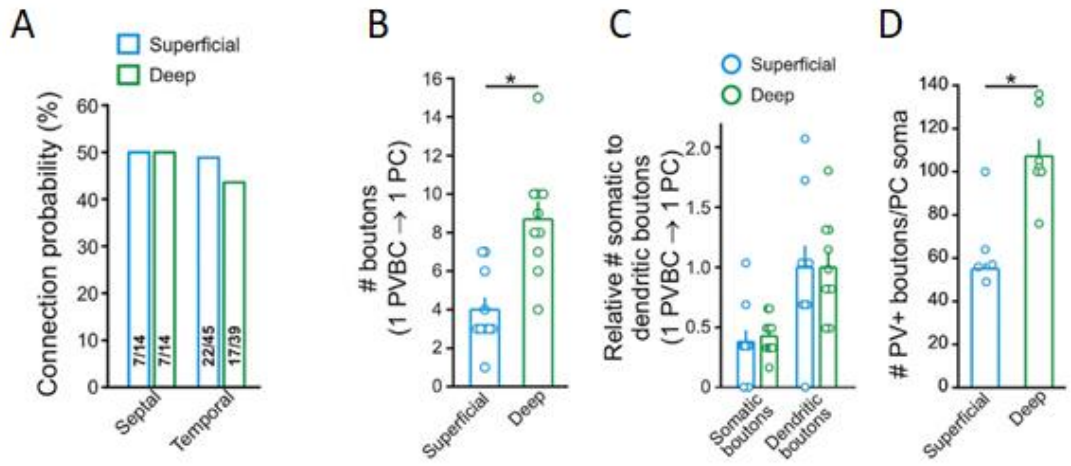

Fig. S 1 Parvalbumin basket cell connections to CA1 pyramidal cells.
A: Bar graph showing the connection probability from PVBCs to PCs. Numbers in bars indicate connected/tested pairs.
B: Number of putative axon terminals of single PVBCs on single sPCs (n = 10) and dPCs (n = 10).
C: Relative number of somatic to proximal dendritic boutons of single PVBCs on single sPCs (n = 10) and dPCs (n = 10); data normalized by the average number of dendritic boutons in each group.
D: Summary data of the number of putative synaptic PV+ boutons around the somata of biocytin-filled dPCs and sPCs.
As adapted from Lee *et al*., 2014 Figure 1F, J, K, L.

From Fig. S1 above and values obtained through WebPlotDigitizer, in the superficial layer, one PVBC innervates one PC via 3.97 boutons with a connection probability of 50%. Considering the somatic to dendritic bouton ratio (0.38:1) and the number of PV+ boutons on a PC soma (55.1), PVBCs have a convergence of about 50.6 cells on one superficial PC (sPC).

In contrast, in the deep sublayer, one PVBC innervates one PC via 8.68 boutons. Considering the somatic to dendritic bouton ratio of 0.43:1 and the number of PV+ boutons on a PC soma of 107.2, then PVBCs have a convergence of about 41.1 cells on one deep PC (dPC). The average connection probability from PVBCs and dPCs is of 46.8%.

In the superficial layer, one PVBC innervates one PC via 3.97 boutons with a connection probability of 50%. PVBCs have a convergence of about 50.6 cells on one sPC. In contrast, in the deep sublayer, one PVBC innervates one PC via 8.68 boutons. PVBCs have a

convergence of about 41.1 cells on one dPC. The average connection probability from PVBCs and dPCs is of 46.8%.

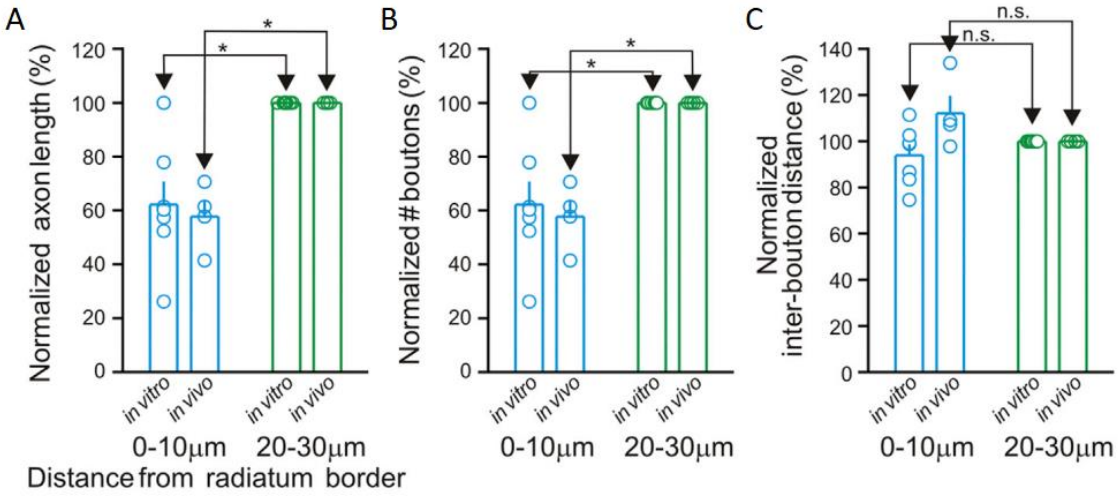

Fig. S 2 Bouton distribution of Parvalbumin Basket cells.
(A, B, and C) Summary of morphological measurements of the length (A), number of boutons (B), and interbouton distance (C) of axons originating from individual PVBCs filled in vitro and in vivo in the septal CA1. Means and SEM are plotted. n.s., not significant (in this and subsequent figures). As adapted from Lee *et al*., (2014) Figure 2 G,H,I.

PVBCs preferentially innervate deep PCs over superficial PCs. As observed by Lee *et al*., (2014), and as shown in **Fig. S2** showing a PVBC from the septal CA1, while the inter-bouton distance throughout the axon appears constant, a higher innervation density is achieved by a significantly higher proportion of the axon present in the deep sublayer. Unfortunately, the values given by Lee and colleagues are the normalized values and not the actual values.

10. Appendix B: Quantifications extended.

Table S1

Numerical densities from Yamada and Jinno (2017)

		Hippocampal CA1 strata							
		dSO	vSO	dSP	vSP	dSR	vSR	dSLM	vSLM
PV+ interneurons ND (cells*1000/mm3)	PV BC	-	-	3.38 ± 0.26	2.90 ± 0.22	-	-	-	-
	ACC	-	-	0.75 ± 0.17	0.54 ± 0.25	-	-	-	-
	BSC	-	-	0.99 ± 0.26	0.27 ± 0.16	-	-	-	-
	PV+ O-LM	0.52 ± 0.07	0.71 ± 0.08	-	-	-	-	-	-
	PV+ HS	0.44 ± 0.11	0.52 ± 0.25	-	-	-	-	-	-

Table S2

Percentages of CCK+ interneuron categories in the rat.

		Hippocampal CA1 strata		
		dSO	dSP	dSR+dSLM
Percentages from Somogyi *et al*. 2004	CCK only (% of CCK+)	28.9	49.5	28.2
	CCK/vGluT3 (% of CCK+)	12.4	16.2	41.6
	CCK/CB (% of CCK+)	31.7	12.4	25.9
	CCK/VIP (% of CCK+)	27	21.9	4.3

Table S3

Calculation of CCK+ colocalisation with vGluT3, CB and VIP

		Hippocampal CA1 strata							
		dSO	vSO	dSP	vSP	dSR	vSR	dSLM	vSLM
Jinno & Kosaka 2006	CCK ND (cells*1000/mm3)	0.290	0.560	0.760	1.080	0.410	0.700	0.170	0.660
Kim *et al*. 2017	CCK/VIP ND (cells*1000/mm3)	0.005	0.005	0.019	0.019	0.014	0.014	0.016	0.016
divided according to CCK dorso-ventral distribution	CCK/VIP ND (cells*1000/mm3)	0.003	0.007	0.016	0.022	0.010	0.018	0.007	0.025
	CCK/VIP (% of CCK+)	1.176	1.176	2.065	2.065	2.523	2.523	3.855	3.855
Amended percentages from Somogyi *et al*. 2004	CCK only (% of CCK+)	37.507	37.507	56.110	56.110	28.793	28.793	28.347	28.347
	CCK/vGluT3 (% of CCK+)	21.007	21.007	22.810	22.810	42.193	42.193	41.747	41.747
	CCK/CB (% of CCK+)	40.307	40.307	19.010	19.010	26.493	26.493	26.047	26.047
	CCK/VIP (% of CCK+)	1.180	1.180	2.070	2.070	2.520	2.520	3.860	3.860
	CCK only ND (cells*1000/mm3)	0.109	0.210	0.426	0.606	0.118	0.202	0.048	0.187
	CCK/vGluT3 ND (cells*1000/mm3)	0.061	0.118	0.173	0.246	0.173	0.295	0.071	0.276
	CCK/CB ND (cells*1000/mm3)	0.117	0.226	0.144	0.205	0.109	0.185	0.044	0.172
	CCK/VIP ND (cells*1000/mm3)	0.003	0.007	0.016	0.022	0.010	0.018	0.007	0.025

Table S4

Calculation of colocalisation of SST+ and nNOS+ interneurons for the estimation of BPC ND.

		Hippocampal CA1 strata							
		dSO	vSO	dSP	vSP	dSR	vSR	dSLM	vSLM
Kim *et al*. (2017)	Volume of ROI (mm3)	0.915	0.915	0.955	0.955	1.415	1.415	1.165	1.165
Jinno and Kosaka (2006)	Total ND and SD of SST (cells*1000/mm3)	3.09 ± 0.16	5.79 ± 0.48	0.46 ± 0.12	0.67 ± 0.17	0.07 ± 0.06	0.11 ± 0.05	0.03 ± 0.03	0
Jinno and Kosaka (2006)	Total ND and SD of nNOS (cells*1000/mm3)	1.27 ± 0.07	0.76 ± 0.10	4.23 ± 0.26	2.44 ± 0.29	0.70 ± 0.19	0.76 ± 0.18	1.96 ± 0.43	1.84 ± 0.56
Jinno and Kosaka (2004)	nNOS (% of SST)	4.3	3.3	0	4.1	10	12.5	25.5	0
Jinno and Kosaka (2004)	SST (% of nNOS)	10	23.8	0	1.5	1.9	1.3	0.6	0
	Nº of nNOS, SST interneurons	121.58	174.83	0	26.23	9.91	19.46	8.91	0
	Nº of SST, nNOS interneurons	116.21	165.51	0	34.95	18.82	13.98	13.70	0
	Average interneuron Nº	118.89	170.17	0	30.59	14.36	16.72	11.31	0
	ND of SST+/nNOS+ (cells*1000/mm3)	**0.13**	**0.06**	**0**	**0.07**	**0.01**	**0.24**	**0.01**	**0**

Table S5

Calculation of O-LM numerical densities.

		Hippocampal CA1 strata	
		dSO	vSO
Jinno *et al*. (1998)	Total GABAergic ND (cells*1000/mm3)	6.48	10.50
Chittajallu *et al*. (2013)	31.5% in SO are CGE derived (cells*1000/mm3)	2.041	3.308
Chittajallu *et al*. (2013)	39% of CGE in SO are SOM+ (cells*1000/mm3)	0.796	1.290
Chittajallu *et al*. (2013)	8/29 SO-A SOM+ cells are O-LM (cells*1000/mm3)	**0.220**	**0.356**
Yamada and Jinno (2017)	ND of PV+ OLM (cells*1000/mm3)	0.522	0.712
	ND of Unclaimed SO SST+ interneurons (cells*1000/mm3)	0.166	0.354
	Total ND of MGE O-LM (cells*1000/mm3)	**0.689**	**1.066**
	Total ND of O-LM cells (cells*1000/mm3)	**0.908**	**1.421**

Table S6

Number of cells per hippocampal sub-layer

		Hippocampal CA1 strata							
		dSO	vSO	dSP	vSP	dSR	vSR	dSLM	vSLM
Jinno and Kosaka (2006)	Total ND of SST (cells*1000/mm3)	3.09	5.79	0.46	0.67	0.07	0.11	0.03	0
Jinno and Kosaka (2006)	Total ND of PV (cells*1000/mm3)	1.34	2.68	5.73	3.83	0.23	0.04	0.06	0
Kim *et al*., (2017)	Volume of ROI (mm3)	0.915	0.915	0.955	0.955	1.415	1.415	1.165	1.165
	number of SST+ cells	2827	5298	439	640	99	156	35	0
	number of PV+ cells	1226	2452	5472	3658	325	57	70	0

Table S7

Calculating ND of SST+ HS cells.

		number of cells	Average ND in SO (cells*1000/mm3)
Yamada and Jinno (2017)	22.5% of total SST+	332	1.17
	2.5% of total PV+	2136	0.18
	PV+ HS cells (cells*1000/mm3)		0.48
	SST+ HS cells (cells*1000/mm3)		3.09

Table S8

Calculation of ND of total HS and DPC

		Hippocampal regions	
		dSO	vSO
ND (cells*1000/mm3)	Unclaimed SST+ cells	2.15	4.56
	3.09 divided according to d:v ratio above	1.98	4.21
	Total HS	**2.07**	**4.41**
	CB+ HS cells	**1.18**	**2.52**
	NPY+ HS cells	0.296	0.629

Table S9

Reproduced from: Jinno *et al*. (2007), Supplementary Table 2. Subsets of hippocampo-subicular and hippocampo-septal projection neurons tested for three frequently expressed molecules by GABAergic cells in str. oriens of the CA1 area

Molecular profiles	hippocampo-subicular projection neurons (n=21)	hippocampo-septal projection neurons (n=38)	Similar *in vivo* recorded cells in str. oriens
SST+ mGluR1α+ M2R-	43% (9)	50% (19)	T87c, C25a
SST+ mGluR1α+ M2R+	10% (2)	16% (6)	
SST+ mGluR1α- M2R+	0%	21% (8)	P13c, K98c?
SST+ mGluR1α- M2R-	5% (1)	11% (4)	K98c?
SST- mGluR1α- M2R+	29% (6)	0%	T80a*, T85a**
SST- mGluR1α- M2R-	10% (2)	0%	
SST- mGluR1α+ M2R-	5% (1)	0%	
SST- mGluR1α+ M2R+	0%	3% (1)	

Values represent the proportion of a given subset to all hippocampo-subicular or hippocampo-septal projection neuron tested for the 3 molecules. Percentages are rounded to integers.

Values in parenthesis represent the number of cells belonging to each subset detected by retrograde labelling.
* T80a was not tested for SST; it could belong to this or the third group above.
** T85a has been reported in an earlier study (Ferraguti *et al*., 2005).

Table S10

Numerical densities of various molecular profiles of various H-Sub interneurons.

Molecular profiles	hippocampo-subicular projection neurons (n=21)	ND of H-Sub dSO (cells*1000/mm3)	ND of H-Sub vSO (cells*1000/mm3)
SST+ mGluR1α+ M2R-	43%	1.04	2.20
SST+ mGluR1α+ M2R+	10%	0.24	0.51
SST+ mGluR1α- M2R+	0%	0.00	0.00
SST+ mGluR1α- M2R-	5%	0.12	0.26
SST- mGluR1α- M2R+	29%	0.70	1.49
SST- mGluR1α- M2R-	10%	0.24	0.51
SST- mGluR1α+ M2R-	5%	0.12	0.26
SST- mGluR1α+ M2R+	0%	0.00	0.00
Total ND of interneurons projecting only to subiculum (cells*1000/mm3)*		1.06	2.26
Total ND of H-Sub		2.46	5.23

* This includes SST-/mGluR1α-/M2R+, SST-/mGluR1α-/M2R- and SST-/mGluR1α+/M2R-. This is the minimum value as it is possible that other molecular profiles also include a percentage of cells which only project to the subiculum.

Table S11

Calculation of ND of colocalised CR and nNOS in CA1.

	Hippocampal CA1 strata							
	dSO	vSO	dSP	vSP	dSR	vSR	dSLM	vSLM
percentages of CR containing nNOS*	0.00	7.60	27.10	56.00	19.20	45.40	18.20	41.20
percentages of nNOS containing CR*	0.00	6.10	16.60	41.00	13.40	31.70	6.20	26.90
Total CR+ ND (cells*1000/mm^3)**	0.35	0.57	2.68	1.92	0.47	0.52	0.63	1.18
Total nNOS+ ND (cells*1000/mm3)**	1.27	0.76	4.23	2.44	0.70	0.76	1.96	1.84
ND of CR+ nNOS cells(cells*1000/mm^3)	0.00	0.04	0.73	1.08	0.09	0.24	0.11	0.49
ND of nNOS+ CR cells(cells*1000/mm^3)	0.00	0.05	0.70	1.00	0.09	0.24	0.12	0.49
Average CR:nNOS (cells*1000/mm^3)	0.00	0.05	0.71	1.04	0.09	0.24	0.12	0.49

* Jinno and Kosaka (2002a) ** Jinno and Kosaka (2006)

Table S12

Calculations of NDs of IS-I, IS-II, IS-III and IS-III bipolar cells.

	Hippocampal CA1 strata							
	dSO	vSO	dSP	vSP	dSR	vSR	dSLM	vSLM
Total VIP+ ND (cells*1000/mm^3)*	0.24	0.45	2.79	2.38	0.37	0.58	0.44	1.32
VIP+ CCK BCs ND (see above) (cells*1000/mm^3)	0.00	0.01	0.02	0.02	0.01	0.02	0.01	0.03
ND of "Unclaimed" VIP+ interneurons (cells*1000/mm^3)	0.24	0.44	2.77	2.36	0.36	0.56	0.43	1.29
total CR+ ND (cells*1000/mm^3)*	0.35	0.57	2.68	1.92	0.47	0.52	0.63	1.18
ND of the 6%*** of HS that are CR+ (cells*1000/mm^3)	0.12	0.26	0.00	0.00	0.00	0.00	0.00	0.00
ND of "Unclaimed" CR+ interneurons (cells*1000/mm^3)	0.23	0.31	2.68	1.92	0.47	0.52	0.63	1.18
Average distribution ratio of "unclaimed" VIP+ and CR+ interneuron NDs	0.39	0.61	0.56	0.44	0.43	0.57	0.30	0.70
ND of VIP+/CR+ (cells*1000/mm^3)**	0.068		0.198		0.105		0.086	
ND of VIP+/CR+ according to distribution ratio above (cells*1000/mm^3)	0.05	0.08	0.22	0.17	0.09	0.12	0.05	0.12
ND of CR+/nNOS+ (cells*1000/mm^3)	0.00	0.04	0.71	1.04	0.09	0.24	0.12	0.49
IS-III bipolar ND (cells*1000/mm^3)	0.00	0.06	0.95	1.38	0.12	0.32	0.16	0.65
IS-III ND (cells*1000/mm^3)	**0.05**	**0.10**	**0.46**	**0.52**	**0.12**	**0.20**	**0.09**	**0.28**
IS-II ND (cells*1000/mm^3)	**0.18**	**0.35**	**2.31**	**1.84**	**0.24**	**0.36**	**0.34**	**1.01**
IS-I ND (cells*1000/mm^3)	**0.17**	**0.22**	**2.46**	**1.75**	**0.38**	**0.40**	**0.58**	**1.06**

* Values from Jinno and Kosaka, (2006) **Values from Kim *et al*., (2017) ***Value from Jinno *et al*., 2007

Table S13

Calculation of MGE derived NGF and Ivy cells.

		Hippocampal CA1 strata							
		dSO	vSO	dSP	vSP	dSR	vSR	dSLM	vSLM
interneuron ND (cells*1000/mm^3)	Total nNOS**	1.17	0.76	4.23	2.44	0.70	0.76	1.96	1.84
	IS-III Bipolar cells	0.00	0.06	0.95	1.38	0.12	0.32	0.16	0.65
	BPC	0.13	0.06	0.00	0.07	0.01	0.24	0.01	0.00
	Unclaimed nNOS	1.04	0.65	3.28	0.99	0.57	0.20	1.79	1.19
	Ivy	1.04	0.65	3.28	0.99	0.45	0.16	0.00	0.00
	MGE NGF	0.00	0.00	0.00	0.00	0.11	0.04	1.79	1.19

**Jinno and Kosaka, (2006)

Table S14

Calculation of CGE NGF cells

		Hippocampal CA1 strata							
		dSO	vSO	dSP	vSP	dSR	vSR	dSLM	vSLM
interneuron ND (cells*1000/mm^3)	Total NPY **	3.12	4.45	5.35	2.15	0.88	0.28	1.68	0.83
	Ivy	1.14	0.65	3.28	0.99	0.28	0.10	0.00	0.00
	MGE NGF	0.00	0.00	0.00	0.00	0.28	0.10	1.79	1.19
	PV+ BSC	0.07	0.10	0.99	0.27	0.01	0.02	0.01	0.00
	BPC	0.13	0.06	0.00	0.07	0.01	0.24	0.01	0.00
	NPY+ H-Sub and HS	0.88	1.88	0.00	0.00	0.22	0.22	0.00	0.00
	Remaining NPY	0.90	1.77	1.08	0.83	0.08	-0.40	-0.13	-0.36

**Jinno and Kosaka (2006)

Table S15

Dorsal numbers

	ND in hippocampal CA1 strata (cells*1000/mm3)			
	dSO	dSP	dSR	dSLM
Perisomatic inhibitory neurons				
PV BC	228	3228	215	46
CCK BC total	158	588	259	91
ACC	50	715	48	10
Dendritic inhibitory neurons				
BSC	67	944	63	13
Total OLM	831	0	0	0
SCA total	0	0	160	0
ADI total	0	0	160	0
PPA total	0	0	0	107
Total NGF	0	0	141	2089
IVY	952	3130	138	0
Interneuron-specific interneurons				
IS-I	158	2345	536	674
IS-II	168	2208	337	399
IS-III	48	440	172	106
Projection interneurons				
Total HS	1896	0	0	0
H-Sub	970		2581	1189
BPC	119	0	14	11

Table S16

Ventral numbers

	ND in hippocampal CA1 strata (cells*1000/mm3)			
	vSO	vSP	vSR	vSLM
.				
Perisomatic inhibitory neurons				
PV BC	1036	2770	44	0
CCK BC total	306	836	443	351
ACC	194	520	8	0
Dendritic inhibitory neurons				
BSC	95	254	4	0
Total OLM	1301	0	0	0
SCA total	0	0	275	0
ADI total	0	0	275	0
PPA total	0	0	0	418
Total NGF	0	0	56	1382
IVY	590	945	225	0
Interneuron-specific interneurons				
IS-I	205	1670	567	1234
IS-II	316	1757	515	1177
IS-III	90	496	281	331
Projection interneurons				
Total HS	4033	0	0	0
H-Sub	2068	-	2581	1189
BPC	50	64	338	0